Normal Conditions of Transport Truck Test of a Surrogate Fuel Assembly

Fuel Cycle Research & Development

Prepared for
U.S. Department of Energy
Used Fuel Disposition Campaign
Paul McConnell, Robert Wauneka,
Sylvia Saltzstein, Ken Sorenson
Sandia National Laboratories
August 29, 2014
SAND2014-20495
FCRD-UFD-2014-000066,
Revision 0.1 (December 15, 2014)

Sandia National Laboratories is a multi-program laboratory managed and operated by Sandia Corporation, a wholly owned subsidiary of Lockheed Martin Corporation, for the U.S. Department of Energy's National Nuclear Security Administration under contract DE-AC04-94AL85000.

Revision 2
12/20/2012

APPENDIX E
FCT DOCUMENT COVER SHEET [1]

Name/Title of Deliverable/Milestone/Revision No.	Normal Conditions of Transport Truck Test of a Surrogate Fuel Assembly
Work Package Title and Number	Transportation – SNL FT-14SN081304
Work Package WBS Number	1.02.08.13
Responsible Work Package Manager	Paul McConnell (Name/Signature)
Date Submitted	8/29/14

Quality Rigor Level for Deliverable/Milestone[2]	☐ QRL-3	☒ QRL-2	☐ QRL-1 Nuclear Data	☐ Lab/Participant QA Program (no additional FCT QA requirements)

This deliverable was prepared in accordance with Sandia National Laboratories
(Participant/National Laboratory Name)

QA program which meets the requirements of

☒ DOE Order 414.1 ☐ NQA-1-2000 ☐ Other

This Deliverable was subjected to:

☐ Technical Review ☒ Peer Review

Technical Review (TR)
Review Documentation Provided

☐ Signed TR Report or,
☐ Signed TR Concurrence Sheet or,
☐ Signature of TR Reviewer(s) below

Peer Review (PR)
Review Documentation Provided

☐ Signed PR Report or,
☐ Signed PR Concurrence Sheet or,
☒ Signature of PR Reviewer(s) below

Name and Signature of Reviewers

ELENA Kalinina

NOTE 1: *Appendix E should be filled out and submitted with the deliverable. Or, if the PICS:NE system permits, completely enter all applicable information in the PICS:NE Deliverable Form. The requirement is to ensure that all applicable information is entered either in the PICS:NE system or by using the FCT Document Cover Sheet.*

NOTE 2: *In some cases there may be a milestone where an item is being fabricated, maintenance is being performed on a facility, or a document is being issued through a formal document control process where it specifically calls out a formal review of the document. In these cases, documentation (e.g., inspection report, maintenance request, work planning package documentation or the documented review of the issued document through the document control process) of the completion of the activity, along with the Document Cover Sheet, is sufficient to demonstrate achieving the milestone. If QRL 1, 2, or 3 is not assigned, then the Lab / Participant QA Program (no additional FCT QA requirements) box must be checked, and the work is understood to be performed and any deliverable developed in conformance with the respective National Laboratory / Participant, DOE or NNSA-approved QA Program.*

SUMMARY

This report describes a test of an instrumented surrogate PWR fuel assembly on a truck trailer conducted to simulate normal conditions of truck transport.

The purpose of the test was to measure strains and accelerations on a Zircaloy-4 fuel rod during the transport of the assembly on the truck. This test complements tests conducted in FY13 in which the same assembly was placed on a shaker and subjected to vertical vibrations and shocks simulating truck transport. The results of those tests are in the report "FUEL ASSEMBLY SHAKER TEST for Determining Loads on a PWR Assembly under Surrogate Normal Conditions of Transport" McConnell, et al., SAND2013-5210P, Rev. 0.1, FCRD-UFD-2013-000190, June 30, 2013 (revised December 1, 2013). This report constitutes the Milestone M2FT-14SN0813041 for the DOE/NE Fuel Cycle Research and Development Used Fuel Disposition Campaign ST Transportation Work Package FT-14SN081304 (Rev. 1).

The strains measured on the instrumented Zircaloy-4 rod over a 40.2 mile route in the Albuquerque area over a variety of road conditions – rough dirt to Interstate highway (Figure S.1) – never exceeded 150 μin./in. – a very low level of strain well below the elastic limit/yield strength of Zircaloy-4, Figure S.1. The strains measured in the truck test were slightly lower than those measured in the shaker tests.

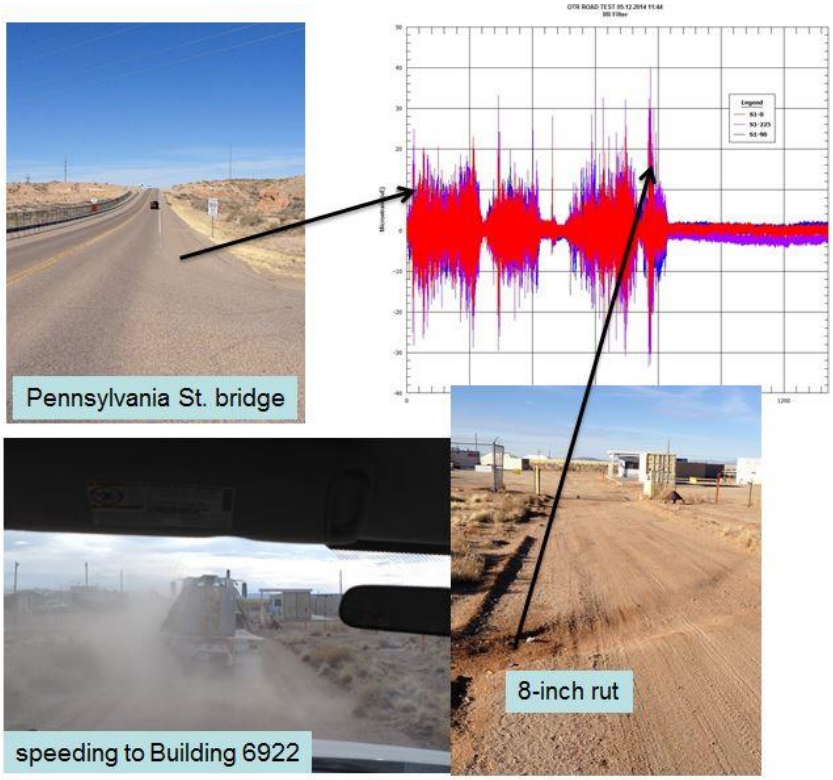

Figure S.1 Rod strains were measured over a 40.2 truck route of varying conditions.

The stresses corresponding to the maximum experimentally measured strains in both the truck test and the previous shaker tests are approximately 2 - 3 ksi (13.8 - 20.6 MPa) as shown in Figure S.2, which is a plot of the elastic portion of the stress-strain curves for unirradiated Zircaloy-4 and low-burnup and high-burnup irradiated Zircaloy-4. The figure also shows the maximum strain result from finite element analyses performed at Pacific Northwest National Laboratory. The figure indicates how low the magnitude of the strains and corresponding stresses were on the rod relative to the elastic limit of unirradiated and irradiated Zircaloy-4. The applied stresses on the rod were low relative to the yield strength of the Zircaloy-4.

The strains and corresponding stresses on the rod in the region of irradiated fuel pellet-pellet interaction could be up to three times higher than the nominal stresses and strains in a region displaced from the pellet-pellet interface. But a factor of three increase in the stress at a pellet-pellet interface based on the stains measured in the assembly tests would be only on the order of 6 – 9 ksi (41 – 62 MPa).

The results suggest that failure of the rods during NCT is unlikely due to a strain- or stress-based failure mechanism. The applied strains on the rods and the corresponding applied stresses may be too low relative to the strength of the cladding to cause failure in the absence of cracks. Further work is underway in other DOE programs to assess Zircaloy-4 performance based on inelastic, brittle fracture material property conditions.

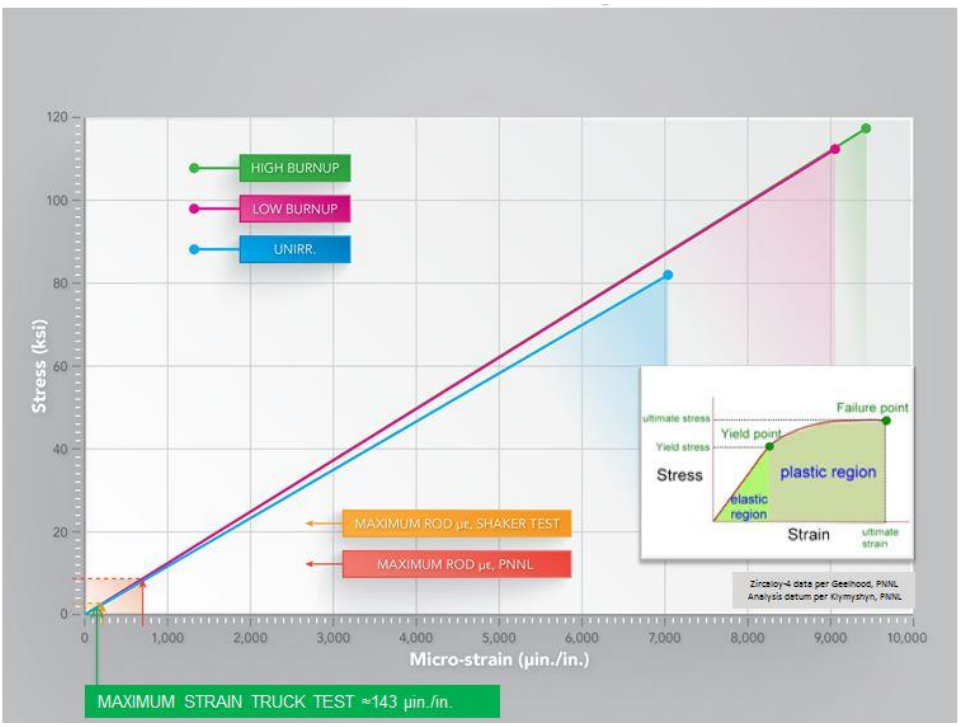

Figure S.2 Strains on Zircaloy-4 rod measured in truck and shaker tests relative to elastic limit / yield strength of Zircaloy-4 were very low.

CONTENTS

SUMMARY iv

CONTENTS vi

FIGURES viii

TABLES xi

1. INTRODUCTION 1-1

2. PURPOSE 2-1
   2.1 Range of Potential Assembly Tests and Application of Data Collected 2-1

3. TEST CONFIGURATION 3-1
   3.1 Test Unit: Assembly / Basket 3-1
      3.1.1 Selection of rods for tests 3-1
      3.1.2 Assembly brackets 3-2
   3.2 Instrumentation 3-3
   3.3 Data Acquisition 3-12
   3.4 TRACTOR/TRAILER 3-14
      3.4.1 Concrete Blocks: Surrogate Cask Mass 3-17

4. TEST ROUTE / ROAD SEGMENTS 4-1

5. TEST DATA / RESULTS 5-1
   5.1 Tabulated Test Results 5-2
   5.2 Correlation of Road Condition with Measured Strain 5-9
   5.3 Visual Examination of the Assembly 5-11
   5.4 Strains Measured in Truck and Shaker Tests Relative to Elastic Limit of Zircaloy-4 5-13
   5.5 Comparison of Truck and Shaker Test Results 5-1
   5.6 Fracture Toughness and Fatigue Assessment 5-2
      5.6.1 Fracture Mechanics Analysis Based on Stresses from Test Data and Analyses 5-2
      5.6.2 Fatigue assessment 5-4

6. FUTURE ASSEMBLY TESTS AND MODELING 6-1
   6.1 Constraints and Compromises to an Ideal Test of an Assembly 6-5

7. CONCLUSION 7-1

8. PLOTS OF STRAIN AND ACCELERATION TIME-HISTORIES AND FAST FOURIER TRANSFORMATIONS FOR ALL FIVE TRUCK ROUTE SEGMENTS 8-1
   8.1 Truck Route Segment 1 Data Plots 8-1
      8.1.1 Strain Gauge Time-Histories (με versus time) 8-2
      8.1.2 Strain Gauge Fast Fourier Transformations (με/Hz versus Hz) 8-7

8.1.3 Accelerometer Time-Histories (g versus time) 8-11
8.1.4 Accelerometer Fast Fourier Transformations (g/Hz versus Hz) 8-13
8.2 Truck Route Segment 2 Data Plots 8-16
8.2.1 Strain Gauge Time-Histories (με versus time) 8-17
8.2.2 Strain Gauge Fast Fourier Transformations (με/Hz versus Hz) 8-22
8.2.3 Accelerometer Time-Histories (g versus time) 8-26
8.2.4 Accelerometer Fast Fourier Transformations (g/Hz versus Hz) 8-29
8.3 Truck Route Segment 3 Data Plots 8-32
8.3.1 Strain Gauge Time-Histories (με versus time) 8-33
8.3.2 Strain Gauge Fast Fourier Transformations (με/Hz versus Hz) 8-38
8.3.3 Accelerometer Time-Histories (g versus time) 8-42
8.3.4 Accelerometer Fast Fourier Transformations (g/Hz versus Hz) 8-45
8.4 Truck Route Segment 4 Data Plots 8-48
8.4.1 Strain Gauge Time-Histories (με versus time) 8-49
8.4.2 Strain Gauge Fast Fourier Transformations (με/Hz versus Hz) 8-54
8.4.3 Accelerometer Time-Histories (g versus time) 8-59
8.4.4 Accelerometer Fast Fourier Transformations (g/Hz versus Hz) 8-62
8.5 Truck Route Segment 5 Data Plots 8-65
8.5.1 Strain Gauge Time-Histories (με versus time) 8-66
8.5.2 Strain Gauge Fast Fourier Transformations (με/Hz versus Hz) 8-71
8.5.3 Accelerometer Time-Histories (g versus time) 8-75
8.5.4 Accelerometer Fast Fourier Transformations (g/Hz versus Hz) 8-78

FIGURES

Figure S.1 Rod strains were measured over a 40.2 truck route of varying conditions. iv

Figure S.2 Strains on Zircaloy-4 rod measured in truck and shaker tests relative to elastic limit / yield strength of Zircaloy-4 were very low. v

Figure 3.1 Technical data used to select copper tubes as surrogate tubes based on Zircaloy-4 tube dimensions. 3-2

Figure 3.2 Schematic of brackets used to limit possible longitudinal motion of assembly within basket. 3-2

Figure 3.3 The red arrows point to some of the copper rods that moved longitudinally within the assembly during the truck test. 3-3

Figure 3.4 Instrumentation on assembly (see Table 3.1). Basket not shown. 3-7

Figure 3.5 Basket / assembly test unit 3-8

Figure 3.6 Assembly in basket with top plate of basket removed (side plates are visible). This figure shows two Zircaloy-4 rods (center and right edge). Only the center Zircaloy-4 rod was used for the truck test. 3-8

Figure 3.7 Instrumentation. Top: uniaxial accelerometer A1 on spacer grid and strain gauge S1 - 0°; bottom: instrumentation on Span 10. 3-9

Figure 3.8 Location of triaxial accelerometer on top of basket. 3-10

Figure 3.9 Triaxial accelerometer below trailer drop deck above rear axle (see Figures 3.11 and 3.13 and Table 3.1). 3-11

Figure 3.10 Copper tube containing a lead rod used as a surrogate Zircaloy/UO_2 rod. Copper rods were not instrumented – only the Zircaloy-4 rod, but all rods contained lead. 3-12

Figure 3.11 Strain gauge bridge completion modules in shielded box, right. Enlarged view on left. 3-13

Figure 3.12 Tractor/trailer with concrete blocks and test unit on top of blocks, top; bottom, brackets on bottom of basket bolted to concrete blocks 3-15

Figure 3.13 Trailer rear spring suspension 3-16

Figure 3.14 Location of triaxial accelerometer below trailer drop deck near trailer rear axle. 3-17

Figure 3.15 Concrete blocks simulating the mass of a truck cask were secured to the trailer. The basket was bolted to the blocks (Figure 3.16). 3-18

Figure 3.16 The basket containing the assembly was bolted to the concrete blocks. Only the assembly had freedom of motion relative to the trailer. The concrete blocks/basket approximated a rigid body. The assembly was free to move within the basket. 3-19

Figure 4.1 Truck route Segments 2, 3, and 4 within the City of Albuquerque. (Segments 1 and 5 were on Kirtland Air Force Base.) 4-3

Figure 4.2 Sandia Area III route Segments 1 and 5 on Kirtland Air Force Base. 4-4

Figure 4.3 Poleline Road, Segment 2, Kirtland Air Force Base. 4-5

Figure 4.4 Pennsylvania Street to Area III, Segment 5. 4-6

Figure 4.5 End of Segment 5, Area III. 4-7

Figure 4.6 Dip on Area III road approaching Pennsylvania St., Segment 1 (going north near beginning of truck route) and Segment 5 (going south near end of test).....4-8

Figure 4.7 Poleline Road looking north, Segment 1. The paved surface near top is a brief section of this dirt road. The highest strains measured on the instrumented rod were on the dirt section just north of the paved section (Figure 4.8).....4-9

Figure 4.8 Poleline Road approaching Eubank Contractors' Gate, Segment 1. This potholed, dirt/gravel portion of the truck route resulted in the highest measured rod strains. 4-10

Figure 4.9 "Big I" transition from I-40W to I-25S, Segment 2 4-11

Figure 4.10 Railroad track crossings on Broadway Blvd. SE, Segment 3. There were two railroad track crossings on Segment 3. 4-12

Figure 4.11 Area III road (rough asphalt), Segments 1 and 5.....4-12

Figure 4.12 Gibson Blvd. (east) concrete plate road surface, Segment 4. Relatively high strains were measured on Gibson Blvd.....4-13

Figure 4.13 Access to Building 6922, Area III, and end of Segment 5. 4-14

Figure 4.14 Dirt road into Building 6922 (southwest, top, and northeast, bottom), Area III, end of Segment 5. The trough shown is over 8 inches deep. The truck traveled directly over the deepest portion of the trough. 4-15

Figure 5.1 Correlation of measured strains on rod to road conditions. Top left is the strain versus time for the S1 strain gauges for truck route Segment 1, top right is the strain versus time for Segment 4 (y-axis is 80 με in both plots ; Figures 8.1 and 8.13). The bottom set of figures are for Segment 5 (y-axis is 50 με; Figure 8.17). Refer to Tables 3.1 and 4.1. Gibson Blvd. has a series of concrete plates separated by gaps which apparently caused peaks in rod strain (Figure 4.12).....5-10

Figure 5.2 Basket cutout, bottom, showing side view of assembly for GoPro® video, top. 5-11

Figure 5.3 Screen capture of GoPro® .MP4 video file. There was no observed motion of the assembly relative to the inside of the top basket plate or the copper rods relative to one another or relative to the spacer grid in the 4 minute 23 second video (240 frames/second). There was occasionally motion observed between the top edge of the top basket plate relative to the clouds in the sky (note bluish-gray patch in top left corner of figure). The perceived curvature is an artifact of the wide angle view of the video. 5-12

Figure 5.4 Strains on rod measured in truck and shaker tests relative to elastic limit/yield strength of Zircaloy-4. 5-14

Figure 5.5 Stress amplitude based upon maximum strain measured in shaker tests relative to irradiated Zircaloy-4 fatigue curve. 5-4

Figure 8.1 Segment 1 strain gauge time-histories.....8-6

Figure 8.2 Segment 1 strain gauge FFTs 8-10

Figure 8.3 Segment 1 accelerometer time-histories.....8-12

Figure 8.4 Segment 1 accelerometer FFTs 8-15

Figure 8.5 Segment 2 strain gauge time-histories.....8-21

Figure 8.6 Segment 2 strain gauge FFTs 8-25

Figure 8.7 Segment 2 accelerometers time-histories 8-28
Figure 8.8 Segment 2 accelerometer FFTs 8-31
Figure 8.9 Segment 3 strain gauge time-histories 8-37
Figure 8.10 Segment 3 strain gauge FFTs 8-41
Figure 8.11 Segment 3 accelerometer time-histories 8-44
Figure 8.12 Segment 3 accelerometer FFTs 8-47
Figure 8.13 Segment 4 strain gauge time-histories 8-53
Figure 8.14 Segment 4 strain gauge FFTs 8-58
Figure 8.15 Segment 4 accelerometer time-histories 8-61
Figure 8.16 Segment 4 accelerometer FFTs 8-64
Figure 8.17 Segment 5 strain gauge time-histories 8-70
Figure 8.18 Segment 5 strain gauge FFTs 8-74
Figure 8.19 Segment 5 accelerometer time-histories 8-77
Figure 8.20 Segment 5 accelerometer FFTs 8-80

TABLES

Table 3.1 Instrumentation on top-center Zircaloy-4 rod in assembly for truck test....3-5
Table 4.1 Truck test route segments....4-1
Table 5.1 Strain gauge maximum values for truck test....5-2
Table 5.2 Maximum strains route Segment 1....5-3
Table 5.3 Maximum strains route Segment 2....5-3
Table 5.4 Maximum strains route Segment 3....5-4
Table 5.5 Maximum strains route Segment 4....5-4
Table 5.6 Maximum strains route Segment 5....5-5
Table 5.7 Maximum vertical rod accelerations all route segments....5-5
Table 5.8 Maximum vertical rod accelerations route Segment 1....5-5
Table 5.9 Maximum vertical rod accelerations route Segment 2....5-6
Table 5.10 Maximum vertical rod accelerations route Segment 3....5-6
Table 5.11 Maximum vertical rod accelerations route Segment 4....5-6
Table 5.12 Maximum vertical rod accelerations route Segment 5....5-7
Table 5.13 Triaxial maximum accelerations all route segments....5-7
Table 5.14 Triaxial maximum accelerations route Segment 1....5-7
Table 5.16 Triaxial maximum accelerations route Segment 3....5-8
Table 5.17 Triaxial maximum accelerations route Segment 4....5-8
Table 5.18 Triaxial maximum accelerations route Segment 5....5-8
Table 5.19 Comparison of acceleration at location and time of maximum measured strain during truck test....5-9
Table 5.20 Comparison of maximum strains measured on Zircaloy-4 rods in truck and shaker tests....5-1
Table 5.21 Estimated applied stress intensities at the tip of circumferential flaws in the cladding of a fuel rod subjected to stresses experimentally measured....5-3
Table 6.1 Potential assembly testing....6-2
Table 6.2 Constraints and compromises to an ideal test of an assembly....6-5

ACKNOWLEDGEMENTS

The authors thank Ned Larson and John Orchard of DOE/LV for their support and advice for the fuel assembly tests.

Technical support for the assembly tests was invaluable. The authors thank Doug Ammerman, John Bignell, Bill Uncapher and Carissa Grey (B&D Consulting Inc.), Melissa C de Baca, Jerry Cap, Rafael Sanchez, Greg Koenig, and Gregg Flores.

Formal technical review of the report was provided by Elena Kalinina.

NORMAL CONDITIONS OF TRANSPORT TRUCK TEST OF A SURROGATE FUEL ASSEMBLY

1. INTRODUCTION

This report describes a truck test of a surrogate fuel assembly. The purpose of the test was primarily to measure strains on a fuel rod when the assembly was subjected to normal conditions of [truck] transport. The assembly was an actual [unirradiated] 17 X 17 PWR assembly. The assembly was populated with copper rods filled with lead "rope" except for one rod which was Zircaloy-4 filled with lead rope. The external surface of the Zircaloy-4 rod was instrumented with strain gauges and accelerometers. Accelerometers were also placed on the assembly spacer grids. The instrumented assembly was placed within a surrogate PWR basket. The internal dimensions of the basket were the same as an actual truck cask PWR basket. The assembly/basket test unit was bolted to concrete blocks which simulated the mass of an actual truck cask. The concrete blocks were securely attached to a trailer. The trailer was driven over a 40.2-mile route with a range of road surface conditions. The data from the instrumentation was recorded by a data acquisition system during the road test and subsequently analyzed so that the strains and accelerations on the Zircaloy-4 rod could be obtained.

The impetus for this test is twofold: 1) Used nuclear fuel (UNF) will be dry stored for significant periods of time before disposal; aging of the fuel cladding may occur during storage which may embrittle the cladding. 2) Fuel will be subjected to higher burnups prior to storage which can cause embrittlement of the cladding. These two factors call into question the integrity of UNF cladding during normal conditions of transport should the stresses and strains applied to the fuel rods during transport exceed the yield strength of the Zircaloy-4 cladding. This test measured strains on the cladding during truck transport which can be compared with mechanical property data for aged, high burnup cladding. Should the strains be sufficiently low compared with the properties of the cladding, a technical basis may exist for the safe transport of high burnup UNF after extended storage.

Virtually all used nuclear fuel in the United States will be shipped by rail. There may be some fuel that will be shipped initially from storage facilities via barge or heavy-haul truck to a rail line. Truck tests rather than rail tests were nevertheless performed for two major reasons: 1) The logistics and cost of performing a truck test were more practicable than those for a rail test. And 2) the shocks and vibrations transmitted to a fuel assembly on a truck are more severe than those transmitted by rail so a truck test provides a conservative measure of strains imposed on fuel rods during rail transport[a].

[a] Refer to Figure 5.15 in Section 5.1.3 in "Used Nuclear Fuel Loading and Structural Performance Under Normal Conditions of Transport –Demonstration of Approach on Used Fuel Performance Characterization", Adkins, et al., FCRD-UFD-2013-000289, August 31, 2013.

2. PURPOSE

A truck test of a surrogate PWR assembly was performed to measure strains directly on a Zircaloy-4 rod in the assembly during normal conditions of transport. Other than a set of previously conducted shaker tests performed at Sandia National Laboratories[b] there is believed to be no direct measurement of strains on rods within an assembly when subjected to conditions of normal truck or rail transport. Knowledge of the loads applied to fuel rods during transport can be compared with material properties of unirradiated and irradiated Zircaloy and Zircaloy/UO_2 rods, including high burnup fuel rods, to assess the potential for failure of the Zircaloy cladding during normal conditions of transport.

Federal Regulations (10CFR71.71) require an assessment of "*Vibration* - Vibration normally incident to transport" imposed on transport packages and contents during "normal conditions of transport". The NRC has approved normal transport of low burnup UNF. However, there is need to establish a technical basis to demonstrate that high burnup fuel rods can withstand all conditions of normal transport after an extended period of dry storage.

Vibrations and shocks have been measured on truck trailers and railcars but not directly on fuel assemblies, baskets, or fuel rods. The margin of safety between the applied loads on fuel rods during transport and the material properties of Zircaloy rods has not been quantified.

The SNL assembly tests provide data – the applied stresses on the rods - related to the issue of the margin of safety:

$$\text{applied rod stress}_{\text{normal transport}}$$

Material property test programs at other national laboratories have been testing to generate data on the properties of high burnup cladding:

$$\text{yield strength}_{\text{cladding}}$$

For safe transport of UNF:

$$\text{applied rod stress}_{\text{normal transport}} << \text{yield strength}_{\text{cladding}}$$

The data from the assembly tests will also be used to validate finite element models of fuel assemblies. The validated models can be used to predict the loads on fuel rods for other basket configurations and transport environments, particularly rail.

2.1 Range of Potential Assembly Tests and Application of Data Collected

The ideal test to obtain strains on an actual irradiated fuel rod during normal conditions of transport would, of course, be a test of an irradiated assembly, preferably of high burnup, in which Zircaloy rods with UO_2 pellets – and pellet-clad interaction - are instrumented, placed within an actual basket within an actual cask mounted on a conveyance per the vendor's design and subjected to normal conditions of transport, either truck or rail, over a representative route. Such a test is unlikely primarily because of the radiological hazards and logistical difficulties inherent to instrumenting an irradiated rod in such a test configuration.

---

[b] FUEL ASSEMBLY SHAKER TEST for Determining Loads on a PWR Assembly under Surrogate Normal Conditions of Transport" McConnell, et al., SAND2013-5210P, Rev. 0.1, FCRD-UFD-2013-000190, June 30, 2013 (revised December 1, 2013). The shaker test report complements the current report and has additional background information relative to the loads imposed on fuel rods during NCT.

Compromises must therefore be made by collecting data from tests of unirradiated assemblies.

Tests using unirradiated assemblies and rods nevertheless generate data which can be useful for approximating the expected behavior of irradiated fuel rods. The compromises and constraints to testing of a fuel assembly are discussed in detail in Section 6.

Among the compromises made for the truck and shaker tests is the rod configuration. The unirradiated Zircaloy-4 tubes were filled with lead rods ("rope") to simulate the mass of UO_2. There was a gap (0.016 in. [0.41 mm]) between the outer surface of the lead and the inner diameter of the Zircaloy[c] - there were neither pellets nor pellet-clad interaction. In addition, the properties of the Zircaloy-4/lead configuration differ from those of irradiated Zircaloy-4/UO_2. The stiffness of the rod is particularly important in terms of the deflection of the rod resulting from transport vibrations and shocks. In terms of the stiffness due to UO_2 pellet-Zircaloy clad interaction, the rod configuration used for these tests with the gap between the lead and the Zircaloy should have a lower stiffness than irradiated Zircaloy/UO_2 and hence a greater displacement and strain when subjected to external loads than if the test rods had pellet-clad interaction. Hence, the strains measured in the shaker and truck tests may be greater than an actual irradiated rod may experience. Another compromise made for the tests is that the assembly was not within an actual cask during the tests although it was within a basket which had the exact weight and length and internal dimensions of an actual NAC-LWT single PWR assembly basket. The basket was bolted to concrete blocks that were within 86% the weight of a fully loaded NAC-LWT truck cask (43920 lbs versus 51200 lbs).

[c] See Figure 3.10.

3. TEST CONFIGURATION

The truck test of the assembly was conducted by placing the instrumented assembly within the basket. The basket was bolted to two concrete blocks which were securely strapped to a trailer. The trailer was then driven over a 40.2-mile route in the Albuquerque area over a variety of road surfaces.

3.1 Test Unit: Assembly / Basket

The assembly used for the truck tests was a surrogate 17 x 17 PWR assembly. This was the same assembly that was used for previous shaker tests. The assembly was populated mostly with copper tubes which were filled with a continuous rod of lead. For the truck test there was one Zircaloy-4 rod placed on the top-center location of the assembly. This Zircaloy-4 tube also contained lead[d].

Figure 3.1 provides the material property data evaluated in selecting the copper/lead surrogate rod for the shaker tests[e]. A SOLIDWORKS™ simulation predicted a bending response difference of less than 5% between the copper-lead rod and Zircaloy-lead rods.

3.1.1 Selection of rods for tests

The combined Modulus/Moment of Inertia properties was checked to assess the combined stiffness of each rod:

- EI_{Cu} = 8.71 K-in^2
- EI_{Zirc} = 5.53 K-in^2.

The conclusion is that copper tubing is slightly stiffer than Zircaloy.

Although the material surrogates do not mimic the true material properties exactly, they are the best as far as availability, constructability, and cost. UO_2 and lead share very similar densities but UO_2 is considerably stiffer than lead. Zircaloy is 30% less dense than copper but Zircaloy has stiffness similar to copper. An actual assembly weighs approximately 1,404 lbs. (637 kg). The experimental assembly weighed approximately 1,446 lbs. (656 kg). The difference in weight between the actual and experimental assemblies is 42 lbs. (19 kg – a 3% difference). Although the stiffness of actual and the experimental surrogate rods were not the same (mostly due to properties of the UO_2 *v*. lead), the weights of the two rods were nearly exact - *weight is considered the most important parameter to simulate*. Thus, dynamic response of the test assembly is expected to closely represent that of a real fuel assembly.

---

[d] Three Zircaloy-4 rods were used for the shaker tests located at the top-center, top-side, and bottom-side positions within the assembly. Shaker test results indicated little difference in the strains measured on the three Zircaloy rods so only one Zircaloy rod was instrumented for the truck test.

[e] Taken from "FUEL ASSEMBLY SHAKER TEST for Determining Loads on a PWR Assembly under Surrogate Normal Conditions of Transport" McConnell, et al., SAND2013-5210P, Rev. 0.1, FCRD-UFD-2013-000190, June 30, 2013 (revised December 1, 2013).

Zirc and Surrogate Material Properties (Based on equivalent thickness and variable EI)									
Zirc		Aluminum		Brass		Carbon Steel		Copper	
E_{zirc} (GPa)	99	E_{Al} (GPa)	70	E_{Brass} (GPa)	110	E_{SS} (GPa)	205	E_{Cu} (GPa)	115
E_{zirc} (ksi)	14359	E_{Al} (ksi)	10153	E_{Brass} (ksi)	15954	E_{SS} (ksi)	29733	E_{Cu} (ksi)	16679
ρ_{zirc} (g/cm^3)	6.55	ρ_{Al} (g/cm^3)	2.7	ρ_{Brass} (g/cm^3)	8.5	ρ_{SS} (g/cm^3)	7.85	ρ_{Cu} (g/cm^3)	8.94
ρ_{zirc} (g/in^3)	107	ρ_{Al} (g/in^3)	44	ρ_{Brass} (g/in^3)	139	ρ_{SS} (g/in^3)	129	ρ_{Cu} (g/in^3)	147
h (in)	151.79	h (in)	144	h (in)	151.79	h (in)	151.79	h (in)	151.79
Vol_{zirc} (in3)	3.77	Vol_{Al} (in3)	5.38	Vol_{Brass} (in3)	5.67	Vol_{SS} (in3)	5.67	Vol_{Cu} (in3)	5.67
Mass (g)	404.80	Mass (g)	238.19	Mass (g)	790.42	Mass (g)	729.98	Mass (g)	831.34
t (in)	0.0225	t (in)	0.03500	t (in)	0.03500	t (in)	0.03500	t (in)	0.03500
D_{zirc} (in)	0.374	D_{Al} (in)	0.375	D_{Brass} (in)	0.375	D_{SS} (in)	0.375	D_{Cu} (in)	0.375
d_{zirc} (in)	0.329	d_{Al} (in)	0.305	d_{Brass} (in)	0.305	d_{SS} (in)	0.305	d_{Cu} (in)	0.305
EI (k*in2)	5.532	EI (k*in2)	5.543	EI (k*in2)	8.710	EI (k*in2)	16.232	EI (k*in2)	8.710
Zirc Rod (lbs)	0.891	Al Rod (lbs)	0.525	Brass Rod (lbs)	1.739	CS Rod (lbs)	1.606	Cu Rod (lbs)	1.829

Moment of Inertia = I $\frac{\pi(D^4 - d^4)}{64}$

Figure 3.1 Technical data used to select copper tubes as surrogate tubes based on Zircaloy-4 tube dimensions.

3.1.2 Assembly brackets

In order to ensure that the assembly would not slide forward nor backward out of the basket during the truck test, especially should a hard brake be required during transport, a set of brackets were placed at either end of the basket. These brackets had a lip that was configured below the top plate of the basket that would allow the assembly to slide only 1.25 inch, Figure 3.2.

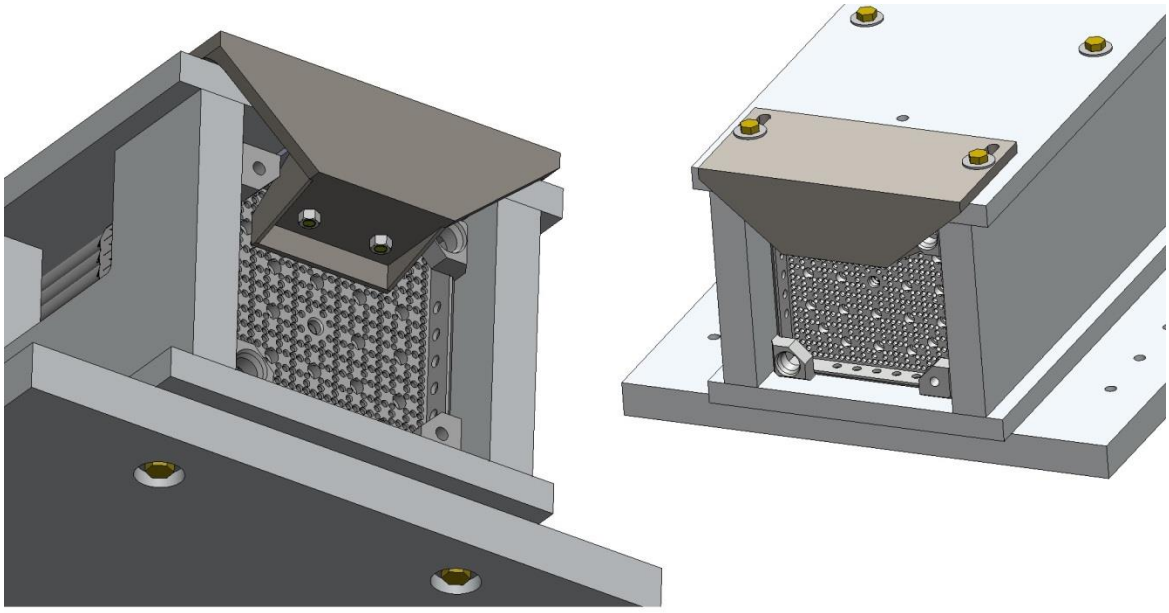

Figure 3.2 Schematic of brackets used to limit possible longitudinal motion of assembly within basket.

Prior to the truck test, a dab of silicone was placed on the edge of these brackets which would contact the assembly if it happened to slide beyond approximately 0.25 inch. Post-test examination revealed that the assembly had not contacted the silicone. It was noted, however, that some of the copper rods within the assembly moved longitudinally during the truck test. Visual examination suggested that the magnitude of this longitudinal motion was less than 0.25 inch (Figure 3.3).

Figure 3.3 The red arrows point to some of the copper rods that moved longitudinally within the assembly during the truck test.

3.2 Instrumentation

The assembly was populated with copper/lead rods with the exception of a Zircaloy-4/lead rod at the top-center of the assembly. This rod was instrumented with strain gauges and uniaxial accelerometers (vertical [Z] direction).

The strain gauges were placed in four axial (longitudinal [X]) locations on the Zircaloy-4 rod. At each axial location three strain gauges were placed circumferentially around the rod at 0° (top), 90°, and 225°. This was done in order to assess strains imposed on the rod due to vertical, lateral, and longitudinal motion of the trailer during the test. There were a total of twelve strain gauges on the rod.

The uniaxial accelerometers were placed at various locations axially along the top of the rod – at the 0° position – and on spacer grids. (Only uniaxial accelerometers were used on the assembly because triaxial accelerometers are too large to be affixed to the rod.) The uniaxial accelerometers measured acceleration in the vertical direction.

A triaxial accelerometer was placed on the top of the basket near its mid-span and another was placed below the drop deck of the trainer just above the rear axle of the trailer.

Table 3.1 lists the instrumentation. Figure 3.4 shows the location of the strain gauges and accelerometers. Photographs of some of the instrumentation are in Figures 3.5 to 3.9.

Table 3.1 Instrumentation on top-center Zircaloy-4 rod in assembly for truck test.

Data Acquisition Channel	Instrument	Instrument ID	Test Nomenclature	Instrument Parameter	Location on Rod	Measured Position (in.)
	Vishay Micro-Measurements[f]			Gauge Factor		Measured from top edge of assembly top nozzle
1	Strain gauge	CEA-03-062UW-350	S1 - 0°	2.15 ± 0.5%	adj. first S.G., Span 10	8.6875
2	Strain gauge	CEA-03-062UW-350	S1 - 90°			9.3125
3	Strain gauge	CEA-03-062UW-350	S1 - 225°			8.6875
4	Strain gauge	CEA-03-062UW-350	S2 - 0°		mid-span, Span 10	17.25
5	Strain gauge	CEA-03-062UW-350	S2 - 90°			17.875
6	Strain gauge	CEA-03-062UW-350	S2- 225°			17.25
7	Strain gauge	CEA-03-062UW-350	S3 - 0°		adj. first S.G., Span 5	70.25
8	Strain gauge	CEA-03-062UW-350	S3 - 90°			70.875
9	Strain gauge	CEA-03-062UW-350	S13 - 225°			70.25
10	Strain gauge	CEA-03-062UW-350	S4 - 0°		Mid-span, Span 5	73.875
11	Strain gauge	CEA-03-062UW-350	S4 - 90°			74.5
12	Strain gauge	CEA-03-062UW-350	S4 - 225°			73.875

[f] Dave England, Vishay Micro-Measurements, personal communication 12/13/13: Resolution = ± 1 με (e.g., 100 με = 99 με - 101 με); accuracy/tolerance ≈± 0.5% (e.g., 100 με X ±0.005 = ±0.5 με). "Realistically at 1000 με, accuracy of 10 με or ± 5 με".

Data Acquisition Channel	Instrument	Instrument ID	Test Nomenclature	Instrument Parameter	Location on Rod	Measured Position (in.)
	Endevco Model/ Serial #			Sensitivity (mV/g)		
13	Uniaxial Accelerometer	2250A-10-R/ 17202	A1	9.83	on first S.G., Span 10	7.75
14	Uniaxial Accelerometer	2250A-10-R/ 16923	A2	10.21	mid-span, Span 10	16.625
15	Uniaxial Accelerometer	2250A-10-R/ 16920	A3	9.80	adj. second S.G., Span 10	26
16	Uniaxial Accelerometer	2250A-10-R/ 16918	A5	10.02	on first S.G, Span 5	69.375
17	Uniaxial Accelerometer	2250A-10-R/ 16916	A7	10.02	adj. second S.G., Span 5	77.625
18	Uniaxial Accelerometer	2250A-10-R/16825	A8	9.94	on second S.G., Span 5	78.375
	Endevco Model/ Serial #			Sensitivity (mV/g)		
19	Triaxial Accelerometer	65-10-R Isotron/ 12984	TA2-X	10.26	on top of basket above mid-span, Span 5	74.125
20			TA2-Y	10.14		
21			TA2-Z	10.17		
22	Triaxial Accelerometer	65-10-R Isotron/ 12987	TA5-X	10.24	below trailer drop-deck above rear axle	between rear two wheels
23			TA5-Y	10.15		
24			TA5-Z	10.15		

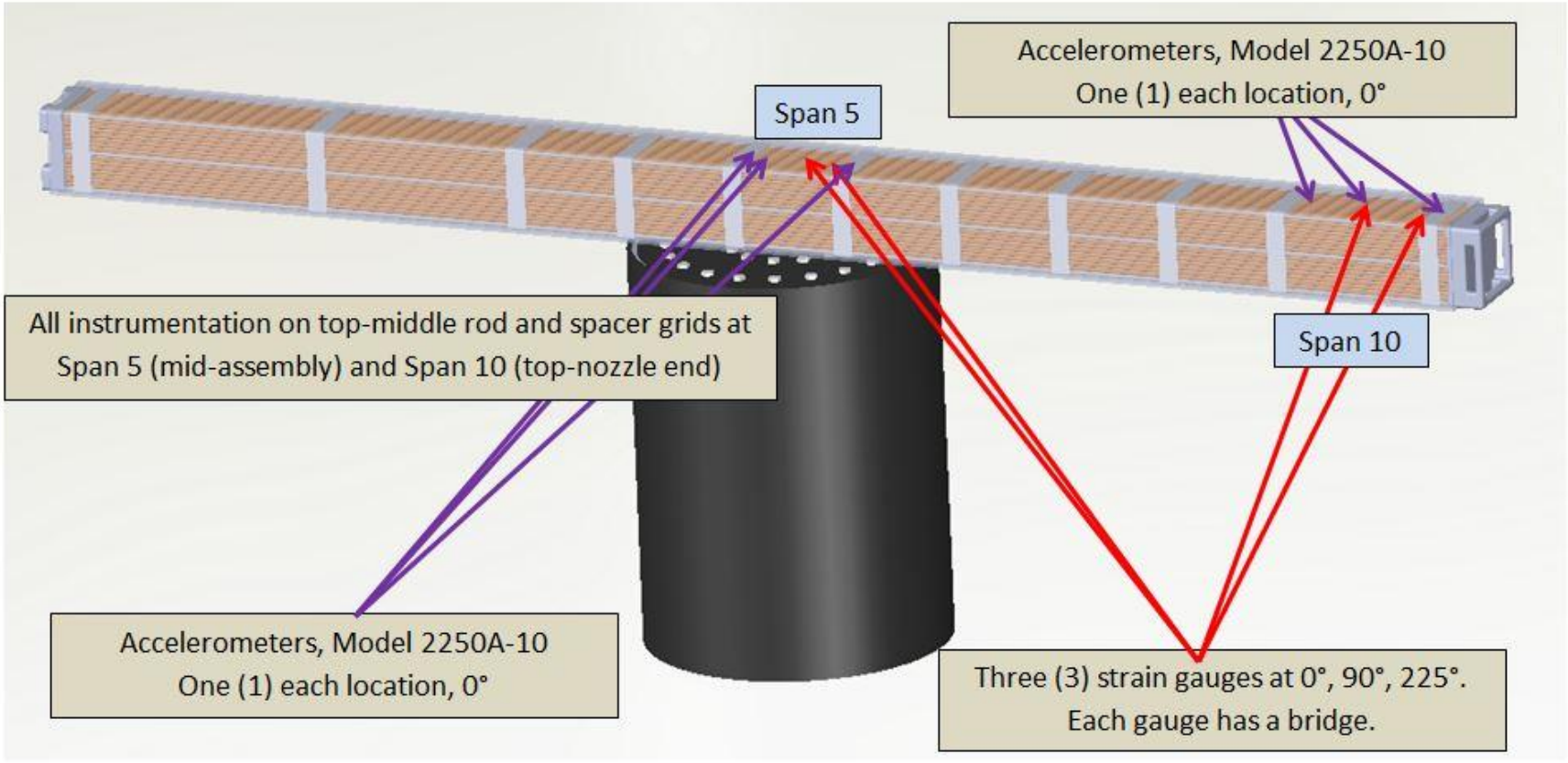

Strain gauges on top-middle Zircaloy-4 rod and accelerometers on top-middle Zircaloy-4 rod and Span 5 and Span 10 spacer grids for over-the-road truck test. Span 10 is the top nozzle end of the assembly. Triaxial accelerometers (2) shall be placed on the top of the basket at the mid-span and the rear axle.

Figure 3.4 Instrumentation on assembly (see Table 3.1). Basket not shown.

REPLACE THIS FIGURE WITH FIGURE FROM WAUNEKA OF 9/5/14

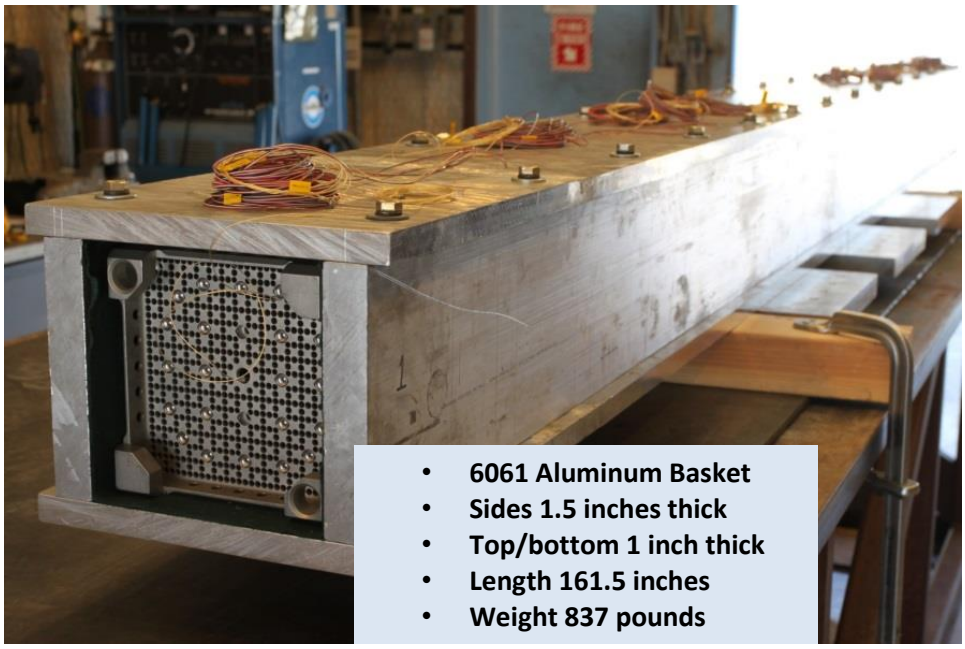

Figure 3.5 Basket / assembly test unit.

Figure 3.6 Assembly in basket with top plate of basket removed (side plates are visible). This figure shows two Zircaloy-4 rods (center and right edge). Only the center Zircaloy-4 rod was used for the truck test.

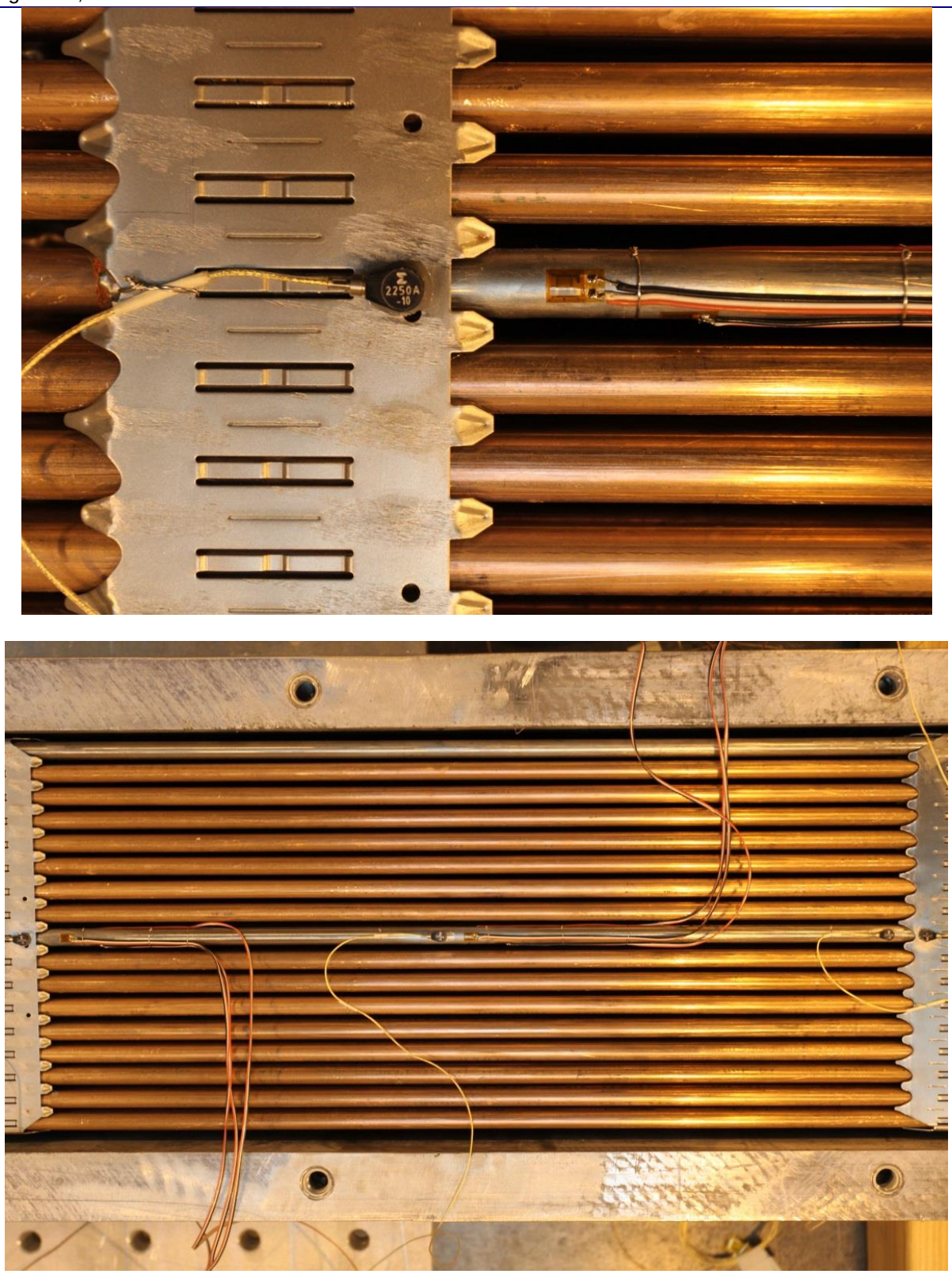

Figure 3.7 Instrumentation. Top: uniaxial accelerometer A1 on spacer grid and strain gauge S1 - 0°; bottom: instrumentation on Span 10.

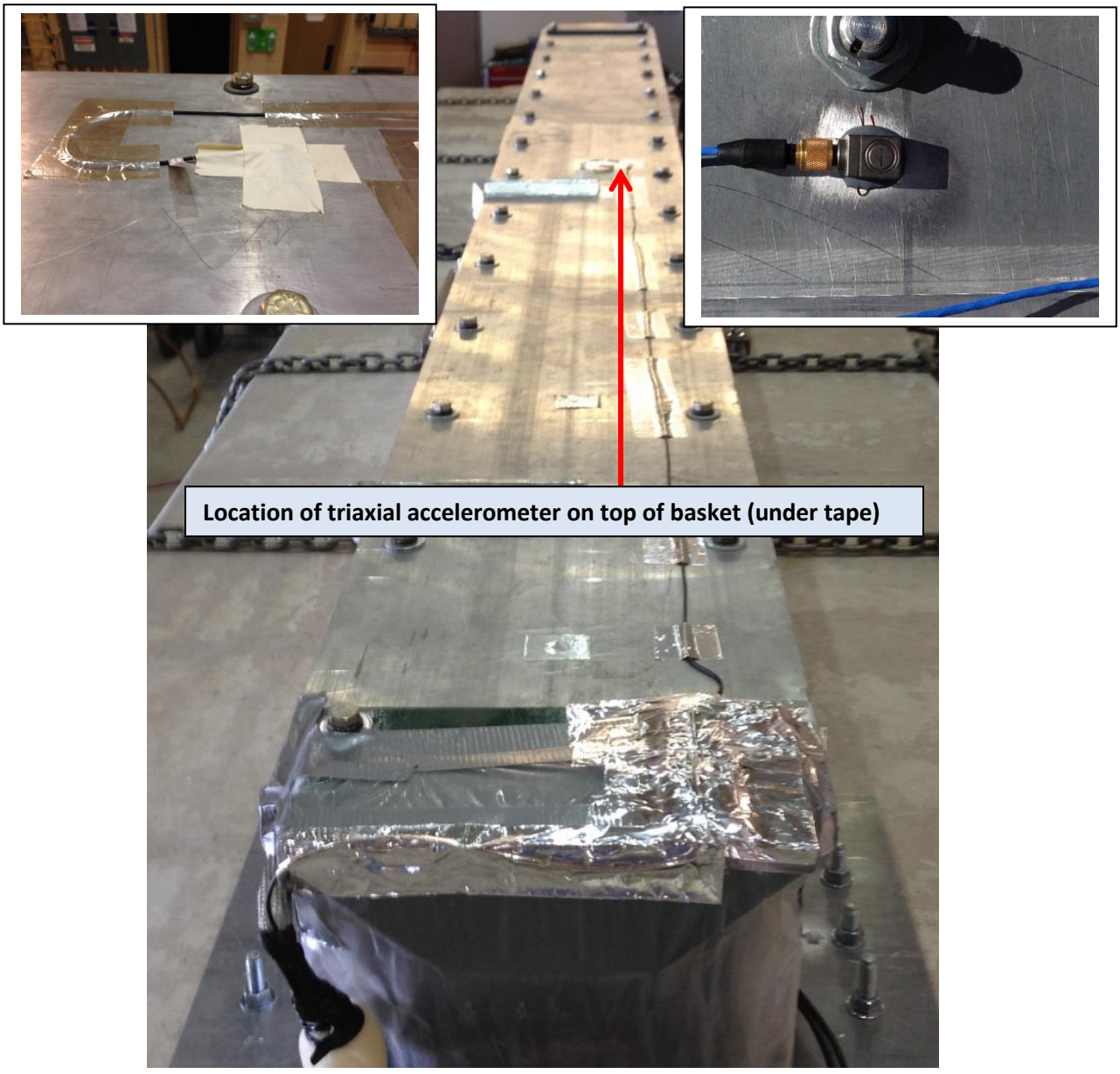

Figure 3.8 Location of triaxial accelerometer on top of basket.

Figure 3.9 Triaxial accelerometer below trailer drop deck above rear axle (see Figures 3.11 and 3.13 and Table 3.1).

Copper tube outer diameter (OD), in. (mm)	0.375 (9.525)
Copper tube inner diameter (ID), in. (mm)	0.312 (7.925)
Copper tube wall thickness, in. (mm)	0.0315 (0.8)
Radial Clearance between copper and lead, in. (mm)	0.016 (0.41)
Lead rod OD, in. (mm)	0.28 (7.11)[g]

Figure 3.10 Copper tube containing a lead rod used as a surrogate Zircaloy/UO_2 rod. Copper rods were not instrumented – only the Zircaloy-4 rod, but all rods contained lead.

3.3 Data Acquisition

The data acquisition system was linked to a Symmetricom XL-GPS global positioning system to mark the start and stop times of the data acquisition to within ±50µs (Coordinated Universal Time / Julian calendar).

All strain gauge instrumentation wires from the point of egress from the aluminum basket were shielded with aluminum tape which was affixed to the lip below the top side of the basket. At the end of the basket (towards the data acquisition system which was within the sleeper cab of the tractor) all wires were enclosed within a RFI (radio frequency interference)-shielded steel braid. The steel braid was wrapped in foam at certain locations to inhibit fretting of the braid.

The wires for the strain gauges went from the basket to a RFI-shielded metal box which contained Vishay Precision Group Micro-Measurements MR1-350-130 strain gauge bridge completion modules. From the bridge completion modules, MicroTek Corp., 4-conductor 30/73 55pc/.06 shielded white cable ran to a terminal strip (#6 screws). This cable had four wires and a steel braid

[g] Zircaloy-4 tubes have an O.D. of 0.379 in. (9.5 mm) and a wall (clad) thickness of 0.0225 in. (0.572 mm). UO_2 fuel pellets have a diameter of 0.322 in. (8.19 mm). The dimensions of the copper tube and lead were selected primarily so the weight of the copper/lead rods would closely match that of a Zircaloy-4/UO_2 rod.

for shielding. Each wire and the steel braid were attached to a terminal lug (NTE Electronics, Inc. electro tin-plated copper 76-15T22-06L PVC-insulated spade terminal 22-18 AWG for #6 screws).

From the terminal strip the strain gauges were connected to 3-pair foil-shielded twisted shielded pair (TSP) cable (Consolidated Electronic Wire & Cable #22 wire (7x30), to +80C; Part # BX06-63452) via spade lugs. The TSP cable is a special Sandia design.

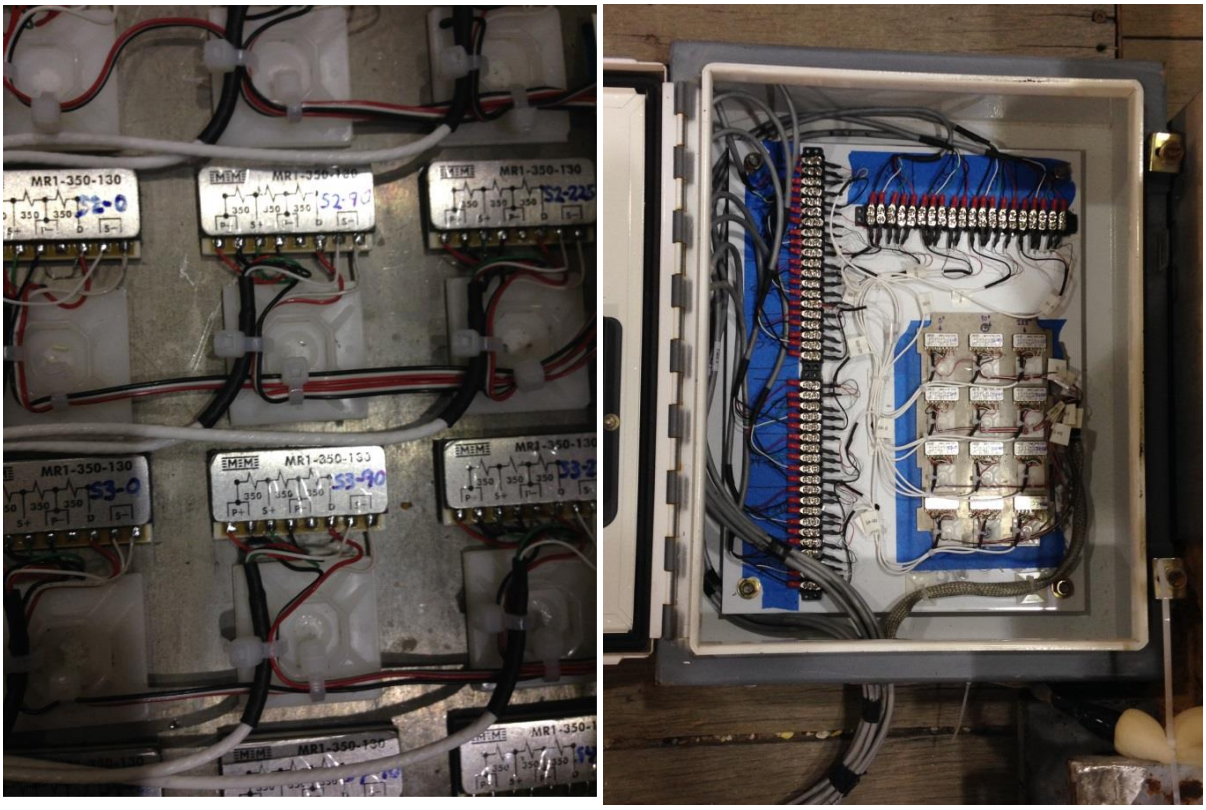

Figure 3.11 Strain gauge bridge completion modules in shielded box, right. Enlarged view on left.

GPS cable and power supply from the generator were separated from instrumentation cables: the GPS/power entered the tractor cab on curb-side (right), the instrumentation entered cab on street side (left).

Within the cab, the GPS antenna was connected to the GPS receiver. Generator power went through an APC BG1500 uninterrupted power supply (UPS) unit.

The Spectral Dynamics Inc. data acquisition system was under computer control using the Spectral Dynamics Impacs proprietary software. Four Spectral Dynamics VX2824B eight channel multi-mode signal conditioners were used.

Strain gauge and accelerometer cables were connected to the data collection system interface panel with Sub-D 15 pin connectors. Each channel of measurement data was terminated in a 15 pin connector.

Data were collected from the analog signal via 16-bit analog to digital converters (±5V). Data were stored on Spectral Dynamics internal memory, 16M samples per channel. The onboard data were transferred after each 22 minute 23 seconds of the truck route (five Segments) to the data collection computer for analysis. The computer converted the data into engineering units which were displayed on a monitor in real time using the Sandia K2 software.

The sample rate for the data acquisition was 12.5 kHz with a 5 kHz anti-aliasing filter. There were 24 channels/file (16MB per data channel). There was a 1 GB network connection.

The Consolidated 4449 RG58A/U stranded coaxial accelerometer cables lead to microdot-to-BNC adapters. The BNC end went to BNC barrels. The accelerometer cable was attached to the BNC barrel with a BNC connector. Electrical tape was wrapped over the adapter, barrel, and BNC connecter to maintain signal isolation.

The ICP accelerometers were connected to three PCB model 482C54 signal conditioner amplifiers each supporting 4 channels of accelerometer data. Each channel of the amplifiers was set to unity gain. The raw acceleration data was converted to analog voltages for recording. The data collection system amplified this signal in the amplifier section of the system before the signal was digitized.

The output of the amplifier was connected to the data collection system using RG58 cable terminated in BNC connector adapters to Sub D 15 Pin connectors at the data collection interface panel.

The raw data was converted to ASCII and plotted using the Sandia developed K2 analysis and plotting package. This analysis package uses algorithms developed by Sterns and Davis[h] and was specifically developed for processing data associated with radioactive and hazardous material package certification testing for DOE and the NRC. The processed data were downloaded and stored on a 1TB USB external hard drive.

3.4 TRACTOR/TRAILER

The assembly/basket test unit was transported via a tractor/trailer, Figure 3.12.

The tractor used for the truck test was a 52000-lb gross vehicle weight rating Peterbilt On-Highway Model 389 with a sleeper cab. The sleeper cab housed the data acquisition system.

The trailer used for the truck test was a 10660-lb KALYN King Goose RDP-70. This was a 35 foot long goose-neck trailer. The test unit was placed on the drop deck of the trailer. The drop deck section was 24-feet long. The raised deck was 11-feet long. The raised deck was 19 inches above the drop deck. The trailer width was 96 inches. The trailer decks were constructed with wood. This trailer had spring suspension. Figure 3.13 shows the spring suspension of the trailer at the rear axle location. The height from the top of the drop deck section of the trailer at the rear axle to the ground was 38.5 inches with no load on the trailer. The height was 36.5 inches when fully loaded for the test with the 43920 lbs of concrete blocks and the 2283 lb assembly/basket test unit.

[h] S. D. Stearns and R. A. Davis, *Signal Processing Algorithms in Matlab*, Prentice-Hall, 1996.

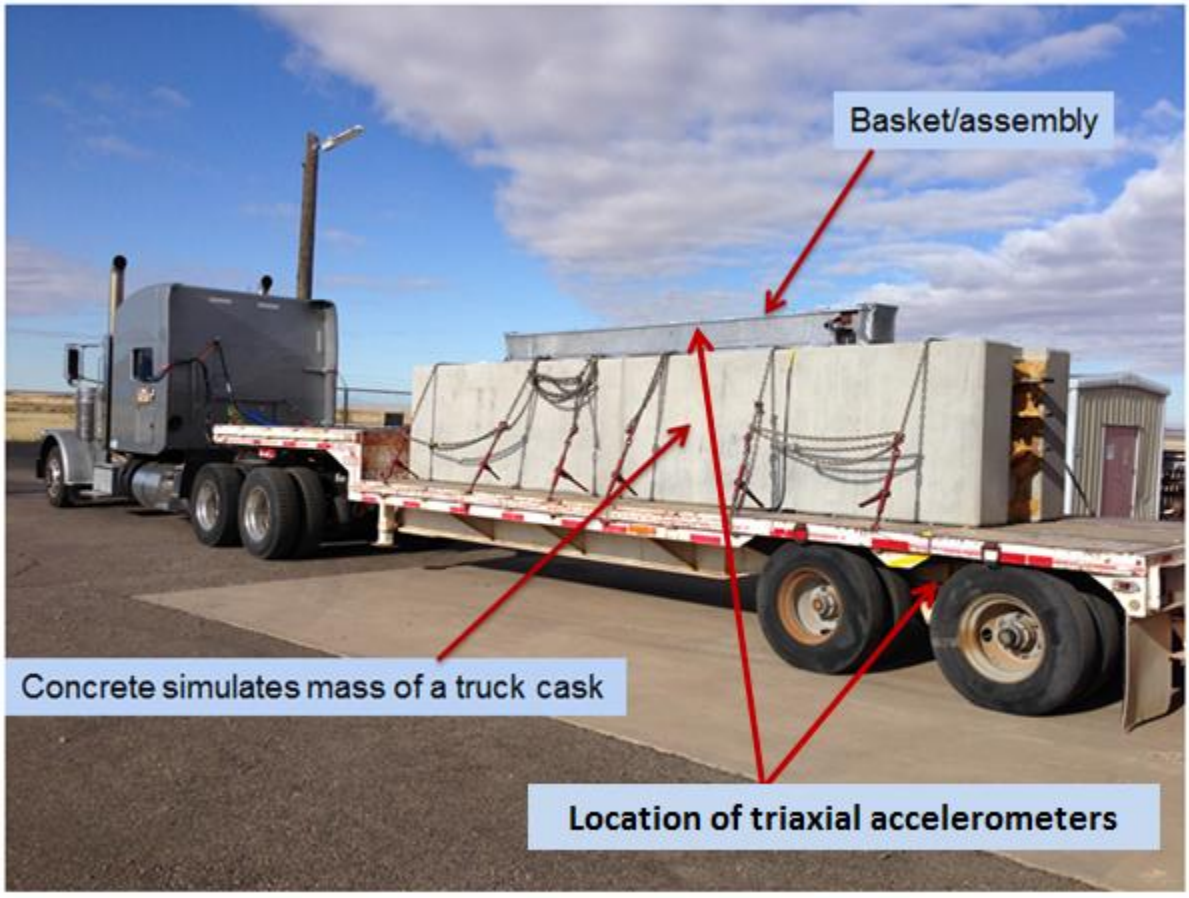

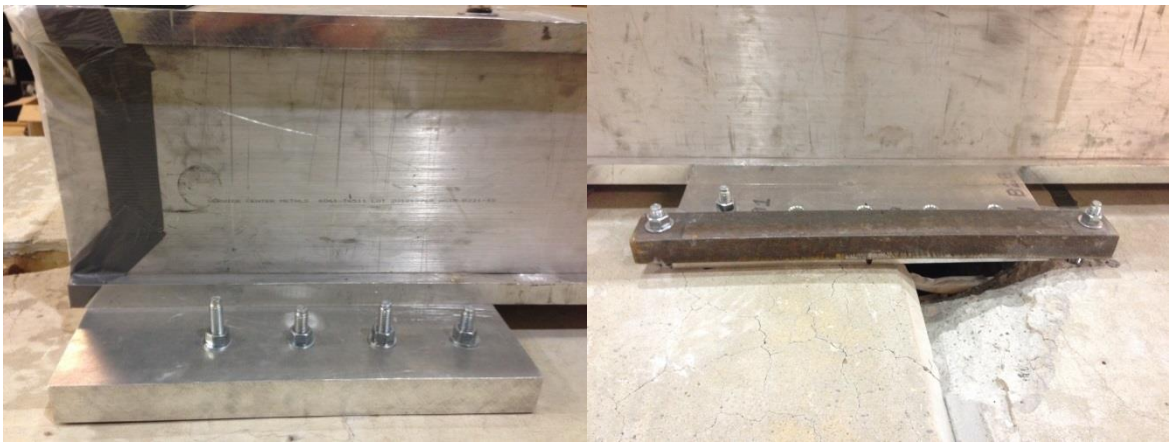

Figure 3.12 Tractor/trailer with concrete blocks and test unit on top of blocks, top; bottom, brackets on bottom of basket bolted to concrete blocks

Figure 3.13 Trailer rear spring suspension.

Figure 3.14 Location of triaxial accelerometer below trailer drop deck near trailer rear axle.

3.4.1 Concrete Blocks: Surrogate Cask Mass

Two concrete blocks were placed on the trailer to simulate the approximate mass of a truck cask. Each block was 10 feet long x 4 feet high x 4 feet wide. Each block weighed 21960 lb; the total weight of both blocks was 43920 lb[i]. These blocks were securely tied down to the trailer with cables. The assembly/basket test unit was bolted to the top of these blocks (Figure 3.12).

[i] The NAC-LWT truck cask weighs 51200 lb loaded with impact limiters.

Figure 3.15 Concrete blocks simulating the mass of a truck cask were secured to the trailer. The basket was bolted to the blocks (Figure 3.16).

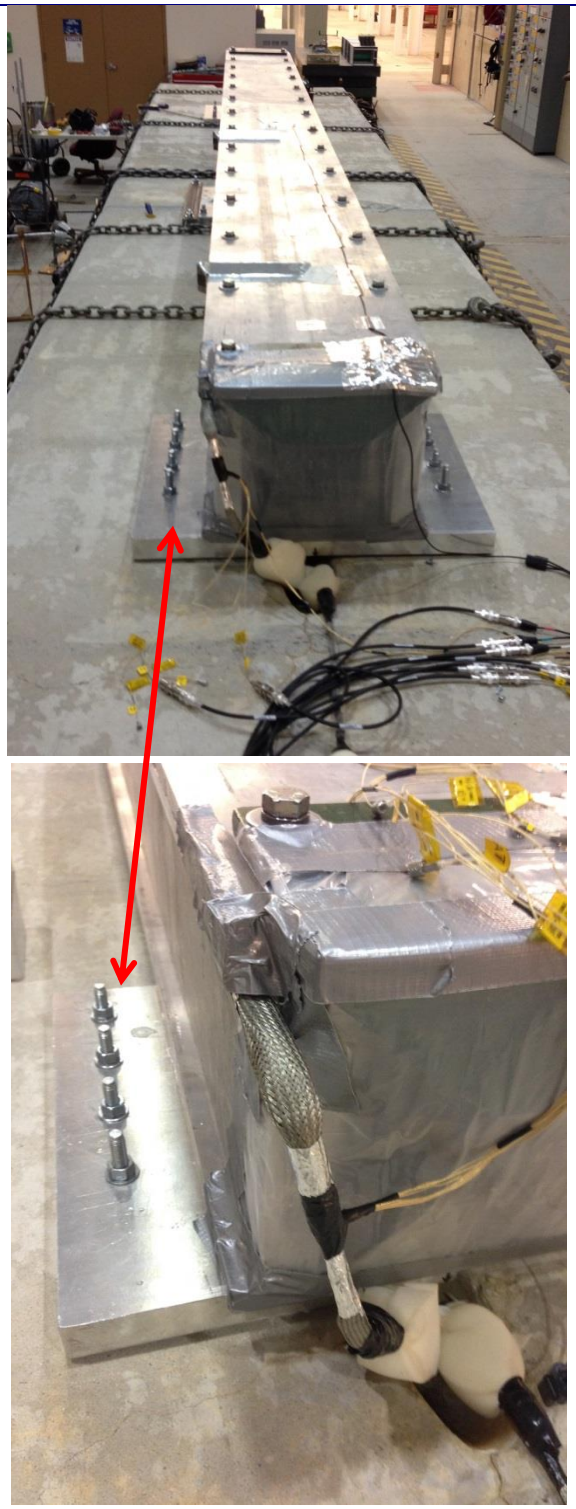

Figure 3.16 The basket containing the assembly was bolted to the concrete blocks. Only the assembly had freedom of motion relative to the trailer. The concrete blocks/basket approximated a rigid body. The assembly was free to move within the basket.

4. TEST ROUTE / ROAD SEGMENTS

The truck test encompassed a 40.2 mile route in the Albuquerque area. Data were collected in five Segments of the route. The data acquisition system could buffer 22 minutes 23 seconds of data after which the system stopped collecting data. At that time, the data from the buffer was downloaded to the computer hard drive. The truck was not in motion for some of the Segments for the full time of data acquisition (22:23). Table 4.1 identifies the route Segments for which data were collected and the times at which data acquisition commenced and was stopped. (The system recorded UTC time; the time has been converted to MDT for the table.) Figures 4.1 to 4.5 show the route of the truck test and the Segments of that route during which data were collected.

Table 4.1 Truck test route segments

Assembly Truck Test – Data Acquisition Road Segments				
Segment	**Location (Albuquerque & KAFB))**	**Time (MDT) 12May2014**	**mile**	**comments**
1	Building 6630 – start data acquisition	08:55:45	0	Includes Poleline Road – dirt; 46°F
	Eubank Contractors' gate – truck stops	09:13:20		
	Stop data acquisition	09:18:15		
2	Eubank Contractors' gate – start data acquisition	09:35:00		Segment includes I-40W, "Big I", I-25S. Pullover just off I-25S Rio Bravo exit
	Rio Bravo Blvd SE – truck stops	≈09:55	22.3	
	Stop data acquisition	09:57:23	22.3	
3	Rio Bravo Blvd SE – pullover point – start data acquisition	10:01:40		Includes crossing of two sets of RR tracks: on Rio Bravo Blvd SE and near Stock Dr SE on Broadway Blvd.
	Truck starts moving	10:02:05		
	Broadway Blvd SE – truck stops near Woodward Rd SE	10:06:24		
	Stop data acquisition	10:24:02		
4	Gibson Blvd SE at Broadway Blvd – start data acquisition	10:30:10	23.2	
	left onto Louisiana Blvd SE			
	right onto Central Ave			
	Eubank Blvd SE at Central Ave - Stop data acquisition	10:52:34	31	
5	Pennsylvania St SE – left off of Wyoming Blvd SE – start data acquisition	11:21:51	34.5	rough dirt road and hard brake near end of Segment; 52°F
	Building 6629 – truck stops	11:35:45	40.2	
	Stop data acquisition	11:44:15	40.2	

A variety of roads were traversed including rough dirt, rough asphalt, typical city streets including necessary stops at intersections and crossing railroad tracks, and Interstate highway. The route selected includes road surfaces more severe than would be expected for transport of an actual truck cask since it is unlikely that the road surfaces to and from facilities where used nuclear fuel would

be transported would include rough dirt roads and rough asphalt secondary streets. Figures 4.6 to 4.14 show some of the roads surfaces traversed during the test.

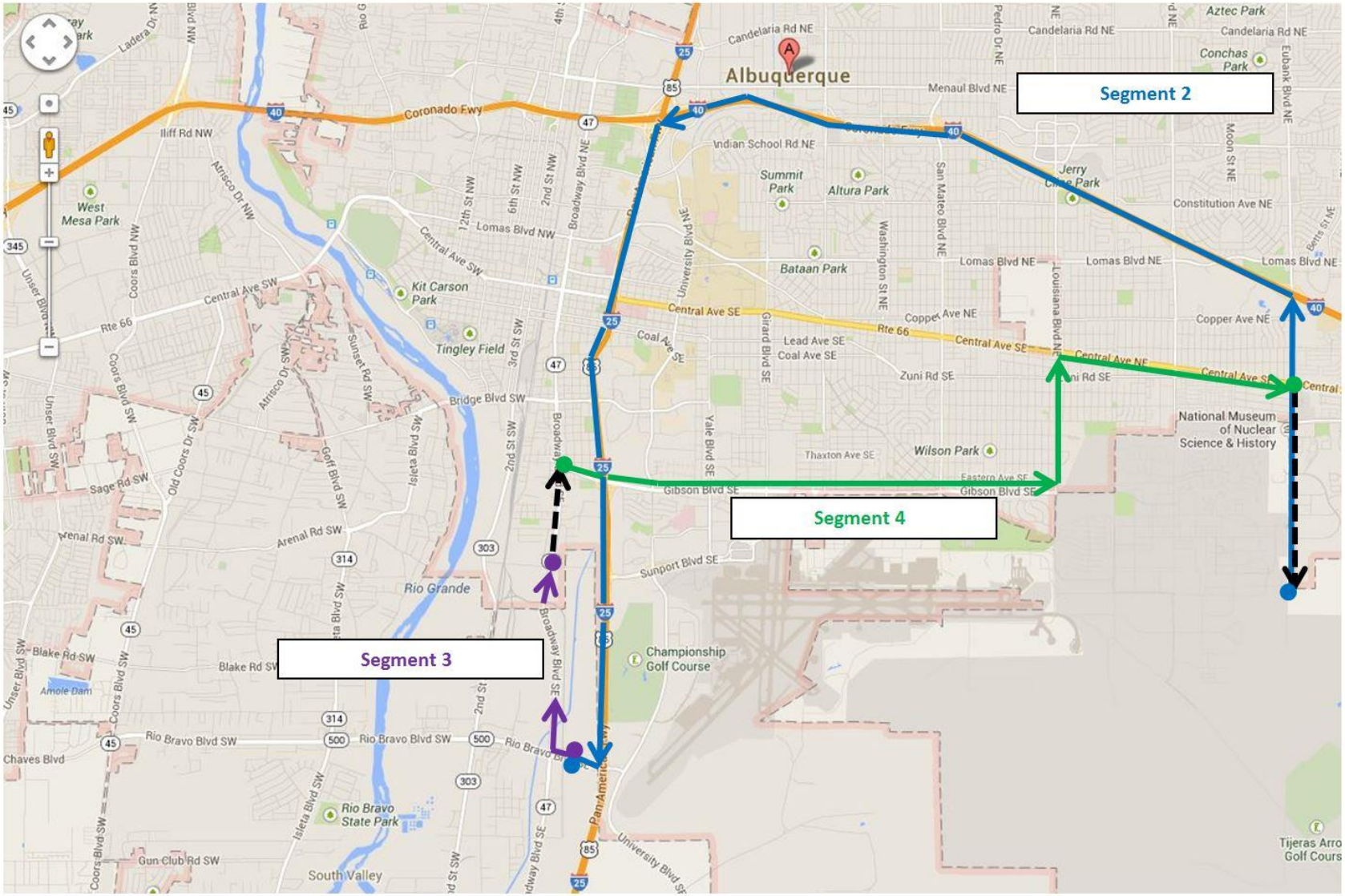

Figure 4.1 Truck route Segments 2, 3, and 4 within the City of Albuquerque. (Segments 1 and 5 were on Kirtland Air Force Base.)

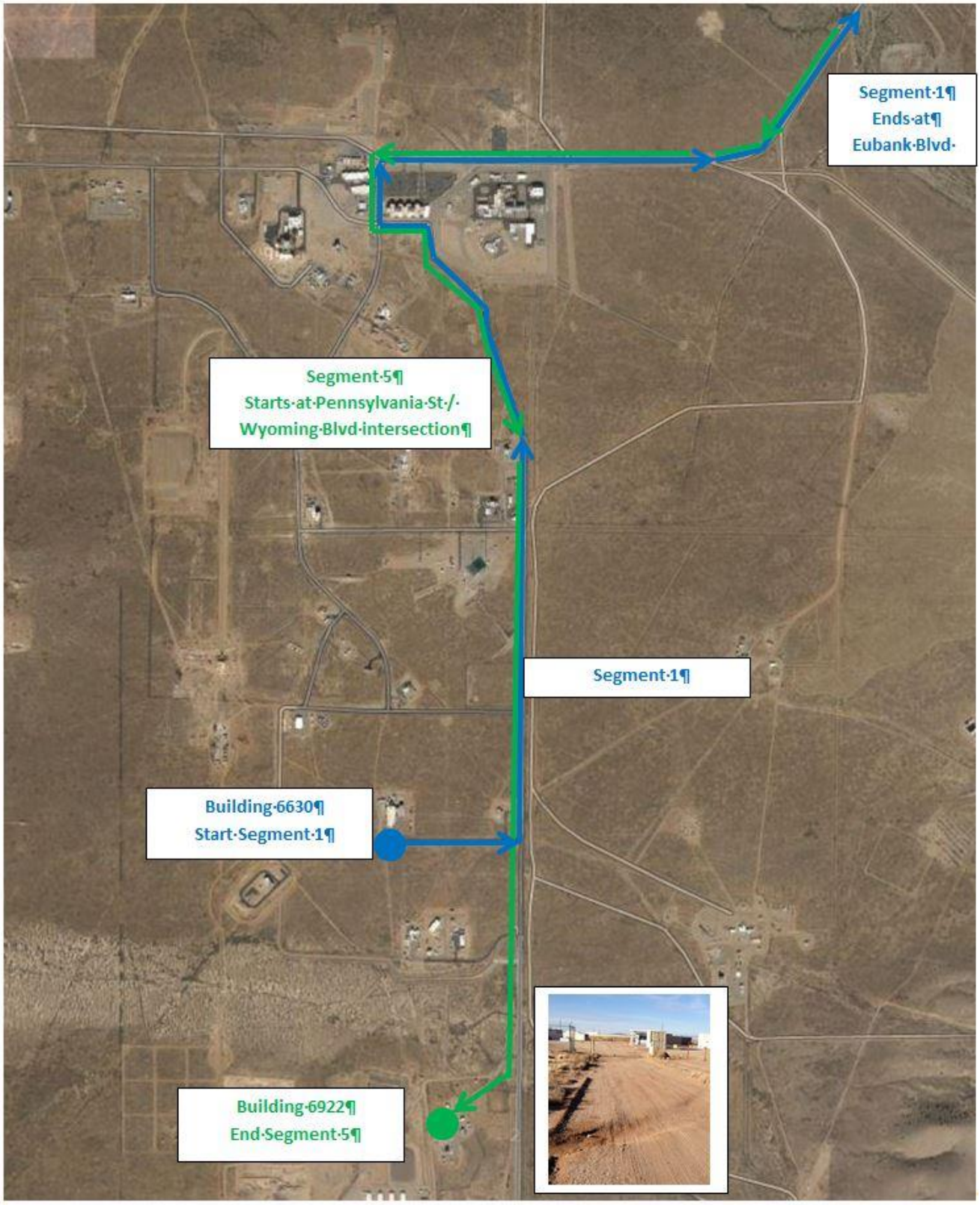

Figure 4.2 Sandia Area III route Segments 1 and 5 on Kirtland Air Force Base.

Figure 4.3 Poleline Road, Segment 2, Kirtland Air Force Base.

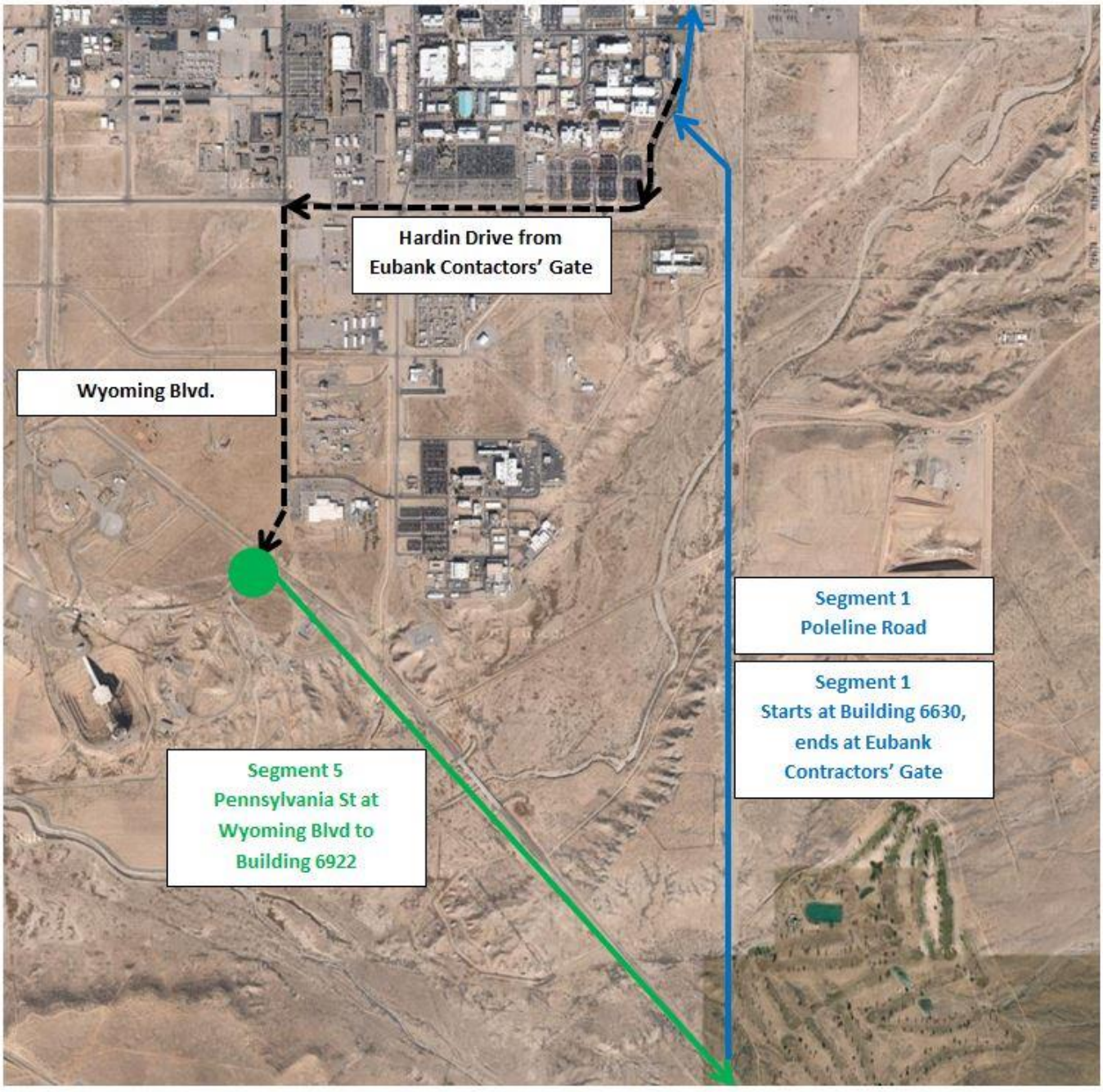

Figure 4.4 Pennsylvania Street to Area III, Segment 5.

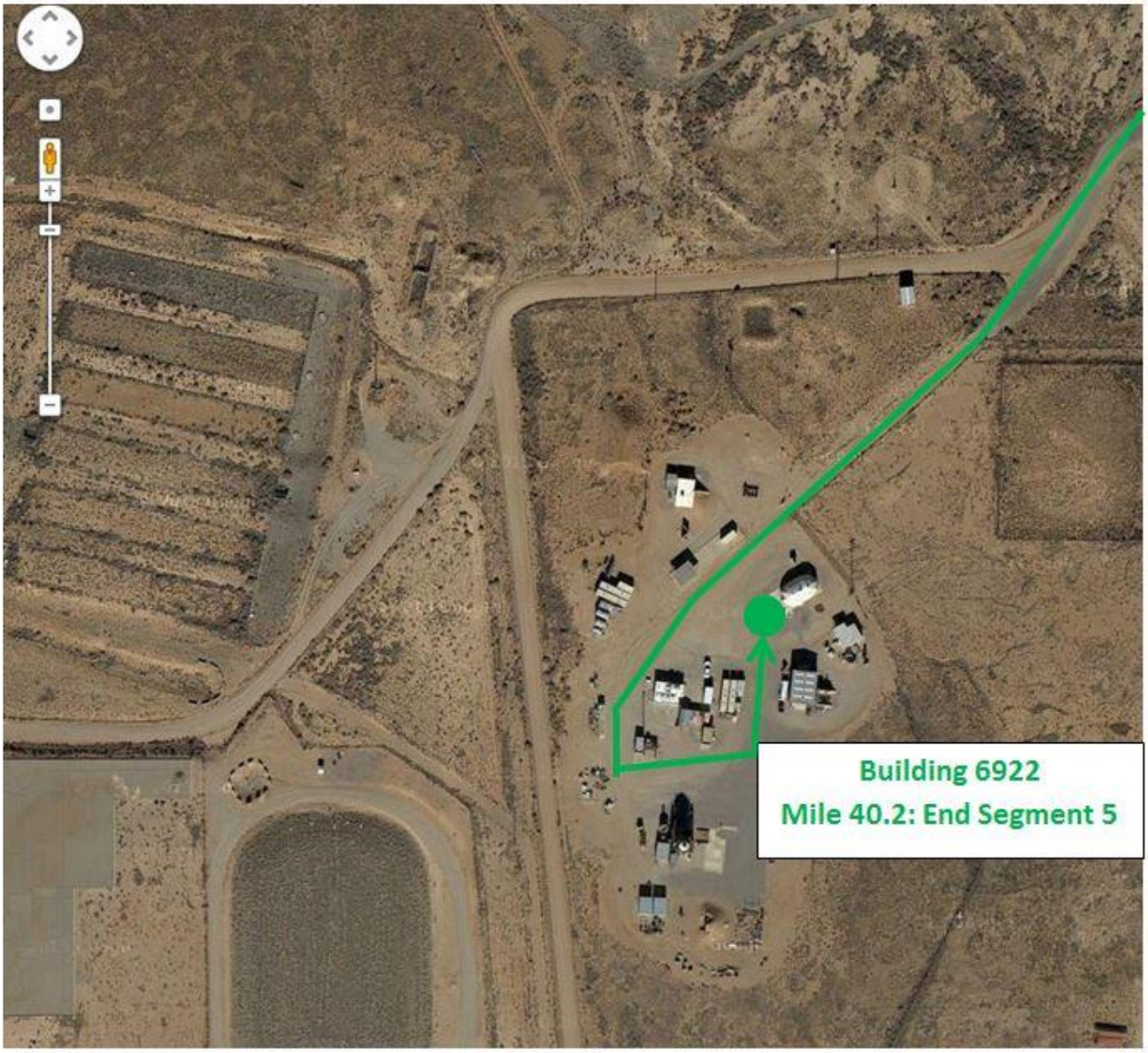

Figure 4.5 End of Segment 5, Area III.

Figure 4.6 Dip on Area III road approaching Pennsylvania St., Segment 1 (going north near beginning of truck route) and Segment 5 (going south near end of test).

Figure 4.7 Poleline Road looking north, Segment 1. The paved surface near top is a brief section of this dirt road. The highest strains measured on the instrumented rod were on the dirt section just north of the paved section (Figure 4.8).

Figure 4.8 Poleline Road approaching Eubank Contractors' Gate, Segment 1. This potholed, dirt/gravel portion of the truck route resulted in the highest measured rod strains.

Figure 4.9 “Big I” transition from I-40W to I-25S, Segment 2

Figure 4.10 Railroad track crossings on Broadway Blvd. SE, Segment 3. There were two railroad track crossings on Segment 3.

Figure 4.11 Area III road (rough asphalt), Segments 1 and 5.

Figure 4.12 Gibson Blvd. (east) concrete plate road surface, Segment 4. Relatively high strains were measured on Gibson Blvd.

Figure 4.13 Access to Building 6922, Area III, and end of Segment 5.

Figure 4.14 Dirt road into Building 6922 (southwest, top, and northeast, bottom), Area III, end of Segment 5. The trough shown is over 8 inches deep. The truck traveled directly over the deepest portion of the trough.

5. TEST DATA / RESULTS

For each of the instruments - strain gauges and accelerometers - time-history data were collected for each of the five route Segments: micro-strains (με) versus time (seconds) for the strain gauges and acceleration (g) versus time for the accelerometers. (The data acquisition system converted input voltage from the instruments to engineering units.) For each of the time-histories for each of the instruments, fast Fourier transformations (FFT) were calculated using the Sandia K2 software. The FFTs are in units of με/Hz versus Hz for the strain gauges and g/Hz versus Hz for the accelerometers.

The data analyzed have been reduced to summary tables (Tables 5.1 through 5.19) and plots of both the time-histories and the FFTs for each instrument (the plots are in Section 8). A 1000 Hz filter was used on all the raw data when generating plots and tables.

The maximum strain measured during the truck test, strain gauge S3 - 0° (vertical direction) was 143 μin./in. which corresponded to a section of Poleline Road, truck route Segment 1 (Tables 5.1 and 5.2 and Figures 8.1 and 8.2). Poleline Road is a rough dirt road unlike any surface an actual shipment of irradiated fuel would be expected to experience.

The maximum strains measured for all the strain gauges occurred at frequencies generally below 60 Hz (Figures 8.2, 8.6, 8.10, 8.14, and 8.18). The accelerations on the rod and spacer grids of the assembly had peaks up to 100 -120 Hz (Figures 8.3, 8.7, 8.11, 8.15, and 8.19).

There was a difference in the accelerations measured at the top of the basket (triaxial accelerometer TA2) and those below the drop deck section of the trailer at the rear axle (accelerometer TA5) by up to a factor of nearly 12 (refer, e.g., to Figure 8.20)[j]. However, as that figure shows, the accelerations on the assembly (uniaxial accelerometers A1, A3, A7, and A8) tended to be higher than those at the top of the basket (TA2), but not as high as those below the trailer on the rear axle (TA5) indicating some relative motion of the assembly within the basket. The basket was bolted to the concrete blocks on the trailer; the blocks were securely strapped to the trailer. The assembly was not attached to the basket and was free to move within the basket. The blocks–basket tended to respond more as a rigid body than the trailer to which they were attached.

The maximum strain measured, 143 μin./in. at the 0° circumferential location (Table 5.1, strain gauge S3 - 0°) is not necessarily the maximum strain experienced by the Zicaloy-4 rod during the truck test. The maximum strain could have (and probably did) occur at some other location around the circumference, and at some location axially removed from the "adjacent to the first spacer grid, Span 5" location on the rod (refer to Figure 3.4). However, the *actual* maximum strain could not have been greater than the maximum *measured* strain (143 μin./in.) than a factor of √2. Therefore, the maximum strain on the Zircaloy-4 rod during the truck test could have be as high as 202 μin./in. (√2 x 143 μin./in.).

[j] For Segment 4, for example, the amplification ratio (trailer response, g, versus basket response, g) for accelerometers TA5 and TA2 in the Z (vertical) direction ranged from a factor of 2 to nearly 12 between 0 and 100 Hz. Nick Klymyshyn, PNNL, personal communication, 7/25/2013.

5.1 Tabulated Test Results

Table 5.1 Strain gauge maximum values for truck test

Strain Gauge	Location on Assembly	Maximum Micro-strain Absolute Value (μin./in.)	Road Segment
S1 - 0°	Adjacent to first spacer grid, Span 10	**55**	
S1 - 90°		**53**	
S1 - 225°		**74**	
S2 - 0°	Mid-span, Span 10	**94**	
S2 - 90°		**99**	
S2 - 225°		**86**	
			1
S3 - 0°	Adjacent to first spacer grid, Span 5	**143**	
S3 - 90°		**84**	
S3 - 225°		**108**	
S4 - 0°	Mid-span, Span 5	**69**	
S4 - 90°		**101**	
S4 - 225°		**93**	
Average 0°		**90**	
Average 90°		**83**	**1**
Average 225°		**90**	

All maximum strains were measured during road Segment 1 at 872.4 – 902.3 seconds into the trip. This corresponds to travel on Poleline Road (dirt).

Table 5.2 Maximum strains route Segment 1

Segment 1		
Strain Gauge	**Location**	**Maximum Micro-strain Absolute Value (µin./in.)**
S1 - 0°	Adjacent to first spacer grid, Span 10	**55**
S1 - 90°		**53**
S1 - 225°		**74**
S2 - 0°	Mid-span, Span 10	**94**
S2 - 90°		**99**
S2 - 225°		**86**
S3 - 0°	Adjacent to first spacer grid, Span 5	**143**
S3 - 90°		**84**
S3 - 225°		**108**
S4 - 0°	Mid-span, Span 5	**69**
S4 - 90°		**93**
S4 - 225°		**101**

Table 5.3 Maximum strains route Segment 2

Segment 2		
Strain Gauge	**Location**	**Maximum Micro-strain Absolute Value (µin./in.)**
S1 - 0°	Adjacent to first spacer grid, Span 10	**29**
S1 - 90°		**31**
S1 - 225°		**35**
S2 - 0°	Mid-span, Span 10	**64**
S2 - 90°		**67**
S2 - 225°		**59**
S3 - 0°	Adjacent to first spacer grid, Span 5	**39**
S3 - 90°		**44**
S3 - 225°		**48**
S4 - 0°	Mid-span, Span 5	**22**
S4 - 90°		**41**
S4 - 225°		**32**

Table 5.4 Maximum strains route Segment 3

Segment 3		
Strain Gauge	**Location**	**Maximum Micro-strain Absolute Value (μin./in.)**
S1 - 0°	Adjacent to first spacer grid, Span 10	**27**
S1 - 90°		**32**
S1 - 225°		**53**
S2 - 0°	Mid-span, Span 10	**49**
S2 - 90°		**65**
S2 - 225°		**50**
S3 - 0°	Adjacent to first spacer grid, Span 5	**73**
S3 - 90°		**38**
S3 - 225°		**43**
S4 - 0°	Mid-span, Span 5	**47**
S4 - 90°		**45**
S4 - 225°		**39**

Table 5.5 Maximum strains route Segment 4

Segment 4		
Strain Gauge	**Location**	**Maximum Micro-strain Absolute Value (μin./in.)**
S1 - 0°	Adjacent to first spacer grid, Span 10	**33**
S1 - 90°		**47**
S1 - 225°		**69**
S2 - 0°	Mid-span, Span 10	**70**
S2 - 90°		**77**
S2 - 225°		**67**
S3 - 0°	Adjacent to first spacer grid, Span 5	**47**
S3 - 90°		**78**
S3 - 225°		**69**
S4 - 0°	Mid-span, Span 5	**26**
S4 - 90°		**94**
S4 - 225°		**61**

Table 5.6 Maximum strains route Segment 5

Segment 5		
Strain Gauge	**Location**	**Maximum Micro-strain Absolute Value (µin./in.)**
S1 - 0°	Adjacent to first spacer grid, Span 10	**31**
S1 - 90°		**29**
S1 - 225°		**40**
S2 - 0°	Mid-span, Span 10	**56**
S2 - 90°		**61**
S2 - 225°		**65**
S3 - 0°	Adjacent to first spacer grid, Span 5	**63**
S3 - 90°		**47**
S3 - 225°		**52**
S4 - 0°	Mid-span, Span 5	**32**
S4 - 90°		**53**
S4 - 225°		**50**

Table 5.7 Maximum vertical rod accelerations all route segments

All Segments			
Uniaxial Accelerometer	**Location**	**Maximum Acceleration, g**	**Road Segment**
A1	On first spacer grid, Span 10	**9.5**	**1**
A2	Mid-span, Span 10	**16.7**	
A3	Adjacent to second spacer grid, Span 10	**14.6**	
A7	Adjacent to second spacer grid, Span 5	**22.0**	
A8	On second spacer grid, Span 5	**11.3**	

Table 5.8 Maximum vertical rod accelerations route Segment 1

Segment 1		
Uniaxial Accelerometer	**Location**	**Maximum Acceleration, g**
A1	On first spacer grid, Span 10	**9.5**
A2	Mid-span, Span 10	**16.7**
A3	Adjacent to second spacer grid, Span 10	**14.6**
A7	Adjacent to second spacer grid, Span 5	**22.0**
A8	On second spacer grid, Span 5	**11.3**

Table 5.9 Maximum vertical rod accelerations route Segment 2

Segment 2		
Uniaxial Accelerometer	**Location**	**Maximum Acceleration, g**
A1	On first spacer grid, Span 10	**1.7**
A2	Mid-span, Span 10	**12.3**
A3	Adjacent to second spacer grid, Span 10	**5.1**
A7	Adjacent to second spacer grid, Span 5	**16.7**
A8	On second spacer grid, Span 5	**1.8**

Table 5.10 Maximum vertical rod accelerations route Segment 3

Segment 3		
Uniaxial Accelerometer	**Location**	**Maximum Acceleration, g**
A1	On first spacer grid, Span 10	**1.8**
A2	Mid-span, Span 10	**6.8**
A3	Adjacent to second spacer grid, Span 10	**6.0**
A7	Adjacent to second spacer grid, Span 5	**15.0**
A8	On second spacer grid, Span 5	**2.3**

Table 5.11 Maximum vertical rod accelerations route Segment 4

Segment 4		
Uniaxial Accelerometer	**Location**	**Maximum Acceleration, g**
A1	On first spacer grid, Span 10	**2.6**
A2	Mid-span, Span 10	**9.4**
A3	Adjacent to second spacer grid, Span 10	**10.6**
A7	Adjacent to second spacer grid, Span 5	**14.5**
A8	On second spacer grid, Span 5	**2.1**

Table 5.12 Maximum vertical rod accelerations route Segment 5

Segment 5		
Uniaxial Accelerometer	**Location**	**Maximum Acceleration, g**
A1	On first spacer grid, Span 10	**4.0**
A2	Mid-span, Span 10	**13.1**
A3	Adjacent to second spacer grid, Span 10	**5.4**
A7	Adjacent to second spacer grid, Span 5	**14.9**
A8	On second spacer grid, Span 5	**2.4**

Table 5.13 Triaxial maximum accelerations all route segments

All Segments		
Triaxial Accelerometer	**Location**	**Maximum Acceleration, g**
TA2 – X (longitudinal)	On top of basket above mid-span of assembly (Span 5)	**2.1**
TA2 – Y (lateral)		**3.6**
TA2 – Z (vertical)		**5.6**
TA5 – X (longitudinal)	Below trailer bed above rear axle	**13.7**
TA5 – Y (lateral)		**10.0**
TA5 – Z (vertical)		**11.8**

Table 5.14 Triaxial maximum accelerations route Segment 1

Segment 1		
Triaxial Accelerometer	**Location**	**Maximum Acceleration, g**
TA2 – X (longitudinal)	On top of basket above mid-span Span 5	**2.1**
TA2 – Y (lateral)		**3.6**
TA2 – Z (vertical)		**5.6**
TA5 – X (longitudinal)	Below trailer bed above rear axle	**2.0 (first 650 s)**
TA5 – Y (lateral)		**2.7 (first 650 s)**
TA5 – Z (vertical)		**4.4 (first 650 s)**

Table 5.15 Triaxial maximum accelerations route Segment 2

Segment 2		
Triaxial Accelerometer	**Location**	**Maximum Acceleration, g**
TA2 – X (longitudinal)	On top of basket above mid-span Span 5	**0.5**
TA2 – Y (lateral)		**1.1**
TA2 – Z (vertical)		**1.1**
TA5 – X (longitudinal)	Below trailer bed above rear axle	
TA5 – Y (lateral)		
TA5 – Z (vertical)		

Table 5.16 Triaxial maximum accelerations route Segment 3

Segment 3		
Triaxial Accelerometer	**Location**	**Maximum Acceleration, g**
TA2 – X (longitudinal)	On top of basket above mid-span Span 5	**0.6**
TA2 – Y (lateral)		**1.5**
TA2 – Z (vertical)		**1.0**
TA5 – X (longitudinal)	Below trailer bed above rear axle	
TA5 – Y (lateral)		
TA5 – Z (vertical)		

Table 5.17 Triaxial maximum accelerations route Segment 4

Segment 4		
Triaxial Accelerometer	**Location**	**Maximum Acceleration, g**
TA2 – X (longitudinal)	On top of basket above mid-span Span 5	**0.6**
TA2 – Y (lateral)		**1.8**
TA2 – Z (vertical)		**1.0**
TA5 – X (longitudinal)	Below trailer bed above rear axle	**13.7**
TA5 – Y (lateral)		**10.0**
TA5 – Z (vertical)		**11.8**

Table 5.18 Triaxial maximum accelerations route Segment 5

Segment 5		
Triaxial Accelerometer	**Location**	**Maximum Acceleration, g**
TA2 – X (longitudinal)	On top of basket above mid-span Span 5	**0.6**
TA2 – Y (lateral)		**1.4**
TA2 – Z (vertical)		**1.3**
TA5 – X (longitudinal)	Below trailer bed above rear axle	**8.0**
TA5 – Y (lateral)		**9.8**
TA5 – Z (vertical)		**19.8**

The maximum strain measured during the entire truck route, 143 µin./in., occurred during Segment 1 on Poleline Road on strain gauge S3 - 0° at 895.965 seconds. The corresponding acceleration measured on uniaxial accelerometer A7 which was near strain gauge S3 - 0° was 15.3 g at 895.963 seconds (refer to Table 5.19). However, that was not the maximum acceleration measured on accelerometer A7 during the truck route (or Segment 1) – the maximum was -21.96 g at 892.468 seconds into Segment 1, slightly before the maximum strain was measured (at 895.965 seconds). The maximum vertical acceleration measured on the top of the basket, -5.58 g, occurred just before the maximum strain at 895.929 seconds (TA2-Z). Note in Table 5.19, however, when all the data are filtered at 100 Hz (versus the normal filtering of 1000 Hz) that the maximum strain for S3 - 0° and maximum acceleration for A7 occurred at the same time.

Table 5.19 Comparison of acceleration at location and time of maximum measured strain during truck test

		1000 Hz data filter		100 Hz data filter	
Instrument nomenclature	**Time (seconds)**	**Micro-strain (µin./in.)**	**g (absolute value)**	**Micro-strain (µin./in.)**	**g (absolute value)**
S3 - 0°	**895.965**	**142.8 (max.)**			
A7	**895.963**		**15.3**		
A7	**892.468**		**21.96 (max.)**		
TA2-X	**895.929**		**1.785**		
TA2-Y	**895.929**		**-2.02**		
TA2-Z	**895.929**		**5.58 (max.)**		
S3 - 0°	**895.964**			**116.0 (max.)**	
A7	**895.963**				**6.07 (max.)**

"max." denotes the maximum strain or acceleration recorded for Segment 1.

5.2 Correlation of Road Condition with Measured Strain

Figure 5.1 correlates strain time-histories with road conditions to illustrate how road surfaces produced displacement and strains on the rod.

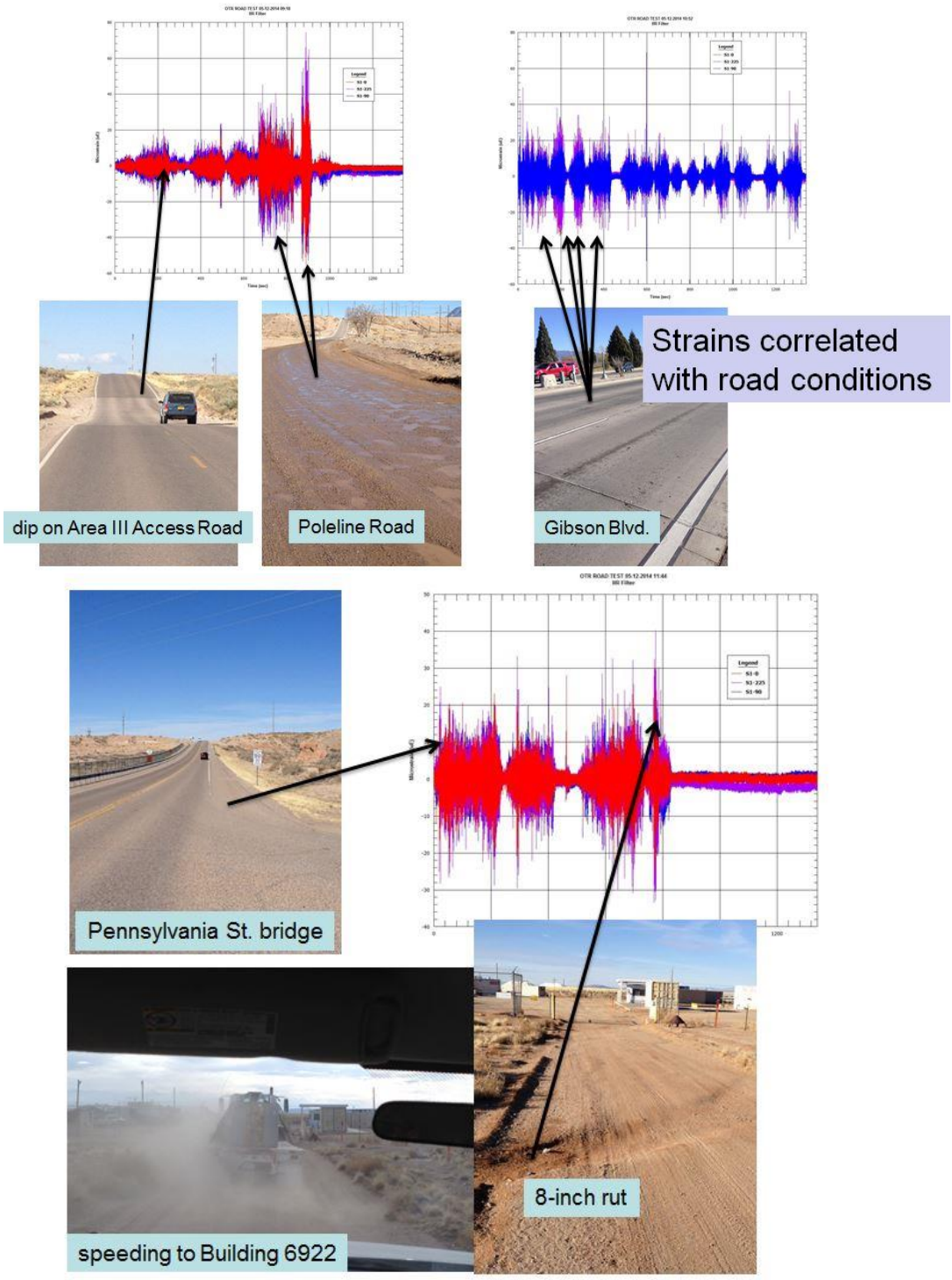

Figure 5.1 Correlation of measured strains on rod to road conditions. Top left is the strain versus time for the S1 strain gauges for truck route Segment 1, top right is the strain versus time for Segment 4 (y-axis is 80 με in both plots ; Figures 8.1 and 8.13). The bottom set of figures are for Segment 5 (y-axis is 50 με; Figure 8.17). Refer to Tables 3.1 and 4.1. Gibson Blvd. has a series of concrete plates separated by gaps which apparently caused peaks in rod strain (Figure 4.12).

5.3 Visual Examination of the Assembly

A GoPro® HERO3+ camera was attached to the basket (Figure 5.2). A video was taken while the tractor/trailer was driven along the Area III access road (rough asphalt) to Building 6922 (rough dirt). This was done to observe whether the assembly moved relative to the basket or if the rods moved relative to one another. The video was recorded at 240 frames/second. The video speed was subsequently reduced to 30 frames/second. In either version of the video, no motion of the assembly relative to the basket or of individual rods relative to one another was observed (Figure 5.3).

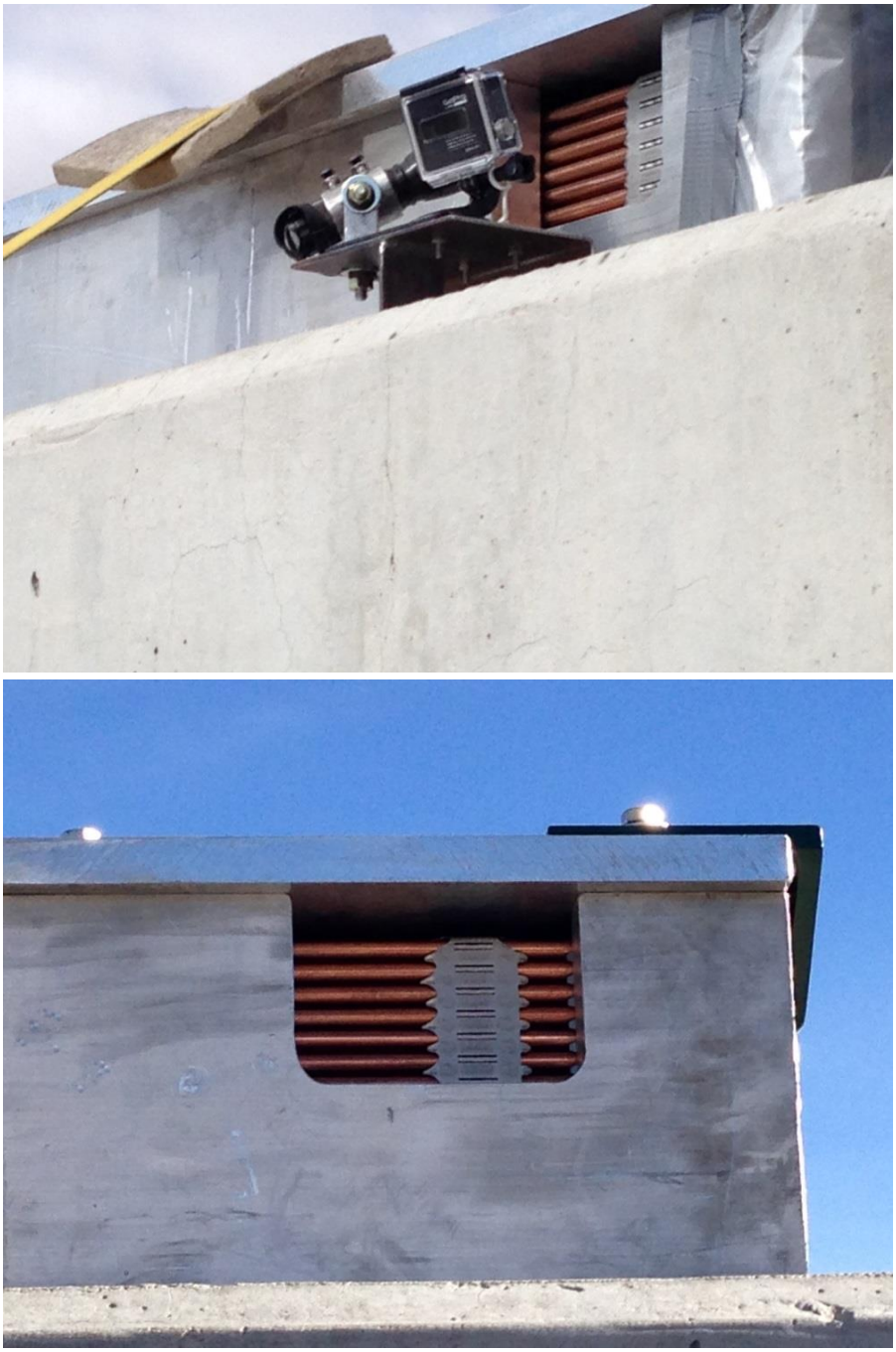

Figure 5.2 Basket cutout, bottom, showing side view of assembly for GoPro® video, top.

Figure 5.3 Screen capture of GoPro® .MP4 video file. There was no observed motion of the assembly relative to the inside of the top basket plate or the copper rods relative to one another or relative to the spacer grid in the 4 minute 23 second video (240 frames/second). There was occasionally motion observed between the top edge of the top basket plate relative to the clouds in the sky (note bluish-gray patch in top left corner of figure). The perceived curvature is an artifact of the wide angle view of the video.

A dab of silicone was placed on top of the assembly spacer grid shown in Figures 5.1 – 5.3 to within about 0.25 inch of the bottom of the top plate of the basket. Post-test examination of the silicone revealed that it had not come into contact with the top plate suggesting that the assembly had not "jumped" vertically during transport.

5.4 Strains Measured in Truck and Shaker Tests Relative to Elastic Limit of Zircaloy-4

The stresses[k] corresponding to the maximum experimentally measured strains in both the truck test and the previous shaker tests are approximately 2 - 3 ksi (13.8 - 20.6 MPa) as shown in Figure 5.4, which is a plot of the elastic portion of the stress-strain curves for unirradiated Zircaloy-4 and low-burnup and high-burnup irradiated Zircaloy-4. The figure also shows the maximum strain result from finite element analyses of the shaker tests performed at Pacific Northwest National Laboratory[l]. The figure indicates how low the magnitude of the strains and corresponding stresses were on the Zircaloy-4 rods relative to the elastic limit of unirradiated and irradiated Zircaloy-4. The applied stresses on the rod were low relative to the yield strength of the Zircaloy-4.

It is estimated that the strains and corresponding stresses on the rod in the region of irradiated fuel pellet-pellet interaction could be up the three times higher than the nominal stresses and strains in a region displaced from the pellet-pellet interface[m]. A factor of three increase in the stress at a pellet-pellet interface based on the stains measured in the assembly tests would be only on the order of 6 – 9 ksi (41 – 62 MPa).

The results suggest that failure of the rods during normal conditions of transport is unlikely due to a strain- or stress-based failure mechanism. The applied strains on the rods and the corresponding applied stresses seem to be too low relative to the strength of the cladding to cause failure in the absence of cracks. Further work is underway in other DOE programs to assess Zircaloy-4 performance based on inelastic, brittle fracture material property conditions which can be compared to the strains measured in the assembly tests.

[k] Stresses were converted from measured strains based on the elastic modulus, E, of unirradiated Zircaloy-4, $\sigma = \varepsilon E$.

[l] Material property data and PNNL analysis from Ken Geelhood and Carl Beyer, "Used Nuclear Fuel Loading and Structural Performance Under Normal Conditions of Transport – Supporting Material Properties and Modeling Inputs", Pacific Northwest National Laboratory, US Department of Energy Used Fuel Disposition Campaign Report FCRD-UFD-2013-000123, March 16, 2013 and Nicholas Klymyshyn, Scott Sanborn, Harold Adkins, and Brady Hanson, "Fuel Assembly Shaker Test Simulation", FCRD-UFD-2013-000168, Pacific Northwest National Laboratory, May 30, 2013, respectively.

[m] Jy-An Wang, ORNL, personal communication.

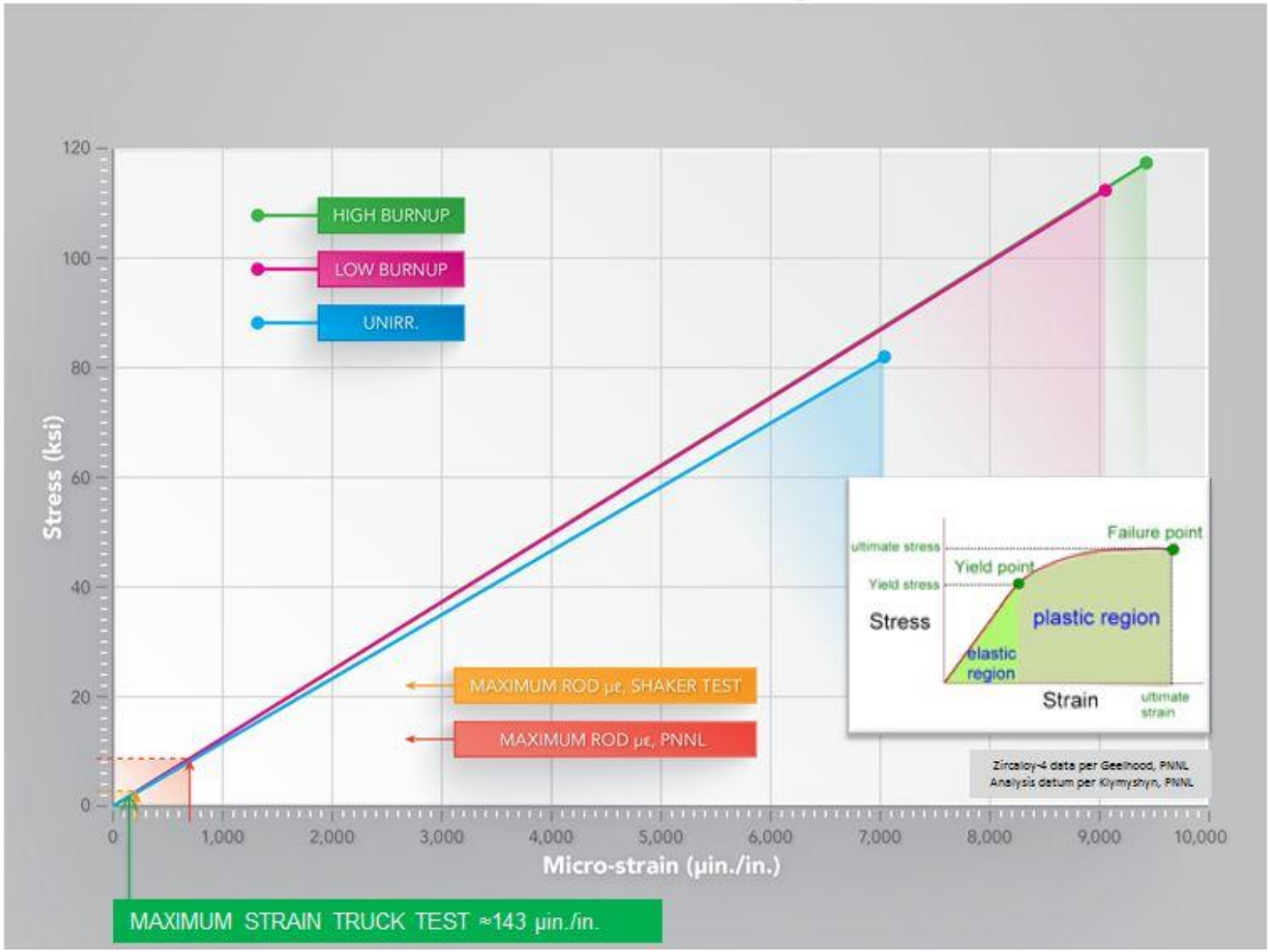

Figure 5.4 Strains on rod measured in truck and shaker tests relative to elastic limit/yield strength of Zircaloy-4.

5.5 Comparison of Truck and Shaker Test Results

The strains measured during the truck test were very similar to those measured during the shaker vibration and shock tests. Table 5.20 compares maximum strains measured at the 0° circumferential position on the top-center Zircaloy-4 rod for both the truck and shaker tests at similar axial (longitudinal) positions on the rod. The shaker maximum strains were generally slightly higher than those measured during the truck test, but all of the strains are very low – the differences can be deemed negligible.

The inputs, accelerations, used for the shaker tests were based on data from two reports[n] which present acceleration data obtained from transport of two casks (56000-lb cask on a spring suspension trailer and 44000-lb cask on an air suspension trailer). The triaxial accelerometers were placed on the four corners of "structures" which supported the casks on the trailer. These supporting structures were "fastened to structural members of the trailer[s]". The shaker test acceleration inputs were somewhat analogous to the accelerations measured below the trailer deck in the truck test.

Table 5.20 Comparison of maximum strains measured on Zircaloy-4 rods in truck and shaker tests

Strain Gauge (Truck/Shaker)	Location on Assembly (Top-middle Rod)	Truck Test Maximum Strain Absolute Value (µin./in.)	Shaker Vibration Test Maximum Strain Absolute Value (µin./in.)	Shaker Shock Test Maximum Strain Absolute Value (µin./in.)
S1 - 0°	Adjacent to first spacer grid, Span 10	55		
TMR-G-S10-3			89	80
S2 - 0°	Mid-span, Span 10	94		
TMR-G-S10-2			207	213
S3 - 0°	Adjacent to first spacer grid, Span 5	143		
TMR-G-S5-2			97	119
S4 - 0°	Mid-span, Span 5	69		
TMR-G-S5-1			156	114

[n] Clifford F. Magnuson, "Shock and Vibration Environments For A large Shipping Container During Truck Transport (Part II)", NUREG/CR-0128, SAND78-0337, May 1978 and Cliff F. Magnuson, "SHOCK AND VIBRATION ENVIRONMENTS FOR A LARGE SHIPPING CONTAINER DURING TRUCK TRANSPORT (PART I)", SAND77-1110, September 1977.

5.6 Fracture Toughness and Fatigue Assessment

The following fracture toughness discussion is taken primarily from the shaker report[o], but because the strains measured in the truck test were so similar in magnitude to those measured in the shaker test, the conclusions apply. The fatigue discussion is based upon rail vibration data provided by the Transportation Technology Center, Inc. for analyses described in Adkins, et al.[p], and is also based upon strains measured in the shaker tests. The material properties for the Zircaloy-4 were taken from Geelhood and Beyer.[q]

5.6.1 Fracture Mechanics Analysis Based on Stresses from Test Data and Analyses

The strain data measured during the tests, for shock and vibration loadings, suggest that the axial strains on the rod—and the corresponding applied stresses—are very low in relation to the elastic limit of unirradiated Zircaloy-4 and the estimated elastic limits for low-burnup and high-burnup Zircaloy-4.[r] This suggests that cladding will not fail during NCT via strain- or stress-based failure criteria (Figure 5.4).

Irradiation of Zircaloy-4 increases the yield strength of the material with little effect on the elastic modulus. The ductility of high-burnup Zircaloy-4 cladding is no doubt degraded meaning that once the yield limit is reached in high-burnup cladding, there will be little or no plasticity—brittle fracture could occur at the yield limit or below. However, the stresses derived from the strains (and associated stresses) measured in the shaker tests are so low that there is a large margin between the applied stresses and the Zircaloy-4 yield strength.

Cladding could fail via a fracture mechanics-based criterion, however. Brittle fracture can occur at any stress below the yield limit in cladding containing damage or flaws, or that develops flaws under fatigue loading. Limited data, some derived from models, suggests a degradation of the fracture toughness of high-burnup Zircaloy-4. In the presence of a crack in the cladding of sufficient size, fracture could occur at relatively low stresses.

An evaluation of the stresses required to cause fracture in the presence of cracks in high-burnup cladding of various sizes has been made. These evaluations required an estimate of the fracture toughness, K_{Ic}, of high-burnup Zircaloy-4. Data for the fracture toughness of Zircaloys has been summarized:

> "The data for irradiated Zircaloy-2 (Zr-2) and Zircaloy-4 (Zr-4) materials shows the lowest room temperature K_{Ic} values to be in the range of 12 MPa-$\sqrt{m}$ to 15 MPa-$\sqrt{m}$ for hydrogen concentrations of the order of 1000 ppm. Such low values, however, are typical of beta-quenched material, which has different microstructural characteristics than fuel cladding. A more typical

[o] FUEL ASSEMBLY SHAKER TEST for Determining Loads on a PWR Assembly under Surrogate Normal Conditions of Transport" McConnell, et al., SAND2013-5210P, Rev. 0.1, FCRD-UFD-2013-000190, June 30, 2013 (revised December 1, 2013).

[p] "Used Nuclear Fuel Loading and Structural Performance Under Normal Conditions of Transport –Demonstration of Approach on Used Fuel Performance Characterization", Adkins, et al., FCRD-UFD-2013-000289, August 31, 2013.

[q] Ken Geelhood and Carl Beyer, "Used Nuclear Fuel Loading and Structural Performance Under Normal Conditions of Transport – Supporting Material Properties and Modeling Inputs", Pacific Northwest National Laboratory, US Department of Energy Used Fuel Disposition Campaign Report FCRD-UFD-2013-000123, March 16, 2013.

[r] The definition of "low burnup" is Zircaloy-4 with a hydrogen concentration of 300 ppm subjected to a fluence of 5.00E+25 n/m^2. "High burnup" corresponds to a hydrogen concentration of 600 ppm subjected to a fluence of 1.00E+26 n/m^2. [per. corr. Ken Geelhood, PNNL, May 2013].

lower-bound value of K_{Ic} for end-of-life burnup at 20°C with relatively high hydrogen concentration (≈750 ppm) is in the range of 18-20 MPa-√m. The corresponding K_{Ic} value for temperatures above 280°C is 30 MPa-√m. These K_{Ic} values are to be contrasted with 50 MPa-√m and higher for moderately irradiated materials with low hydrogen concentrations. The fracture toughness data reviewed in the foregoing supports the following conservative criteria, recommended herein for application to normally discharged fuel with prototypical burnup and hydrogen contents.

(a) K_{Ic}= 18 MPa-√m for T < 100°C, 100<H<500ppm

(b) K_{Ic} = 50 MPa-√m for T > 280°C, H < 100 ppm

(c) K_{Ic} = 30 MPa-√m for T > 280°C, 100 < H < 500 ppm

(d) K_{Ic} = 20 MPa-√m for T > 280°C, 500 < H < 750 ppm

(e) K_{Ic} = 12 MPa-√m for any temperature, H > 1,000 ppm."[s]

The lowest values above most likely correspond to the Zircaloy lower shelf behavior as determined by the ductile-to-brittle transition temperature.

In order to calculate the stress or crack size required to cause fracture of the cladding, equations relating the applied stress intensity, K_I, the crack size, and the applied stress are used. When the applied stress intensity, K_I, exceeds the fracture toughness, K_{Ic}, fracture at the crack tip occurs. A circumferential crack is the most likely to cause fracture in the presence of axial, bending stresses such as those experienced by cladding.

The expression used for the calculations were:

$K_I = Y\sigma_b\sqrt{(\pi a)}$, where Y = 1, σ_b = applied bending stress

The Zircaloy-4 rods have a wall thickness, t, of 0.0225 inches (0.57 mm). Semi-elliptical circumferential surface cracks with a/2c = 1/6 were assumed, where "a" is the crack depth at the deepest point and "2c" is the length of the crack. The assumed applied stress was 3 ksi (20.6 MPa) which corresponded to the maximum strain measured during the shaker tests. The calculations also assumed through-wall flaws of varying depth, a/t = 0.1, 0.25, and 0.5.

Table 5.21 presents results of the applied stress intensities for the maximum applied stresses tests for a range of crack sizes.

Table 5.21 Estimated applied stress intensities at the tip of circumferential flaws in the cladding of a fuel rod subjected to stresses experimentally measured

Crack depth/Zircaloy-rod wall thickness, a/t	Applied stress, (MPa)	Applied stress intensity, K_I, at crack tip, (MPa-√m)
0.10	20.6	0.2 - 0.3
0.25	20.6	0.4 - 0.4
0.50	20.6	0.5 - 0.6

[s] Rashid, Y.R., R.O. Montgomery, W.F. Lyons, "Fracture Toughness Data for Zirconium Alloys – Application to Spent Fuel Cladding in Dry Storage", Electric Power Research Institute Technical Progress Report 1001281, January 2001.

The calculated applied stress intensities are low relative to even a lower bound fracture toughness for Zircaoly-4 of 12 MPa-√m and crack depths up to half the clad wall thickness; the fracture toughness of Zircaloy-4 significantly exceeds the applied stress intensities calculated for the stress levels measured for the shaker tests.

The resulting implication is that the margin against failure in the presence of a crack on the fuel cladding due to a fracture mechanics-based failure mechanism may be acceptable for the stresses measured by the shaker tests that simulate those expected during normal conditions of transport. The measured strains are very low; it would take a significant preexisting flaw in cladding, and/or significantly degraded fracture toughness, and/or large numbers of cycles under these strains for these strains to be of real concern. This issue should be more thoroughly examined, however, particularly by means of generating additional fracture toughness data on high-burnup Zircaloy-4 and assessments of the sizes of potential cracks in cladding.

5.6.2 Fatigue assessment

An estimate was made of the number of shocks a rail car may experience in a typical 2000-mile trip and the number of vibrations over the same distance. The number of shock cycles was estimated to be approximately 25000 and the number of vibration cycles was estimated to be approximately 1000000 to 2000000[t]. Based upon the fatigue curve in Geelhood and Beyer relative to the stress amplitude for cyclic loading based upon the maximum strain measured in the shaker tests, it appears that a fatigue crack would not initiate in Zircaloy-4 cladding, Figure 5.5.

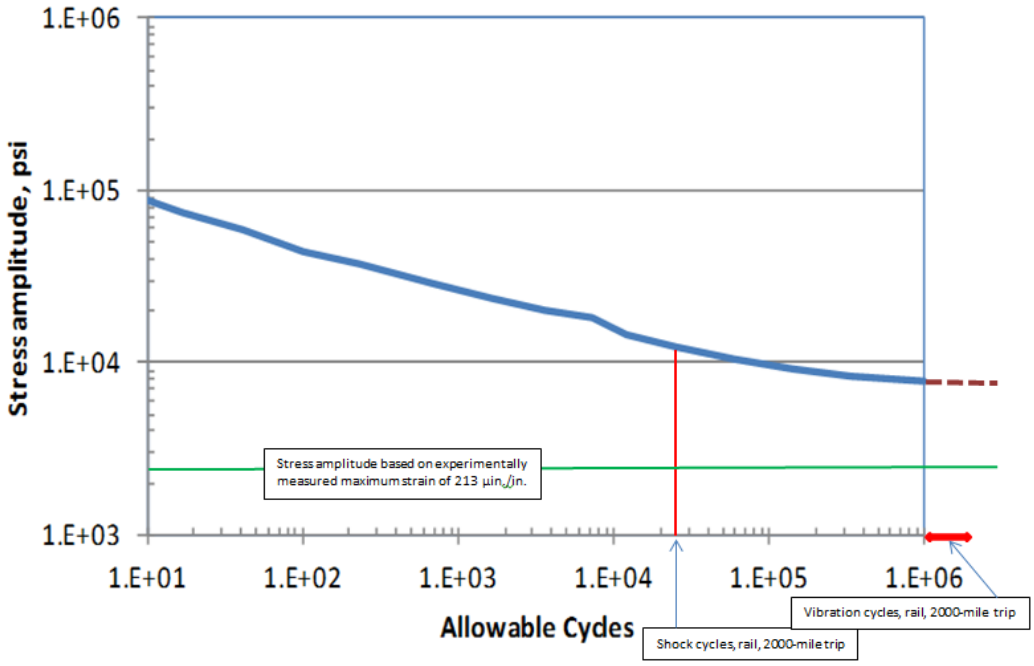

Figure 5.5 Stress amplitude based upon maximum strain measured in shaker tests relative to irradiated Zircaloy-4 fatigue curve.

[t] The shock and vibration estimates were derived from data provided by the Transportation Technology Center, Inc. which was used for the analyses in "Used Nuclear Fuel Loading and Structural Performance Under Normal Conditions of Transport – Demonstration of Approach on Used Fuel Performance Characterization", Adkins, et al., FCRD-UFD-2013-000289, August 31, 2013.

6. FUTURE ASSEMBLY TESTS AND MODELING

The purpose of doing assembly tests is to generate data that can support a technical basis for affirming that high burnup, aged fuel rods can withstand normal conditions of transport. This has been done by conducting shaker tests and the truck test described in this report.

These assembly tests have provided data – a benchmark, or a reasonable approximation, of - the strains on fuel rods when subjected to normal conditions of transport. Each of these tests, of course, entailed compromises to testing of an actual irradiated assembly in an actual cask.

Another purpose of these tests has been to provide data by which finite element models of an assembly could be validated. Data that can be used for finite element model validation does not need to be obtained from an irradiated assembly in an actual cask. Surrogate assemblies and surrogate test configurations can provide useful data for validation of models.

The shaker and truck test of the assembly provided data only for truck transport conditions. Most UNF in the United States will be transported by rail (with perhaps short trips via heavy-haul truck or barge). Truck transport conditions are more severe than rail so the data collected in these tests should be conservative relative to data that could collected via rail. However, due to the predominance of rail transport, it would be prudent to generate assembly test data for rail transport conditions. Such rail tests could be conducted on a shaker, a railcar, or both.

Table 6.1 presents a matrix of possible tests of an assembly. Other test configurations can be envisioned. But, this matrix tries to present a feasible pathway to collect a body of data – evidence – to support the contention that normal transport of irradiated assemblies is not of concern.

Table 6.1 Potential assembly testing

Activity	Test Unit	Status	Advantages / Compromises	Comments
1. SNL Shaker Test	SNL basket/assembly	Completed May 2013	1. Measured low strains on rods 2. Truck inputs only, but conservative[u] 1. Vertical axis only 2. No cask 3. Only > 3 Hz 4. No pellets within rods	
2. SNL Truck Test	SNL basket/assembly	Completed May 2014	1. Actual over-the-road test 2. Multi-axis loading 3. Full Hz range 4. No cask 5. No pellets within rod 6. Truck not rail	Conservative compared to rail loadings (see footnote)

[u] Refer to Figure 5.15 in Section 5.1.3 in "Used Nuclear Fuel Loading and Structural Performance Under Normal Conditions of Transport –Demonstration of Approach on Used Fuel Performance Characterization", Adkins, et al., FCRD-UFD-2013-000289, August 31, 2013.

Activity	Test Unit	Status	Advantages / Compromises	Comments
3. Seismic shaker tests	SNL basket/assembly	Planned FY15	1. Multi-axis; 2. Down to 1 Hz; 3. Both truck and rail inputs	Provides rail data Resolves some SNL shaker issues
4. Rail test with basket/assembly only on railcar using a surrogate mass to simulate a rail cask	Tri-Cities Rail Yard, Richland Washington; assemblies tbd	Test plan FY15, tests FY16?	1. Actual over-the-rail test 2. Multi-axis loading 3. Full Hz range 4. No cask	Provides over-the-rail data
5. Rail test with assembly in actual rail cask/basket	NAC-NLI 10/24, Areva TN-32B, or Ensa cask; assemblies tbd	Test plan FY15, tests FY16?	1. Actual cask/basket; 2. Actual over-the-rail test	Most representative test configuration

There are options for assembly tests that would provide rail transport conditions data.

The most straightforward, timely and least expensive rail-input test is to perform additional shaker tests using rail vibration and shock inputs to the shaker system. Such a set of tests is proposed for FY15 and a test plan has been initiated. These shaker tests would be performed on a "seismic" shaker with six-degrees of freedom (unlike the original Sandia shaker test which had only vertical motion [although vertical motion is the most severe in terms of strains imposed on fuel rods]). The seismic shaker tests can also accommodate frequencies below 1 Hz (the Sandia shaker is limited to a lower bound of approximately 3 – 4 Hz). The test unit would be the assembly/basket used for the Sandia shaker and truck tests.

It is recommended that beyond the rail-input seismic shaker tests that a test of an assembly be performed on an actual railcar and preferably with an actual rail cask (or at least a rail cask basket). Items 4 and 5 in Table 7.1 describe these options. There are at least three current possibilities for an over-the-rail test using an actual rail cask. A proposal has been provided by Areva for a TN-32B cask with surrogate assemblies for both rail and drying tests. The Tri-Cities Rail Yard in Richland Washington has purchased two NAC-NLI 10/24 rail casks which could possibly be used for tests at their facility. Ensa, a Spanish company, has tentatively offered the use for their new ENUN 32P cask for rail tests in the United States. Each of these options has trade-offs in terms of cost, logistics, schedule, and public perception or understanding of the test ("optics").

All of the assembly tests thus far conducted or proposed are surrogate tests in that they are not tests of 1) an actual irradiated assembly with 2) irradiated cladding and UO_2 pellets with 3) pellet-clad interaction in 4) an actual basket with 5) and actual cask transported on 6) an actual conveyance, truck or rail and, in the case of rail transport on 7) an AAR Standard-2043 railcar. Table 6.2 highlights the many constraints and compromises necessary to obtain fuel rod data during normal conditions of transport.

6.1 Constraints and Compromises to an Ideal Test of an Assembly

Table 6.2 Constraints and compromises to an ideal test of an assembly

Ideal Experimental Design	Constraint	Compromise Solution for Test	Comments
Use actual cask	• Available truck casks contaminated • Rail casks unavailable	**Simulate truck transport with a shaker**	Applicable shock/vibration data available from NUREG/CR-0128
Use actual PWR assembly	Use of an irradiated assembly not feasible	**PWR assembly was available**	
Use zirconium alloy rods	Limited number of Zircaloy-4 rods available	• **Use copper alloy tubes for most assembly locations** • **Use Zircaloy-4 rods for those rods to be instrumented**	Among many materials evaluated for surrogates for Zircaloy-4 and UO_2, copper and lead had best combination of material properties (elastic modulus and density, respectively), availability, and cost
Use UO_2 pellets in rods	UO_2 pellets unavailable	**Use lead rods as surrogate**	
Rods have same material properties as used in an actual assembly	• Limited number of Zircaloy-4 rods available • UO_2 pellets unavailable	• **Adjust wall thickness of copper tubes so that $EI_{Cu} \approx EI_{Zircaloy\text{-}4}$** • **Adjust amount of lead in tubes so total assembly weight is that of an actual assembly**	

Ideal Experimental Design	Constraint	Compromise Solution for Test	Comments
Assembly is in an actual basket which is within a cask	Actual basket unavailable	**Construct a basket to contain assembly**	
Basket within a truck cask has some freedom of motion	Experimentally unviable to allow basket to move shaker due to shaker control constraints	**Attach basket to shaker to prevent motion**	
Assembly in basket has freedom of motion	None	**Fuel assembly allowed same freedom of motion as an assembly within an actual NAC-LWT PWR basket**	Within the basket, the assembly had 0.45 in. (1.14 cm) clearance at the top and 0.225 in. (0.57 cm) along the sides
Assembly subjected to actual truck transport environment	Truck cask unavailable	**Derive inputs for shaker from truck vibration/shock data**	• Vibration data and shaker inputs ranged from 5 Hz to 2,000 Hz • Shock data ranges from 0.5 Hz to 420 Hz. Shaker inputs for shock ranged from 4 Hz to 600 Hz
Basket/ assembly within an actual truck cask	Truck cask unavailable	• **Basket constructed to conform to material (aluminum), weight, and internal dimensions of NAC-LWT PWR basket** • **Basket affixed to shaker**	
Instrument assembly and basket (accelerometers and strain gages)	None	• **Apply expert judgment and analyses to define location of instruments** • **Instrument selected rods**	• All rods are expected to respond in a similar manner (per analyses) • Used 16 strain gages and 25 accelerometers

7. CONCLUSION

The strains measured on the Zircaloy-4 rod during the fuel assembly truck test were in the micro-strain levels – well below the elastic limit for either unirradiated or irradiated Zircaloy-4 – and very similar to the strains measured in the previous set of shaker tests.

Based upon the test results, strain- or stress-based failure of fuel rods during normal transport seems unlikely.

Additional testing – assembly rail tests and high burnup Zircaloy rod mechanical property characterization – and continued finite element model analyses - are recommended.

8. PLOTS OF STRAIN AND ACCELERATION TIME-HISTORIES AND FAST FOURIER TRANSFORMATIONS FOR ALL FIVE TRUCK ROUTE SEGMENTS

The following plots were derived from the raw data (με or g versus time) recorded by the data acquisition system for each instrument (strain gauge or accelerometer) using the Sandia K2 software with a 1000 Hz filter on the raw data. All five truck route Segments are represented in the following five Subsections 8.1 through 8.5. A description of the truck route and the route Segments is in Table 4.1 and diagrams showing the truck route are in Figures 4.1 through 4.5. Within each Subsection are four sets of plots: strain versus time (με versus seconds); strain fast Fourier transformations (με/Hz versus Hz); acceleration versus time (g versus seconds); and acceleration fast Fourier transformations (g/Hz versus Hz). The following plots are summarized in tables in Section 5.

8.1 Truck Route Segment 1 Data Plots

8.1.1 Strain Gauge Time-Histories (με versus time)

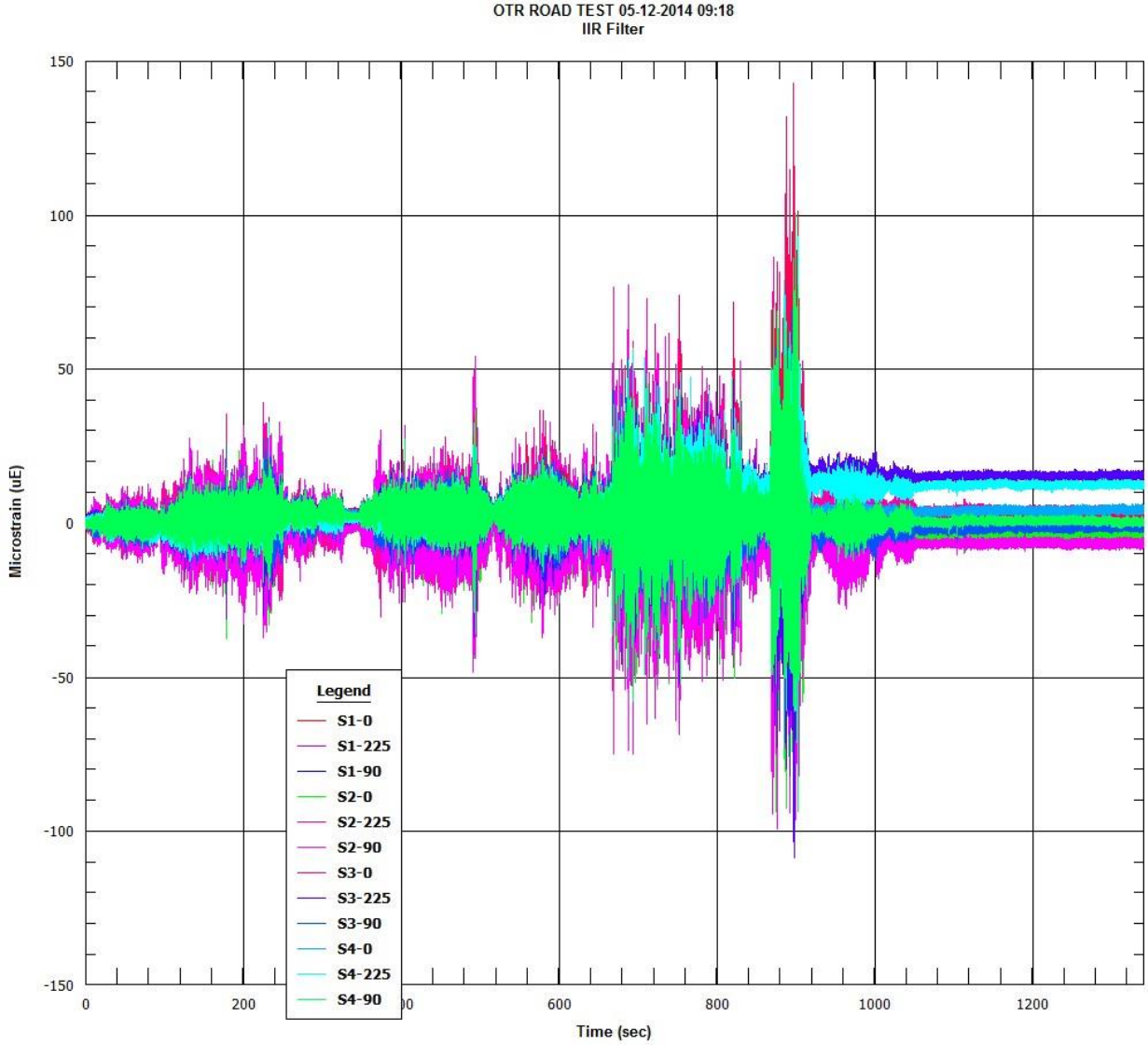

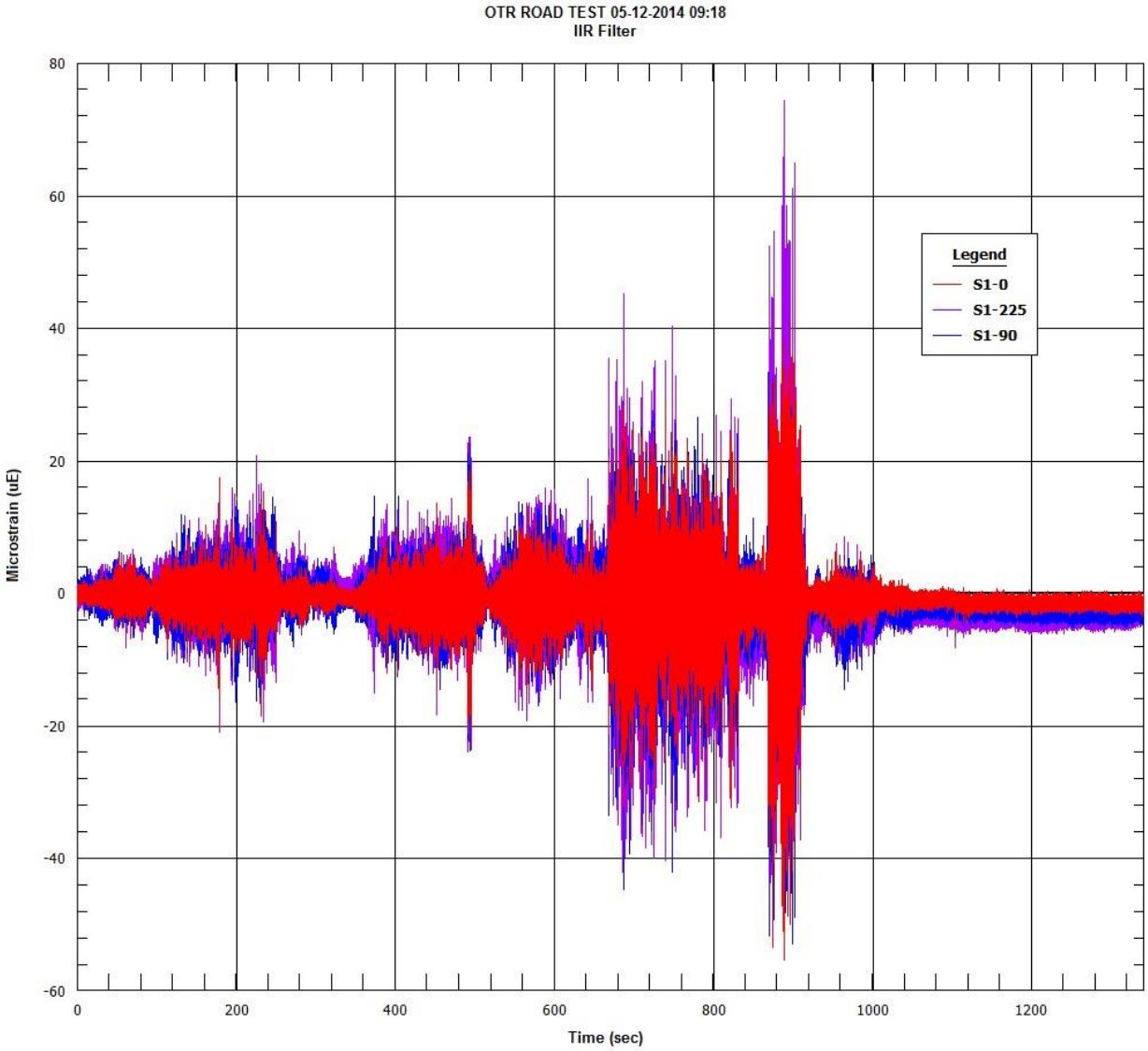
OTR ROAD TEST 05-12-2014 09:18
IIR Filter
Legend
S1-0
S1-225
S1-90
Microstrain (uE)
Time (sec)
80
60
40
20
0
-20
-40
-60
0
200
400
600
800
1000
1200

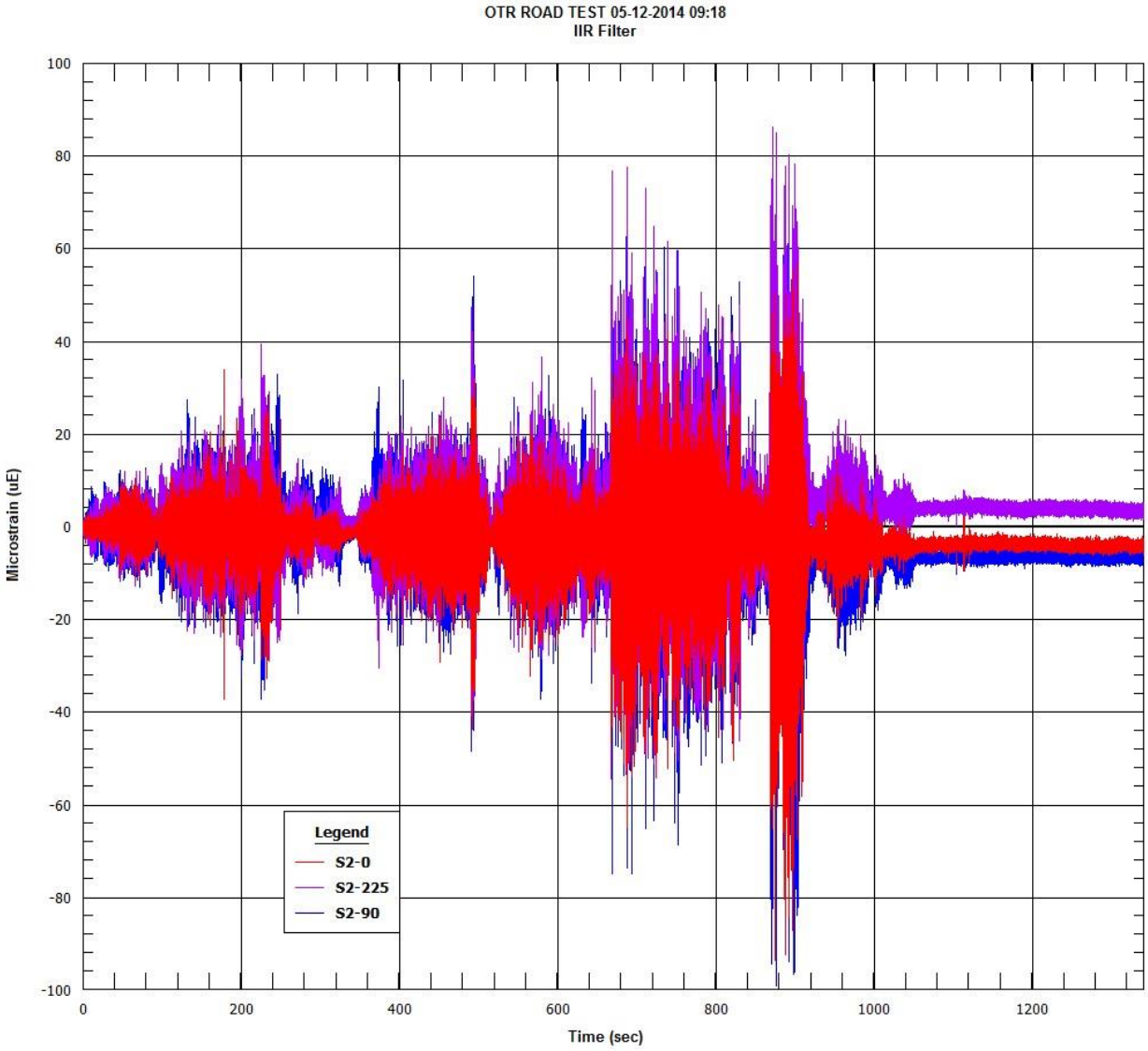
OTR ROAD TEST 05-12-2014 09:18
IIR Filter
Microstrain (uE)
Time (sec)
Legend
S2-0
S2-225
S2-90
100
80
60
40
20
0
-20
-40
-60
-80
-100
0
200
400
600
800
1000
1200

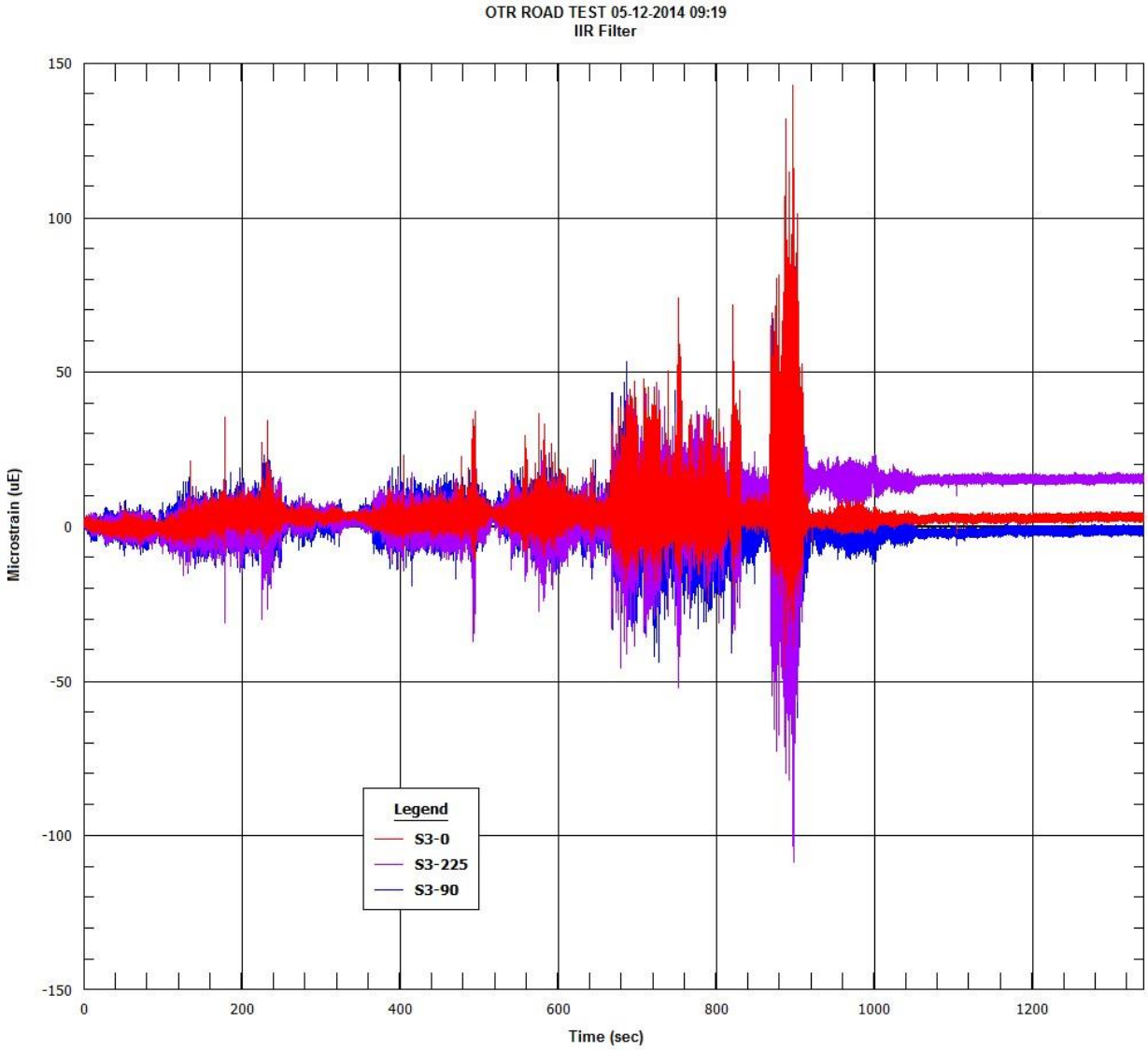
OTR ROAD TEST 05-12-2014 09:19
IIR Filter
Microstrain (uE)
Time (sec)
150
100
50
0
-50
-100
-150
0
200
400
600
800
1000
1200
Legend
S3-0
S3-225
S3-90

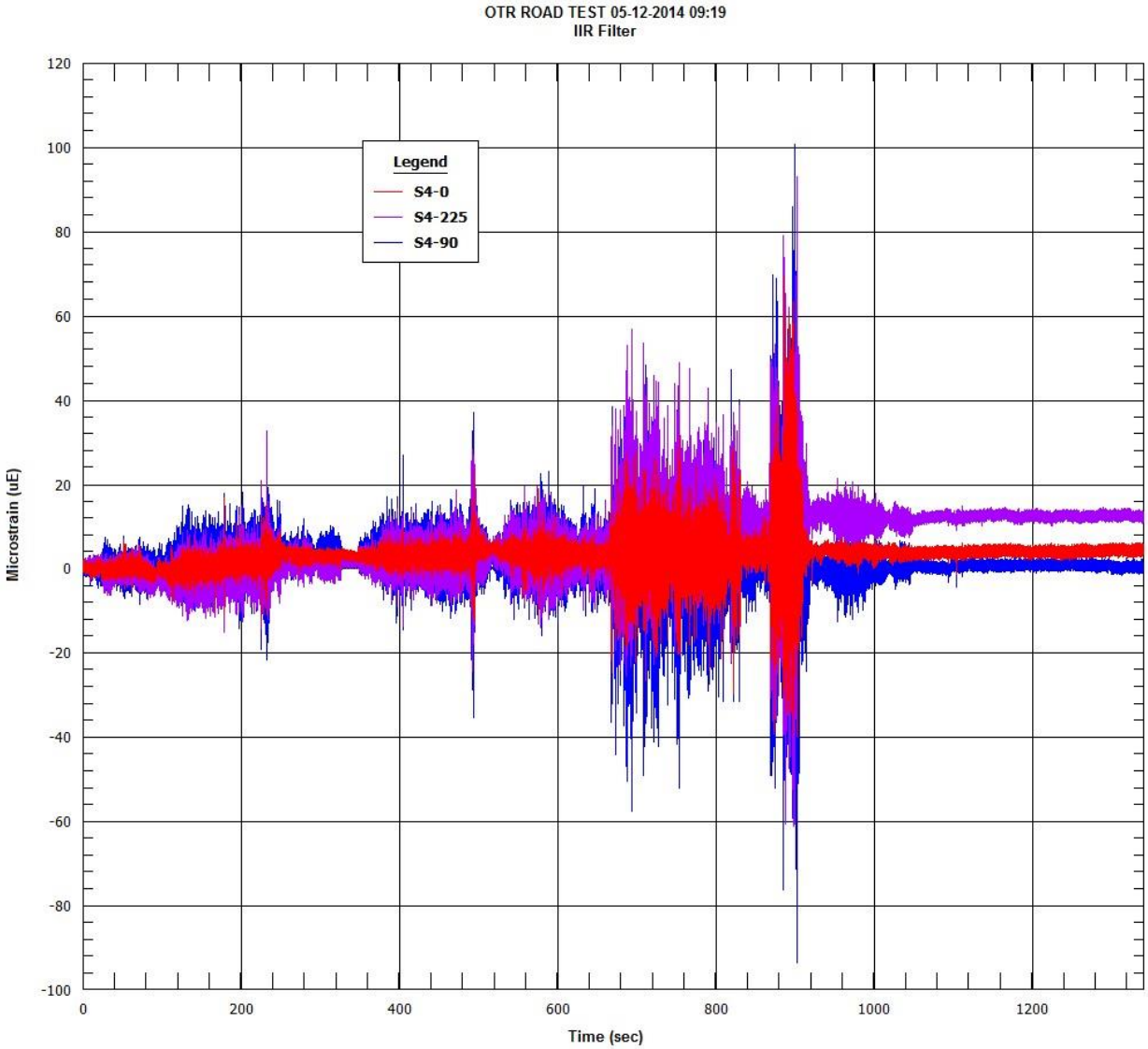

Figure 8.1 Segment 1 strain gauge time-histories

8.1.2 Strain Gauge Fast Fourier Transformations (με/Hz versus Hz)

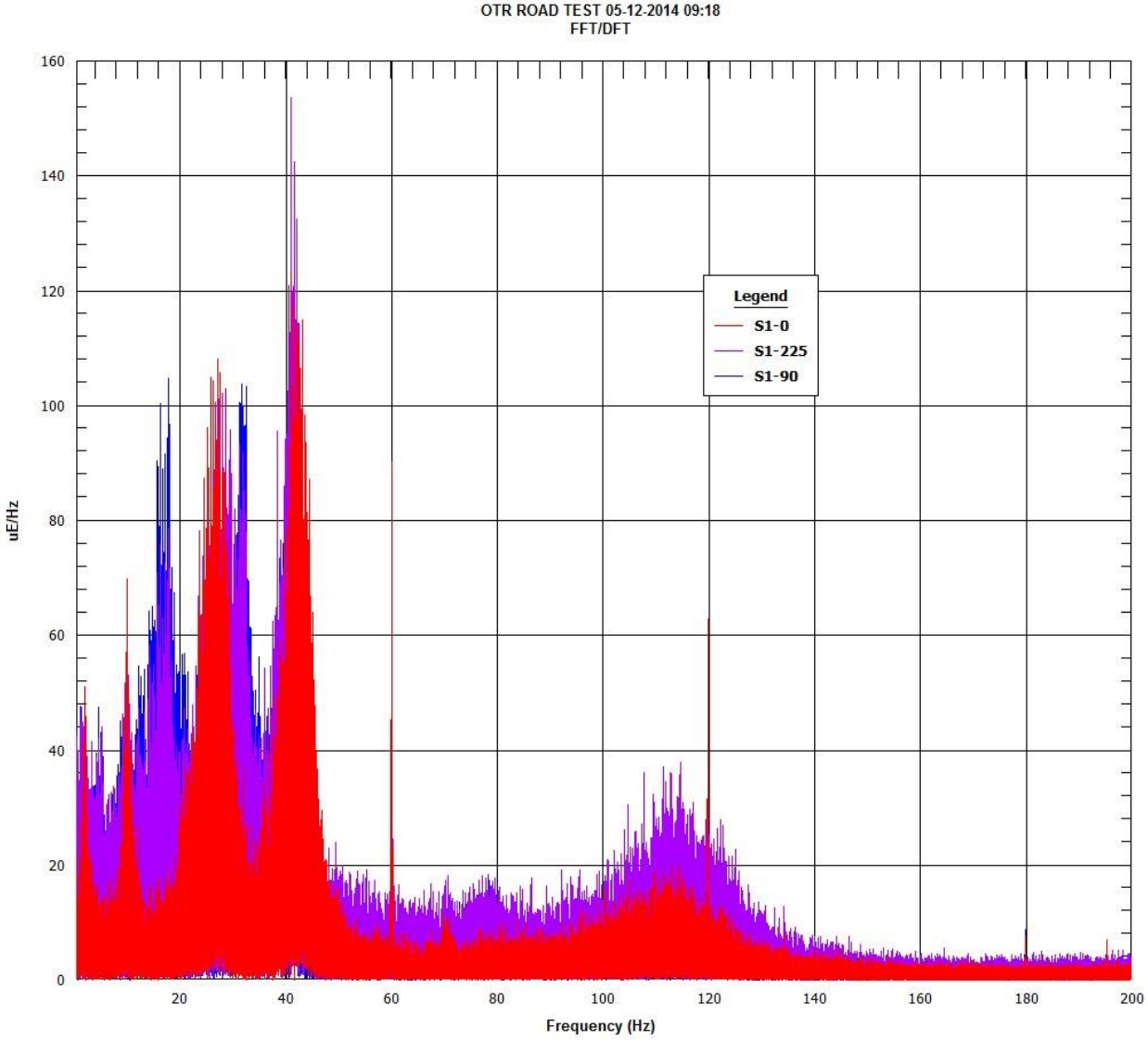

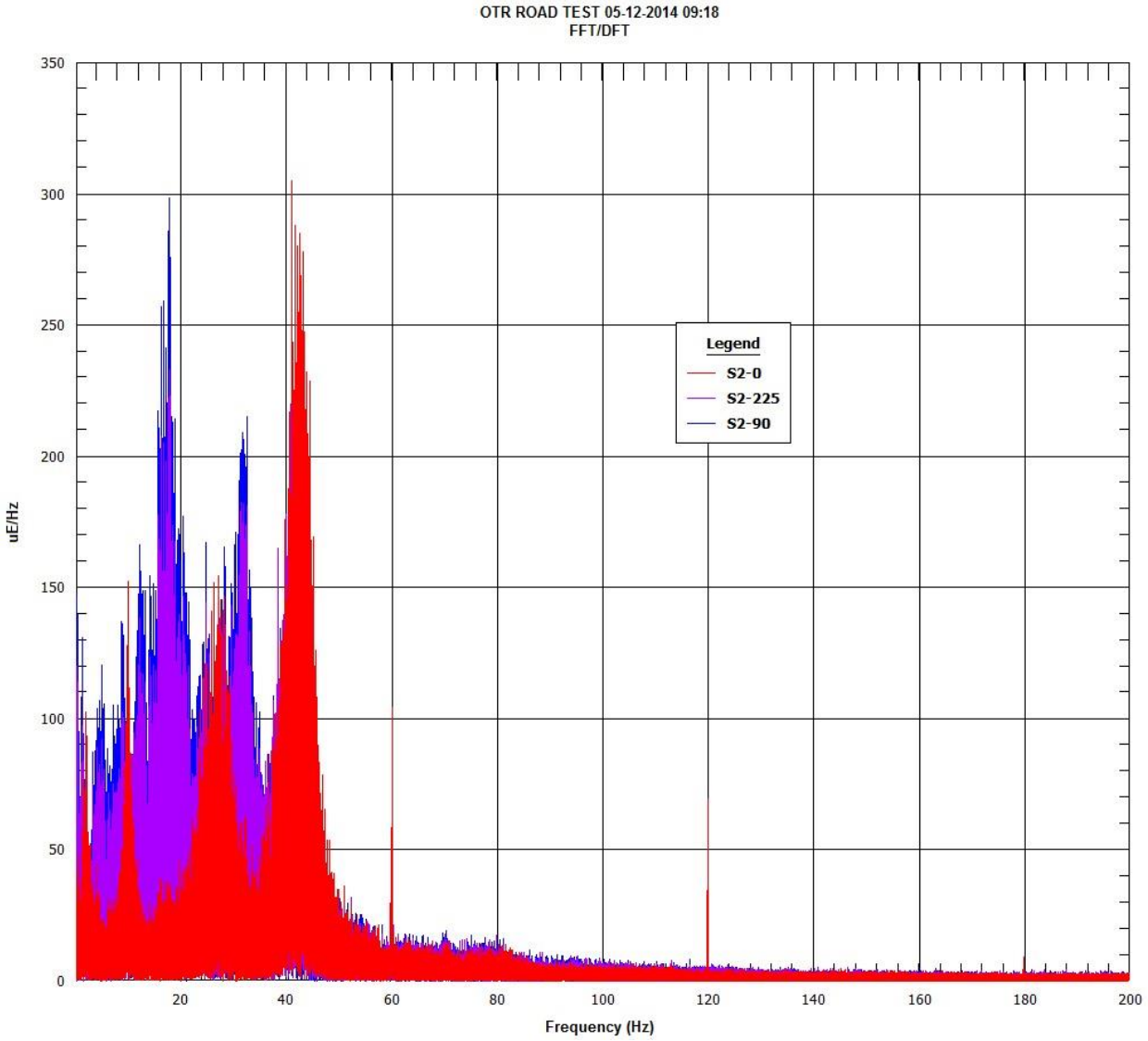
OTR ROAD TEST 05-12-2014 09:18
FFT/DFT
uE/Hz
Frequency (Hz)
Legend
S2-0
S2-225
S2-90
0
50
100
150
200
250
300
350
20
40
60
80
100
120
140
160
180
200

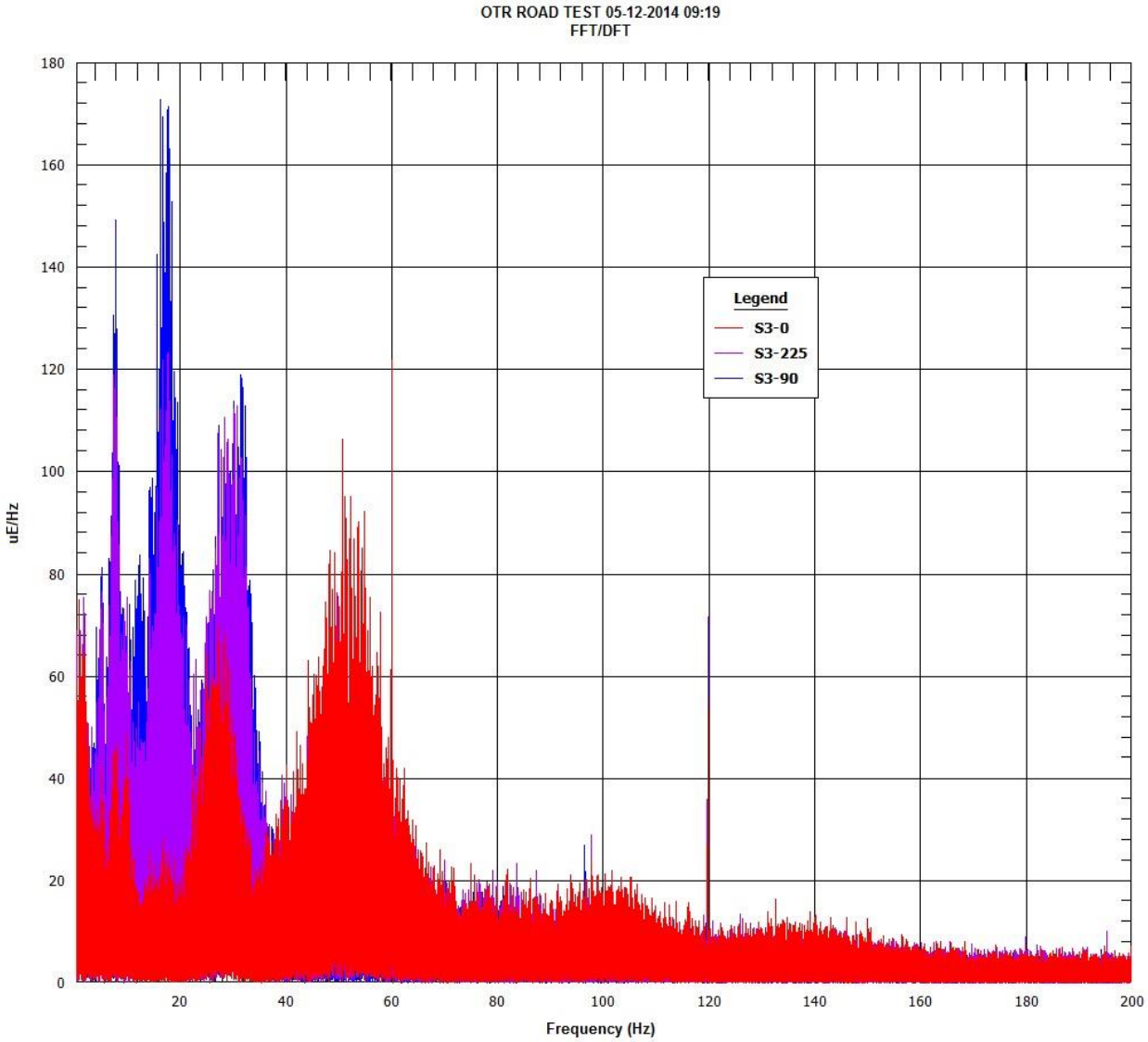
OTR ROAD TEST 05-12-2014 09:19
FFT/DFT
Legend
S3-0
S3-225
S3-90
uE/Hz
Frequency (Hz)
0
20
40
60
80
100
120
140
160
180
200

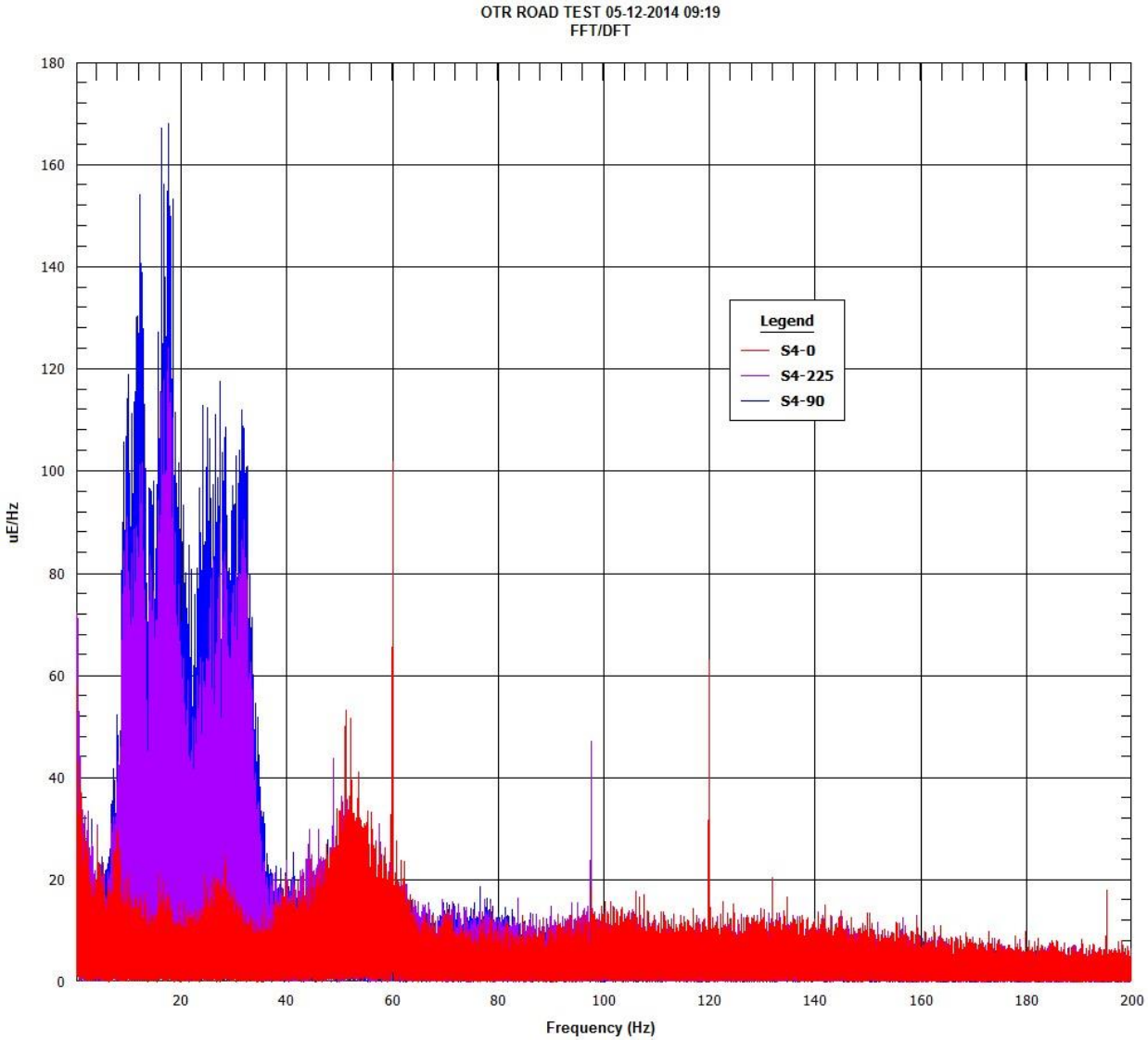

Figure 8.2 Segment 1 strain gauge FFTs

8.1.3 Accelerometer Time-Histories (g versus time)

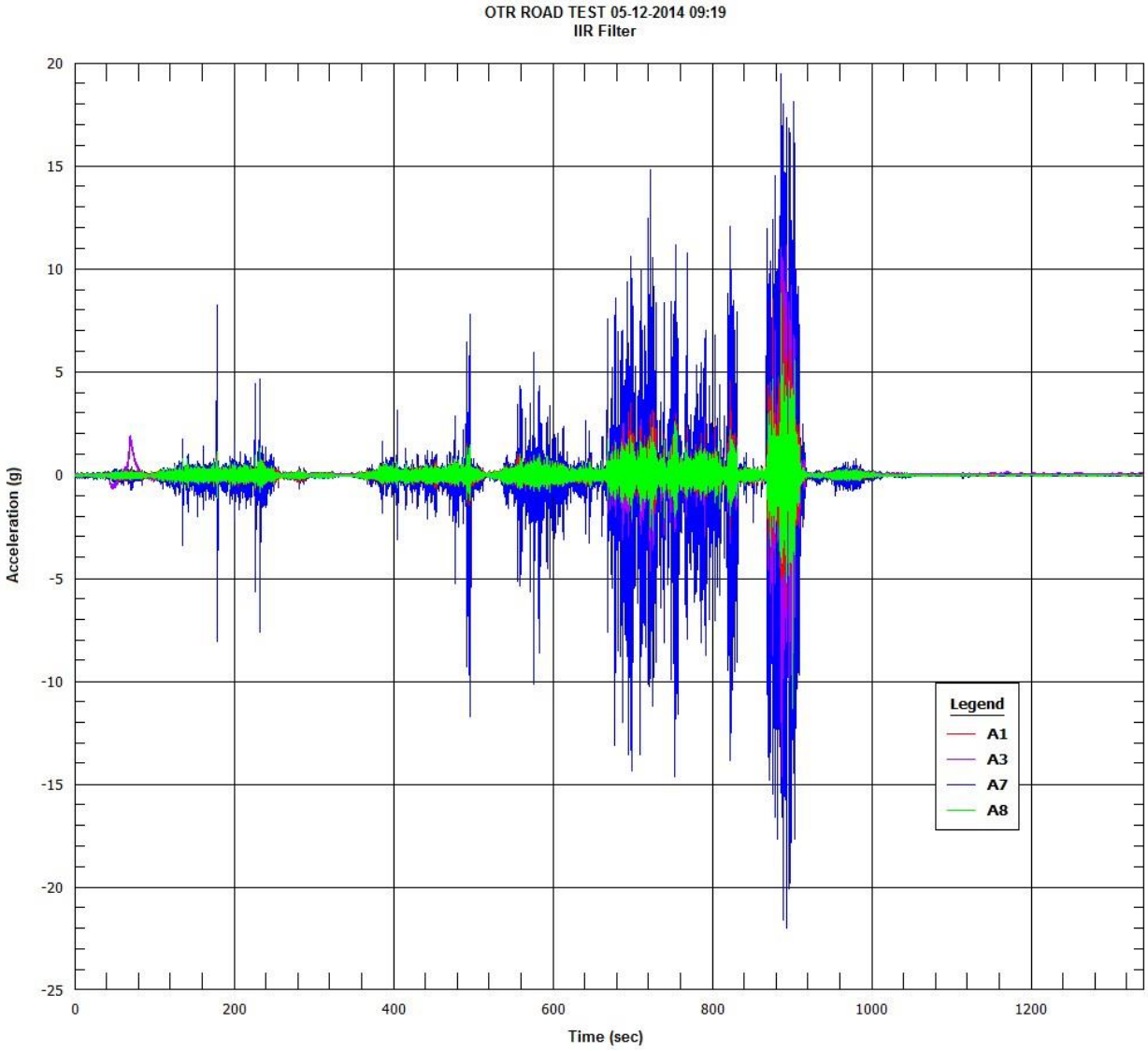

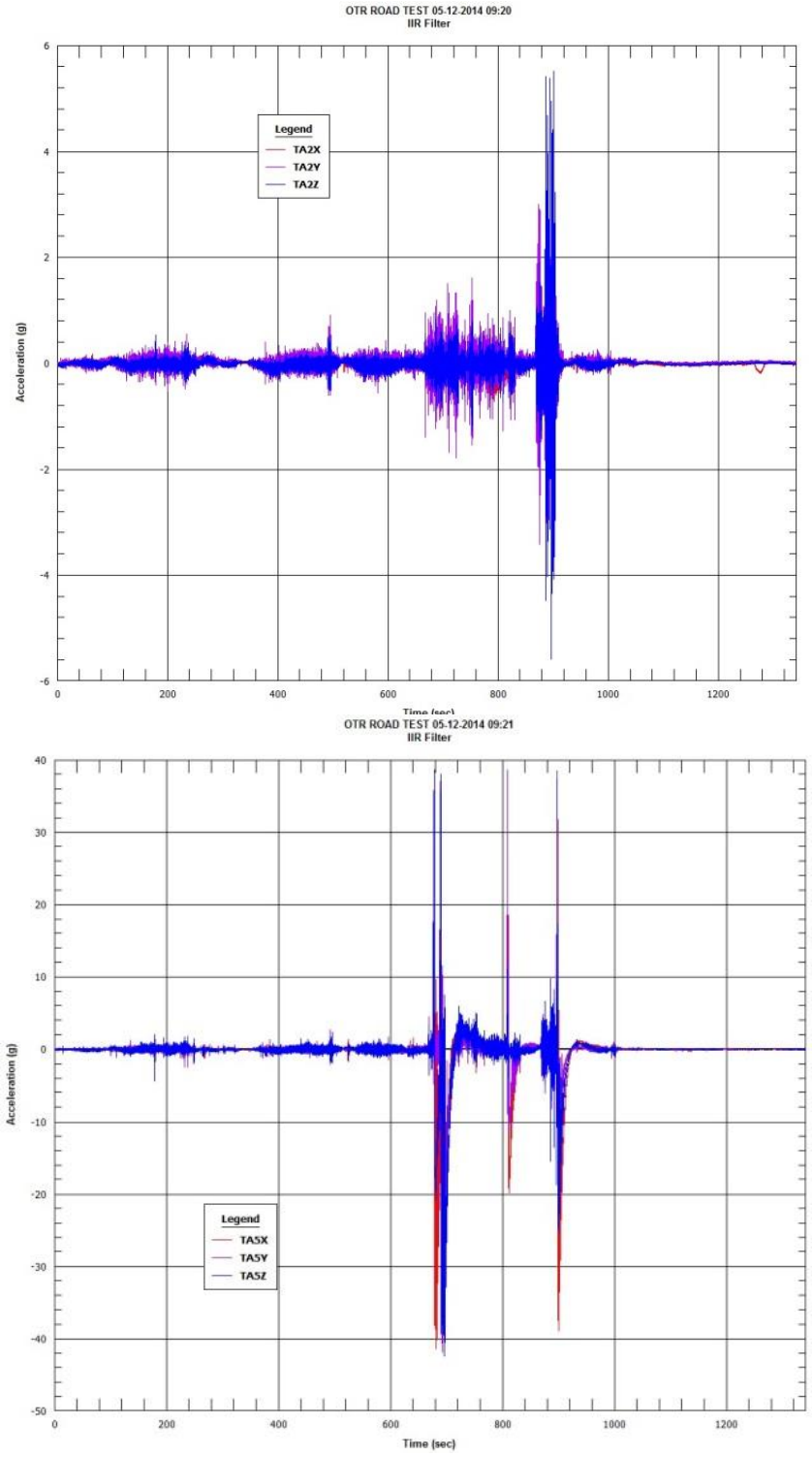

Figure 8.3 Segment 1 accelerometer time-histories

8.1.4 Accelerometer Fast Fourier Transformations (g/Hz versus Hz)

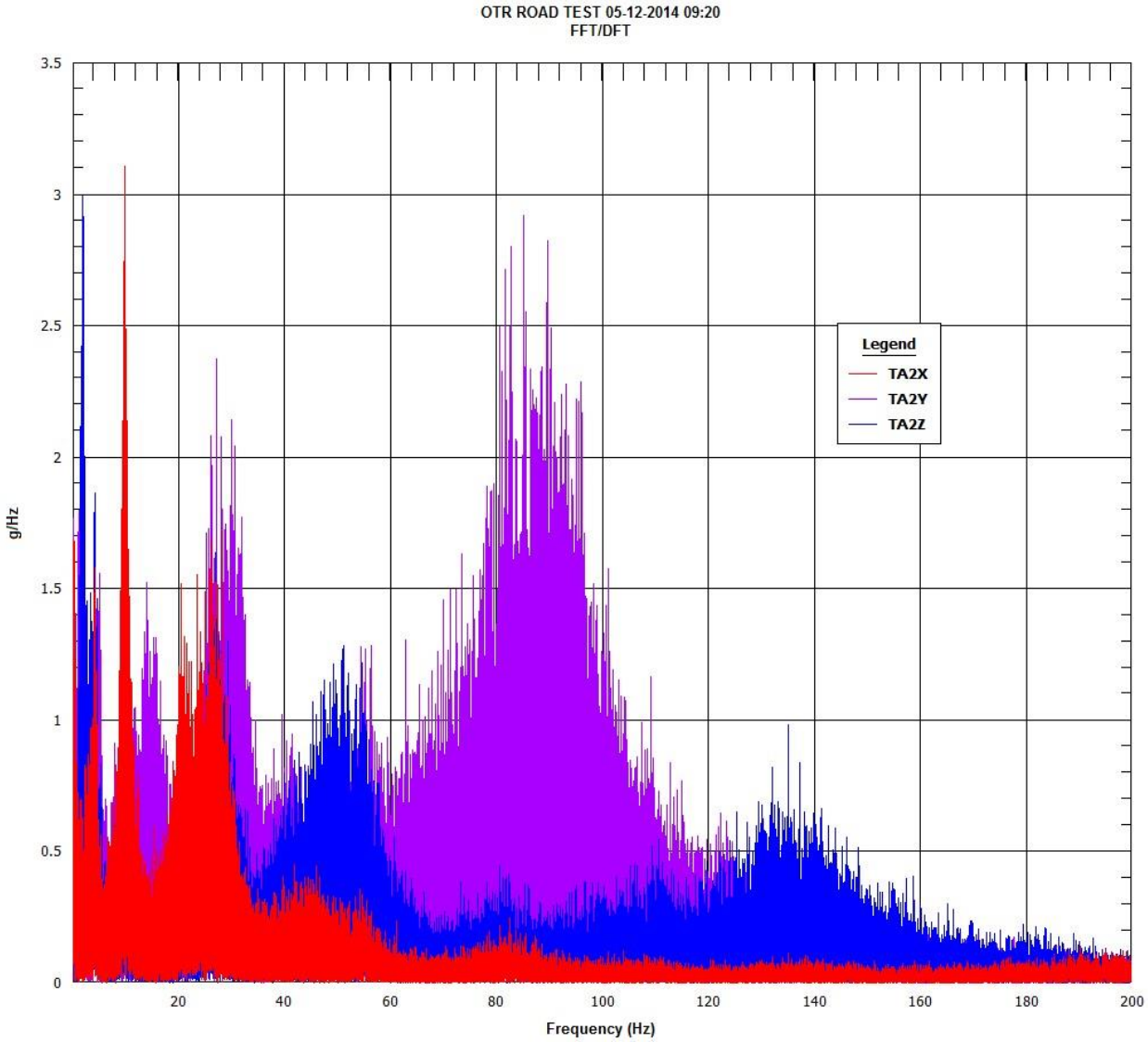

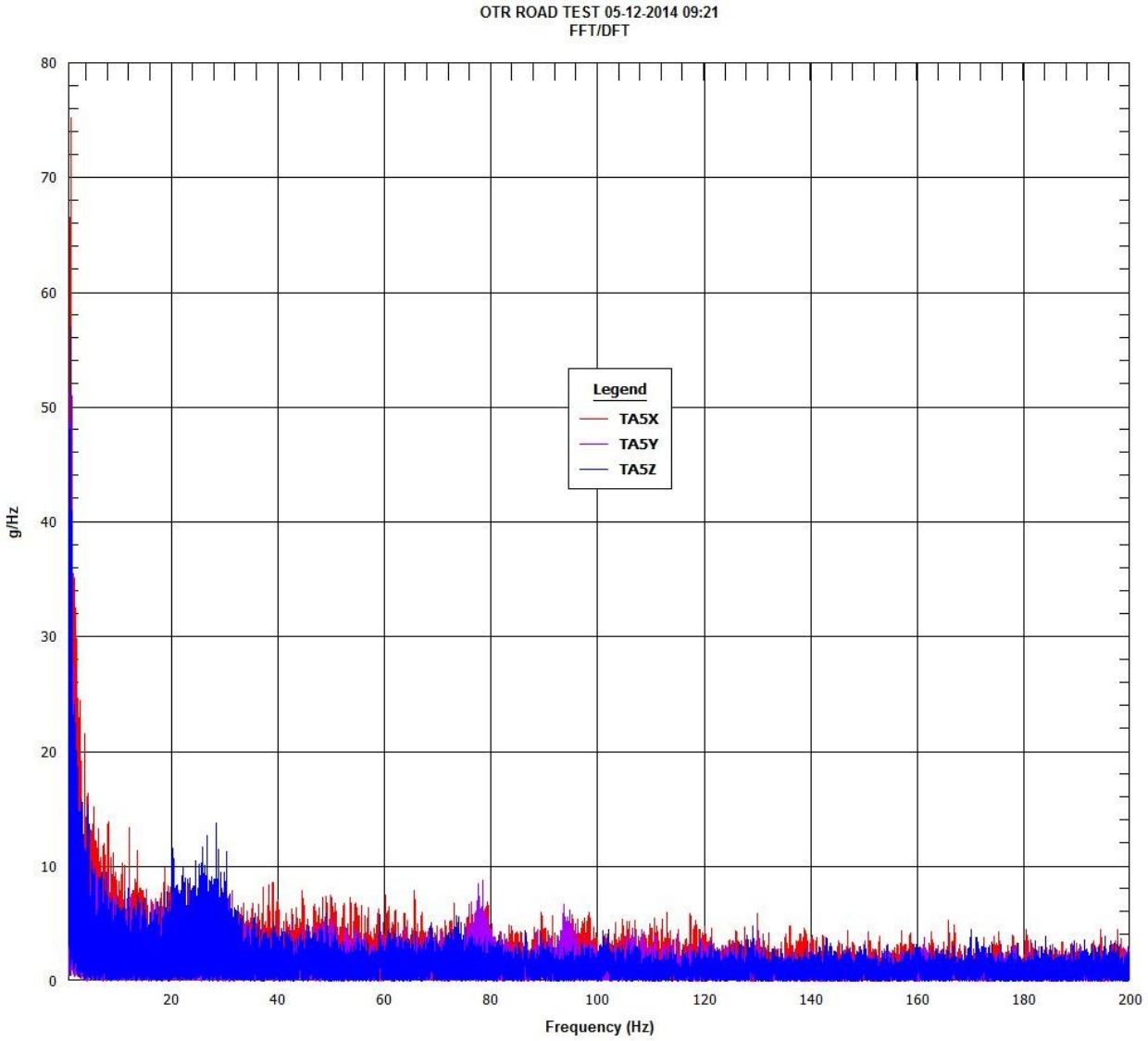
OTR ROAD TEST 05-12-2014 09:21
FFT/DFT
g/Hz
Frequency (Hz)
Legend
TA5X
TA5Y
TA5Z
0
10
20
30
40
50
60
70
80
20
40
60
80
100
120
140
160
180
200

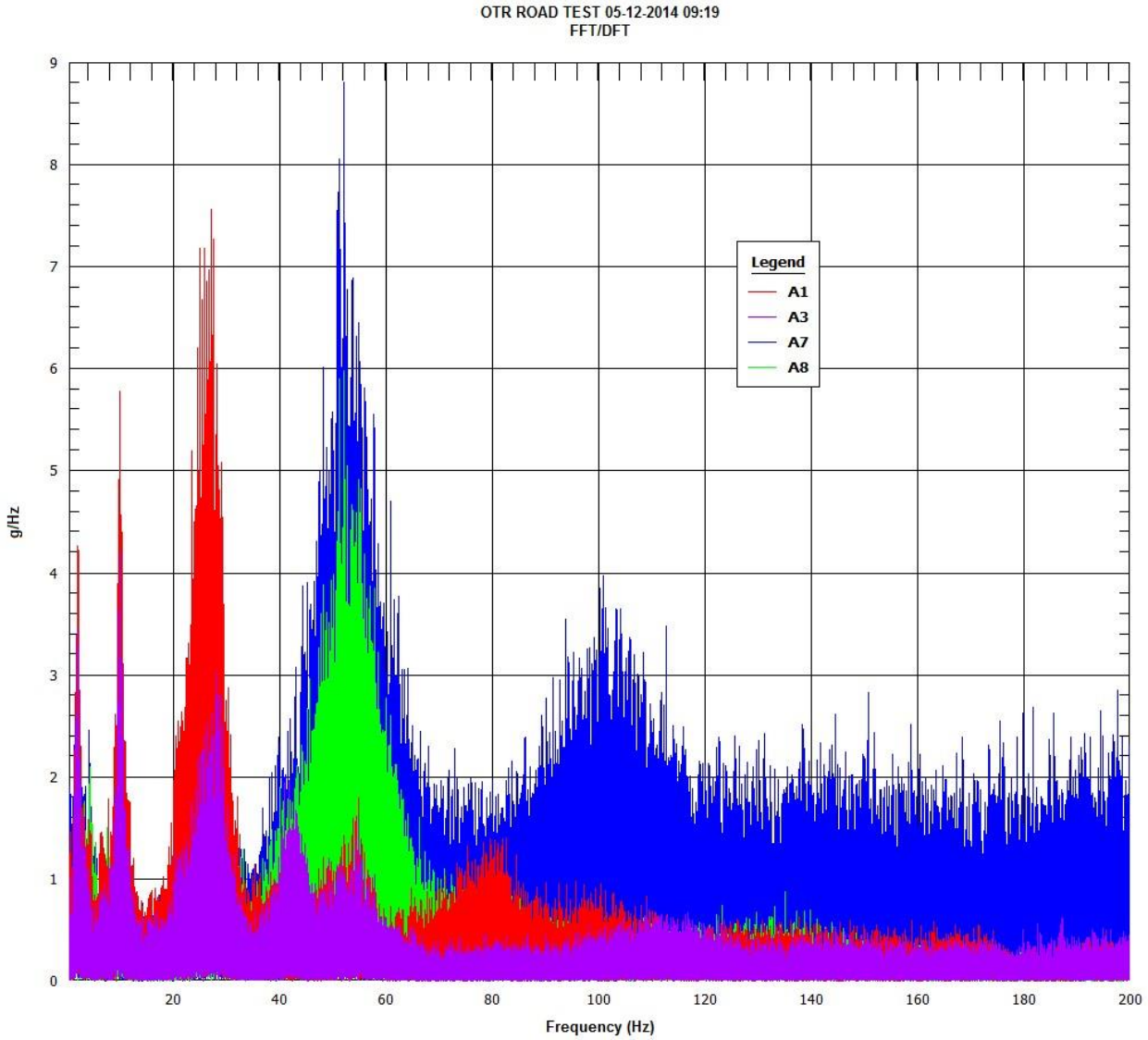

Figure 8.4 Segment 1 accelerometer FFTs

8.2 Truck Route Segment 2 Data Plots

8.2.1 Strain Gauge Time-Histories (με versus time)

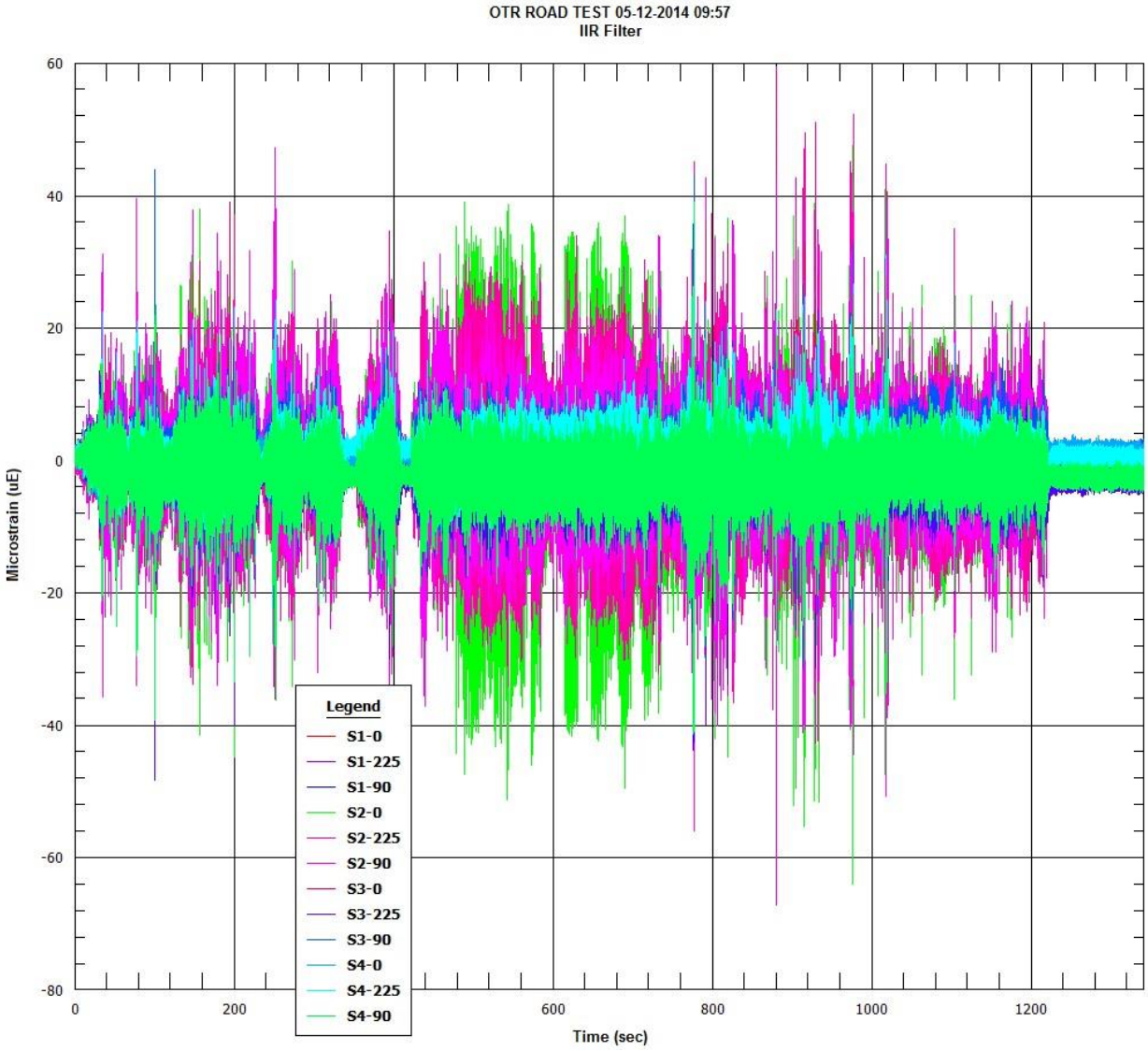

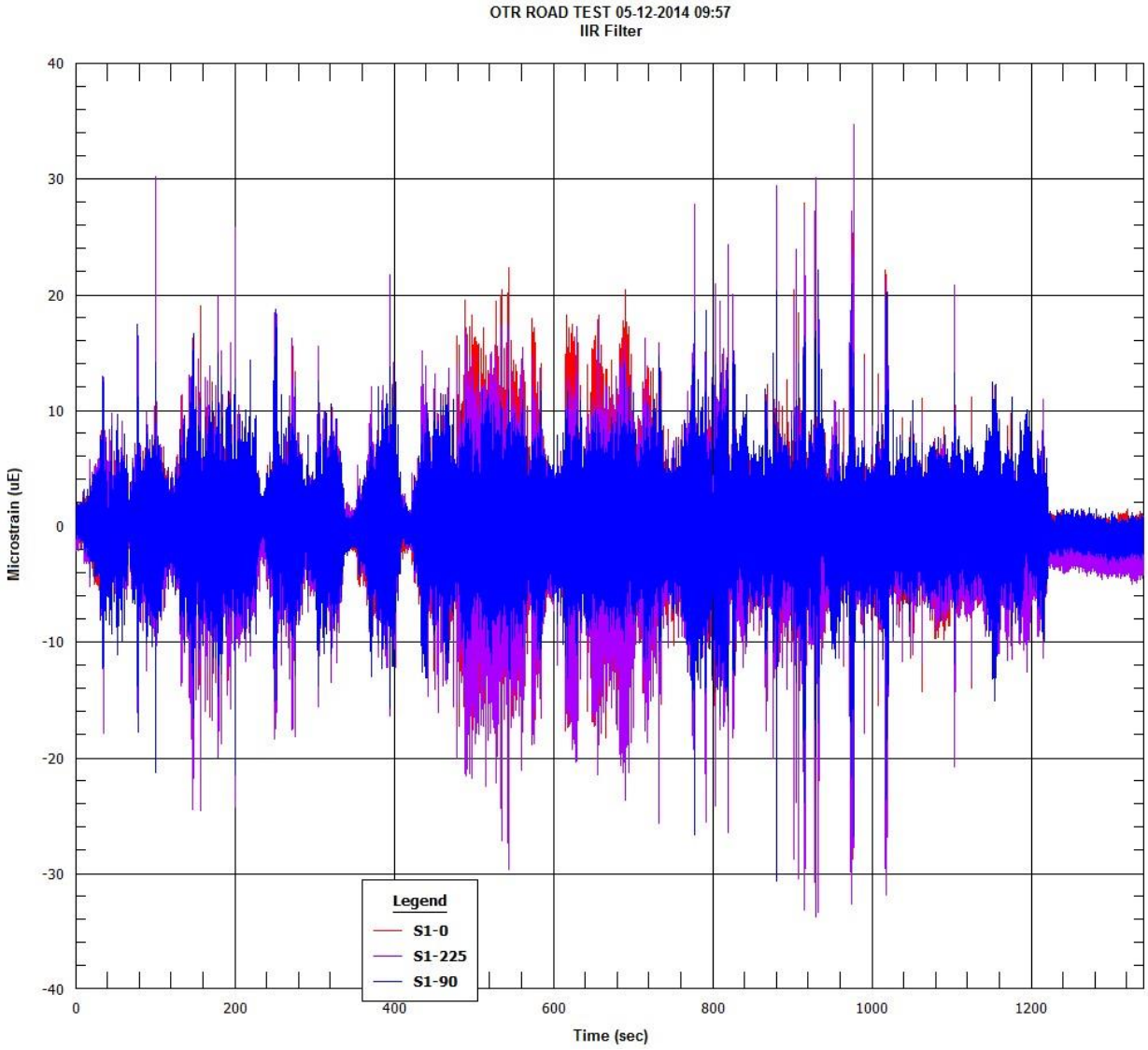
OTR ROAD TEST 05-12-2014 09:57
IIR Filter
Microstrain (uE)
Time (sec)
Legend
S1-0
S1-225
S1-90
40
30
20
10
0
-10
-20
-30
-40
0
200
400
600
800
1000
1200

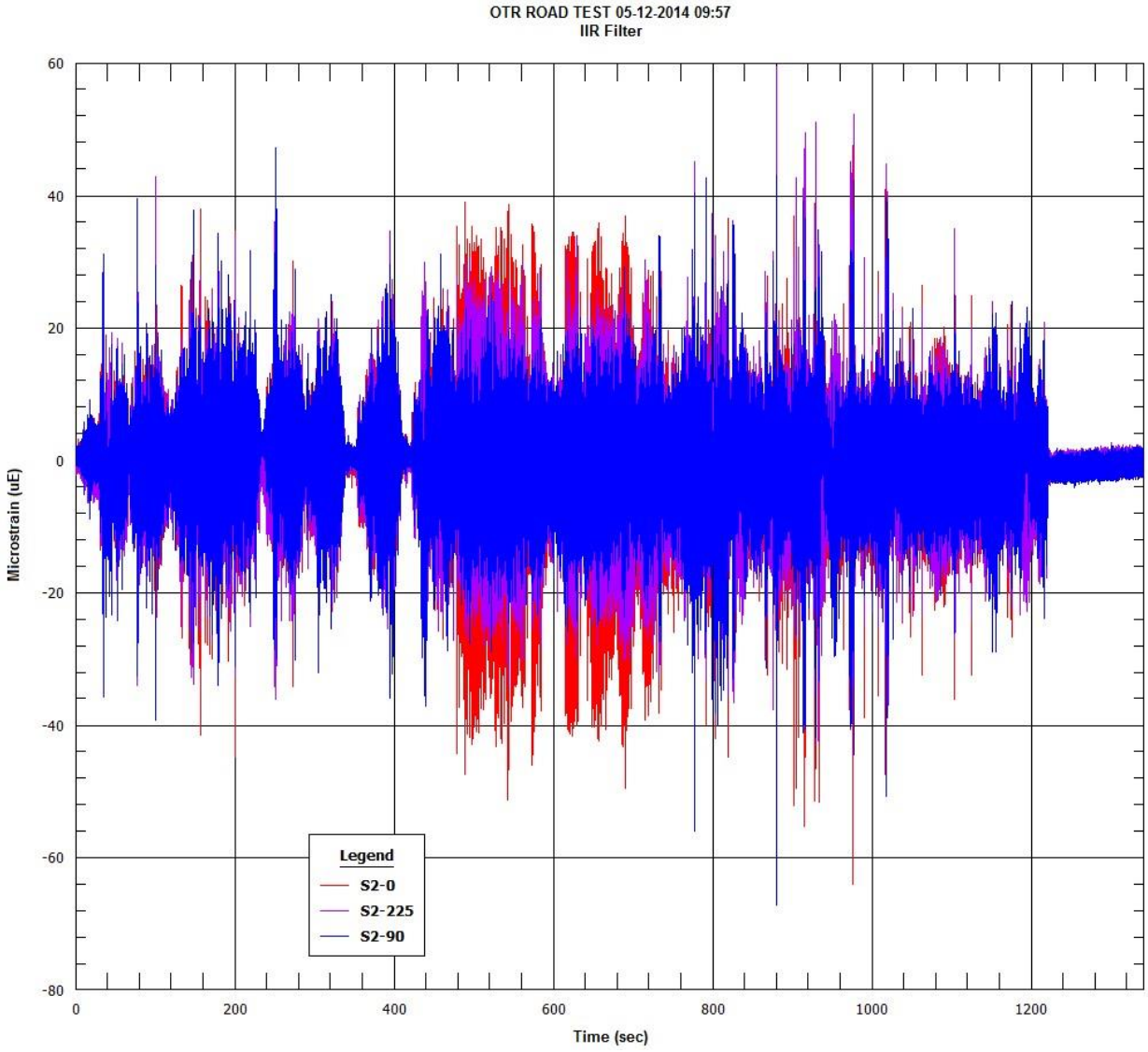
OTR ROAD TEST 05-12-2014 09:57
IIR Filter
Microstrain (uE)
Time (sec)
60
40
20
0
-20
-40
-60
-80
0
200
400
600
800
1000
1200
Legend
S2-0
S2-225
S2-90

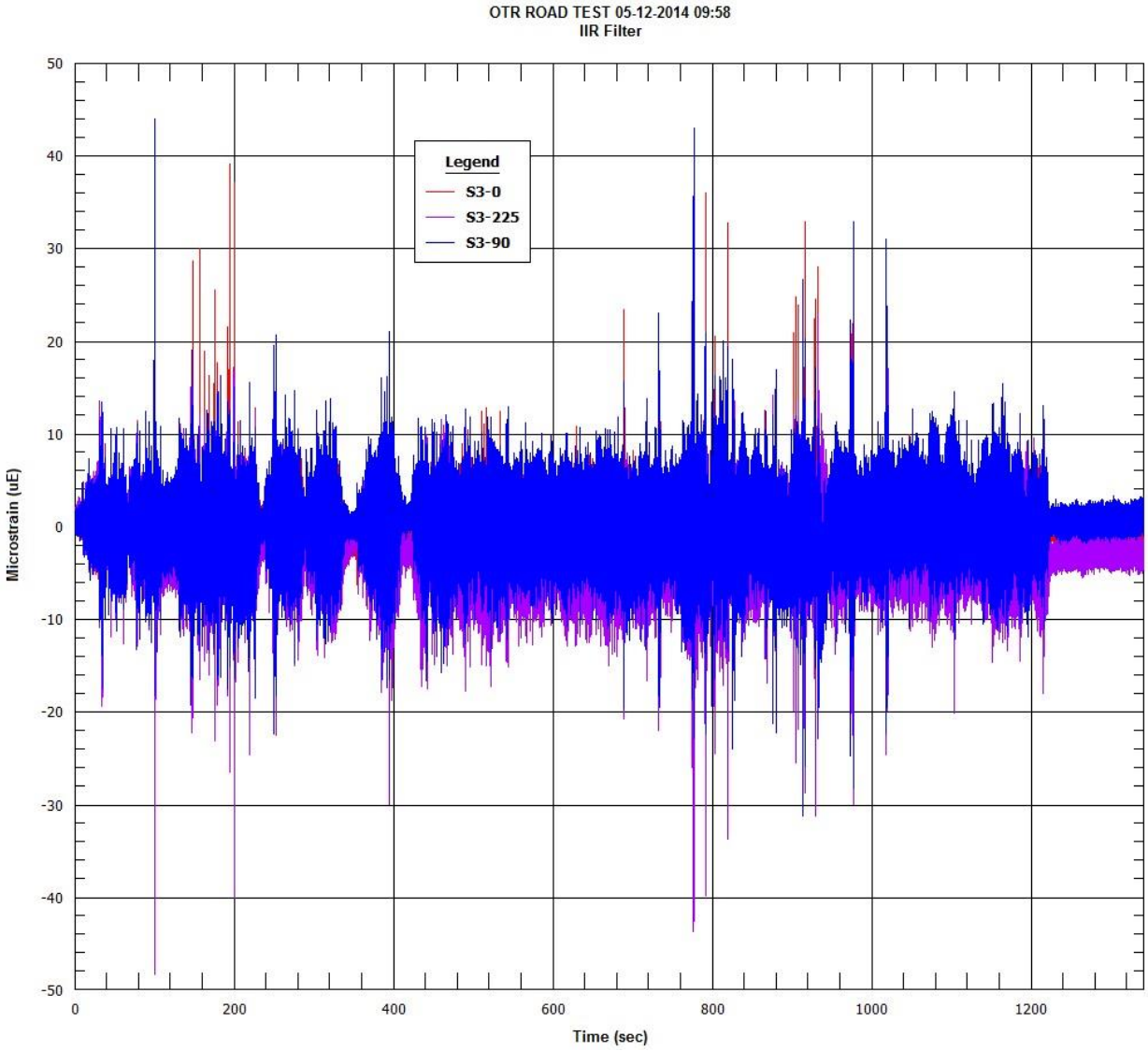
OTR ROAD TEST 05-12-2014 09:58
IIR Filter
Legend
S3-0
S3-225
S3-90
Microstrain (uE)
Time (sec)
50
40
30
20
10
0
-10
-20
-30
-40
-50
0
200
400
600
800
1000
1200

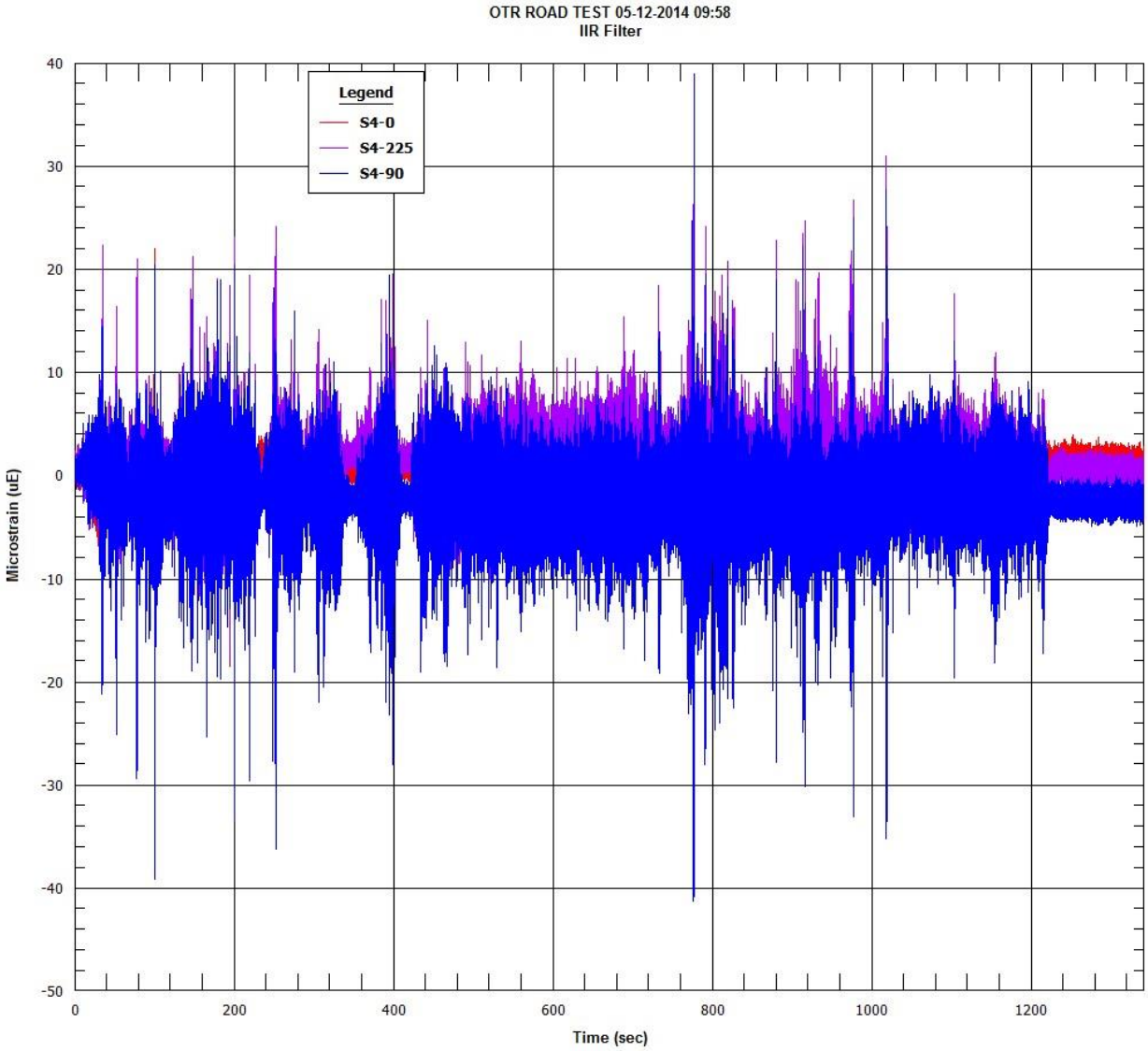

Figure 8.5 Segment 2 strain gauge time-histories

8.2.2 Strain Gauge Fast Fourier Transformations (με/Hz versus Hz)

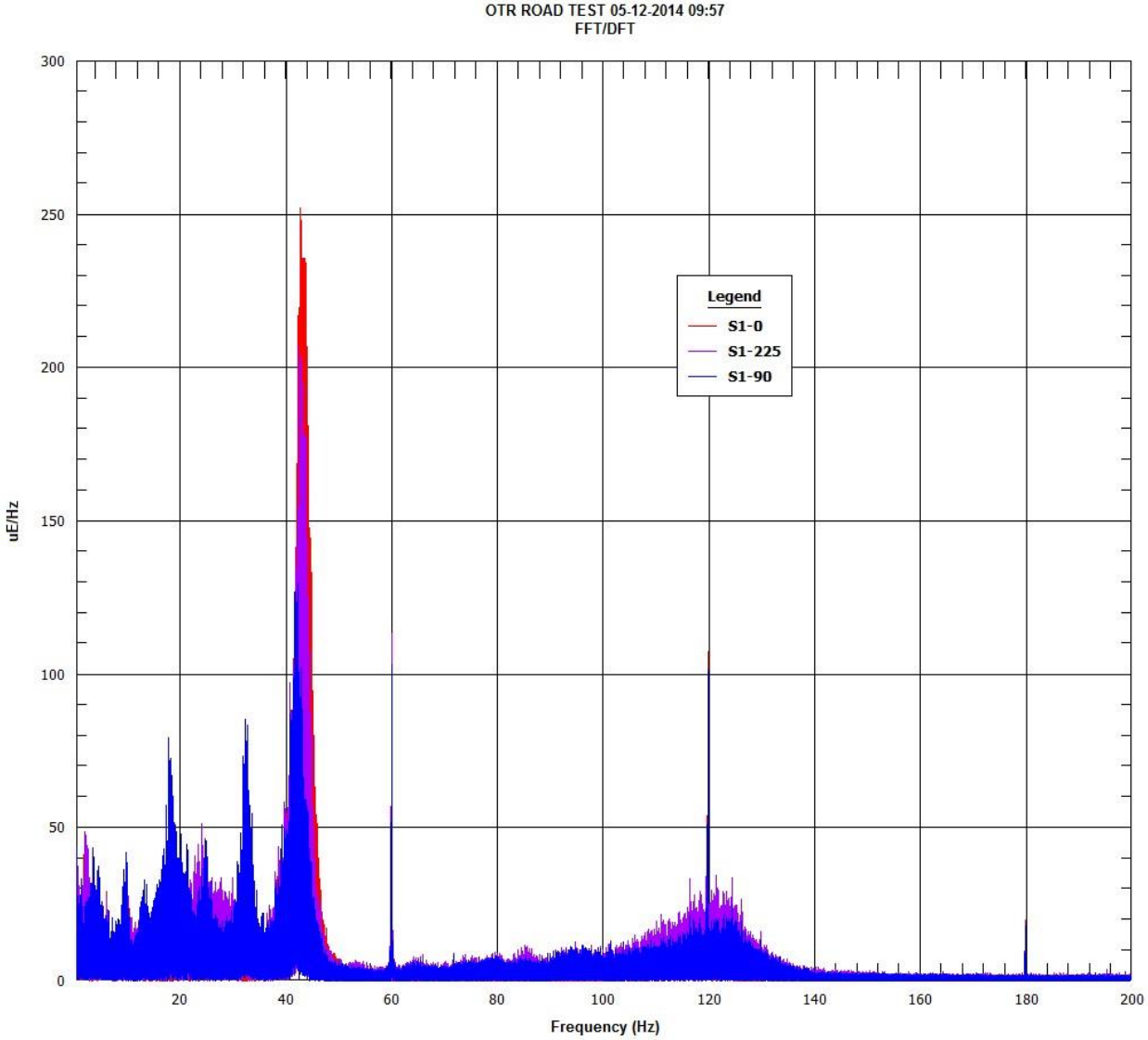

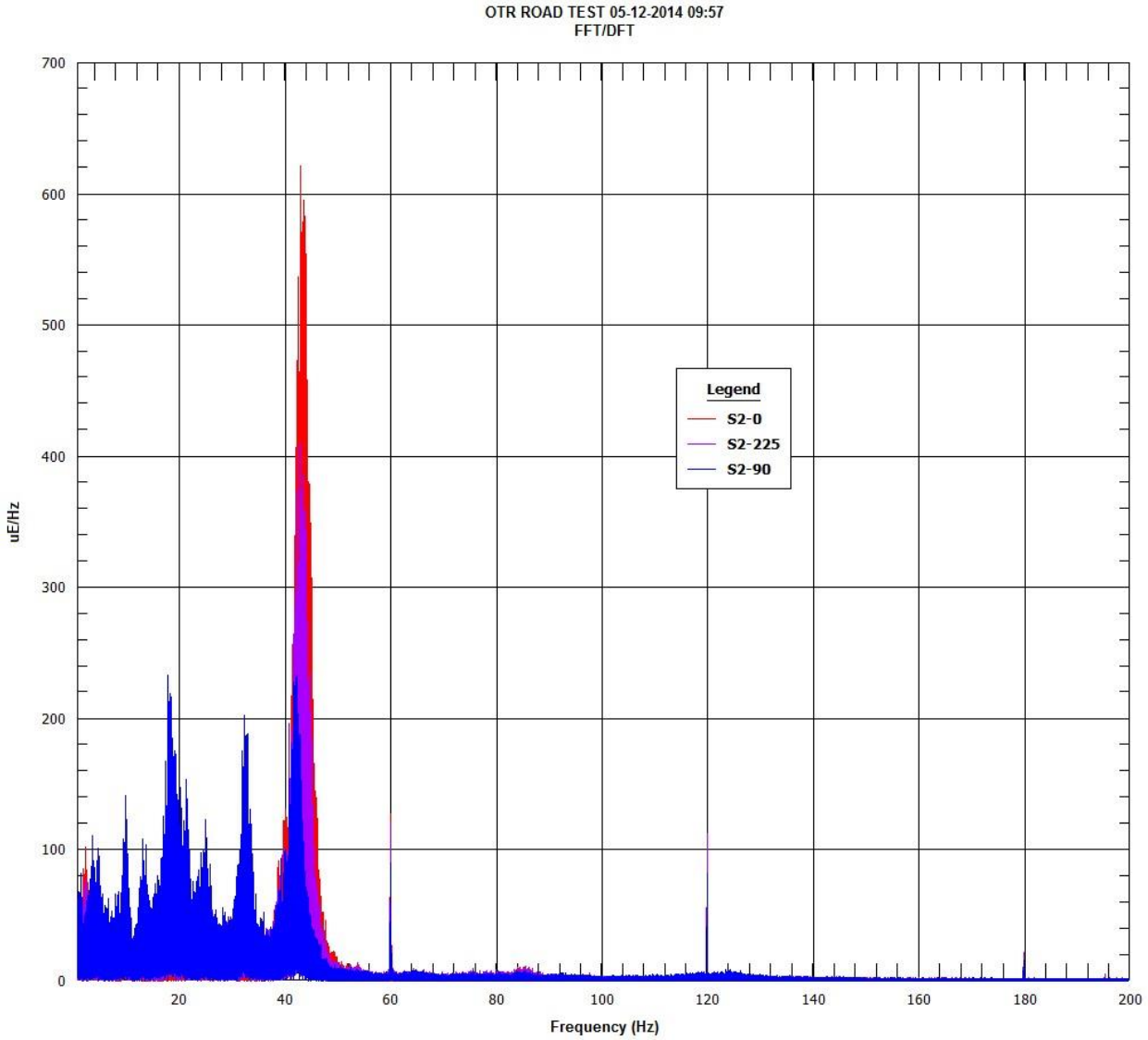
OTR ROAD TEST 05-12-2014 09:57
FFT/DFT
uE/Hz
Frequency (Hz)
Legend
S2-0
S2-225
S2-90
0
100
200
300
400
500
600
700
20
40
60
80
100
120
140
160
180
200

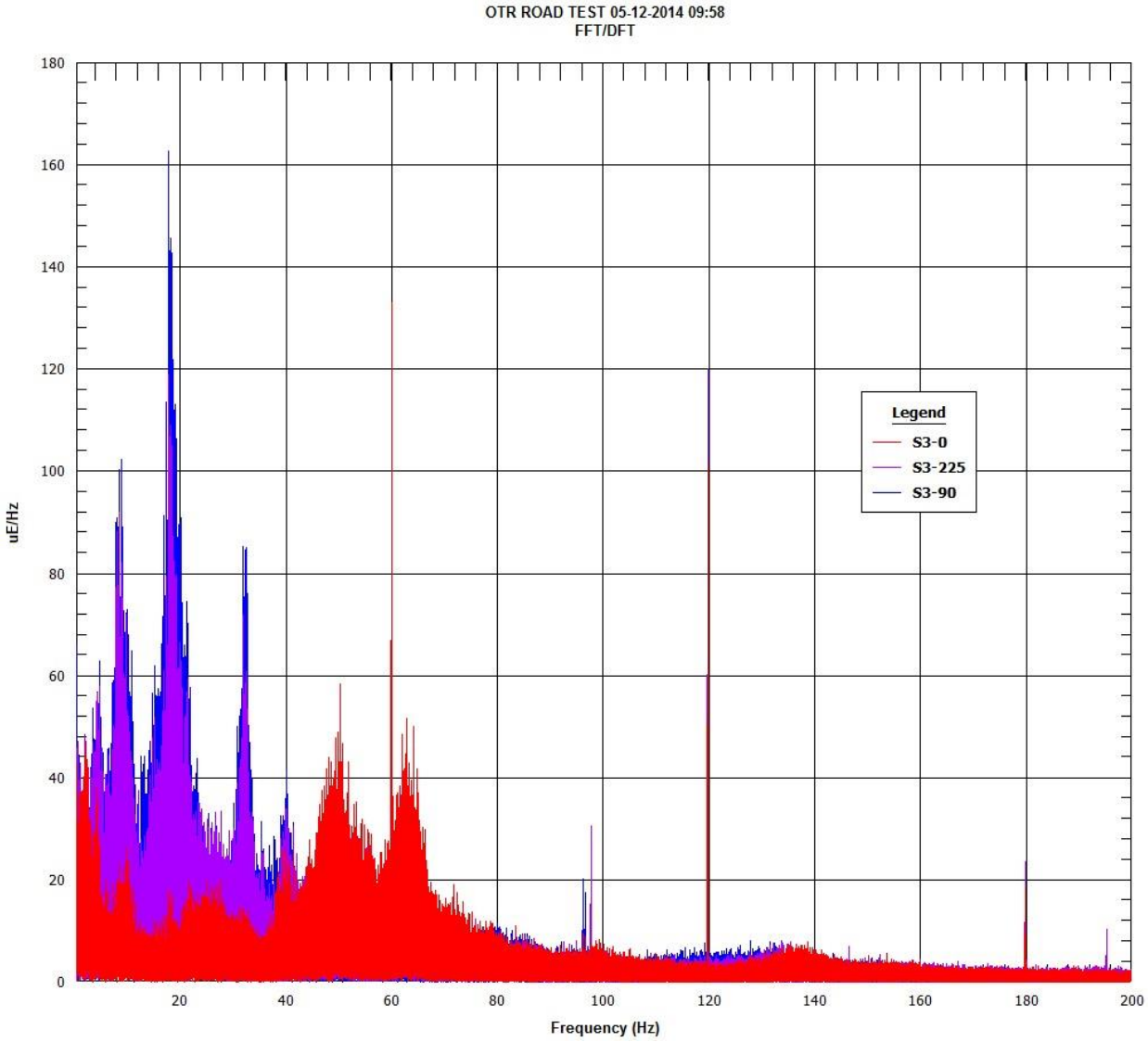
OTR ROAD TEST 05-12-2014 09:58
FFT/DFT
uE/Hz
Frequency (Hz)
Legend
S3-0
S3-225
S3-90
0
20
40
60
80
100
120
140
160
180
200

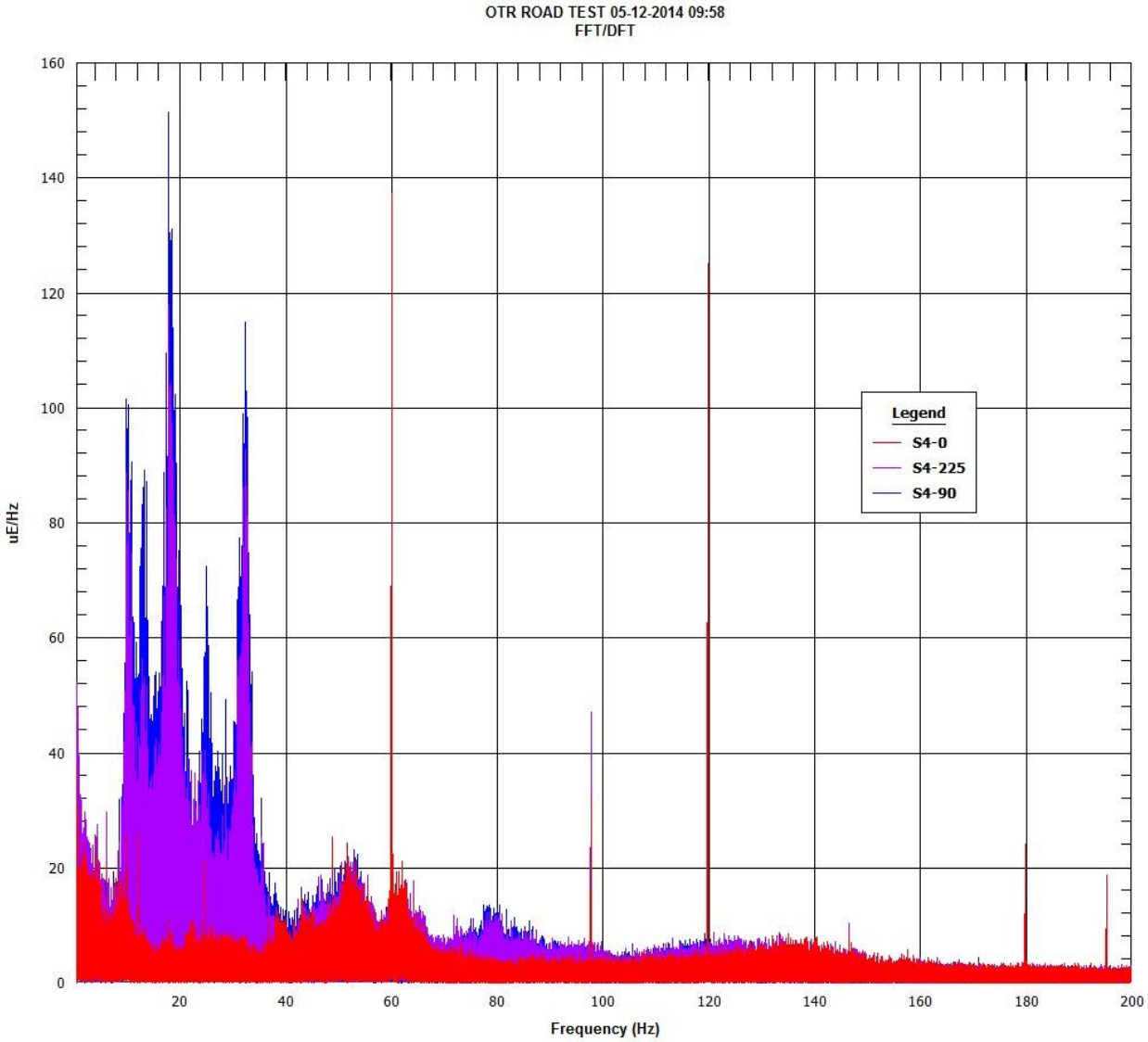

Figure 8.6 Segment 2 strain gauge FFTs

8.2.3 Accelerometer Time-Histories (g versus time)

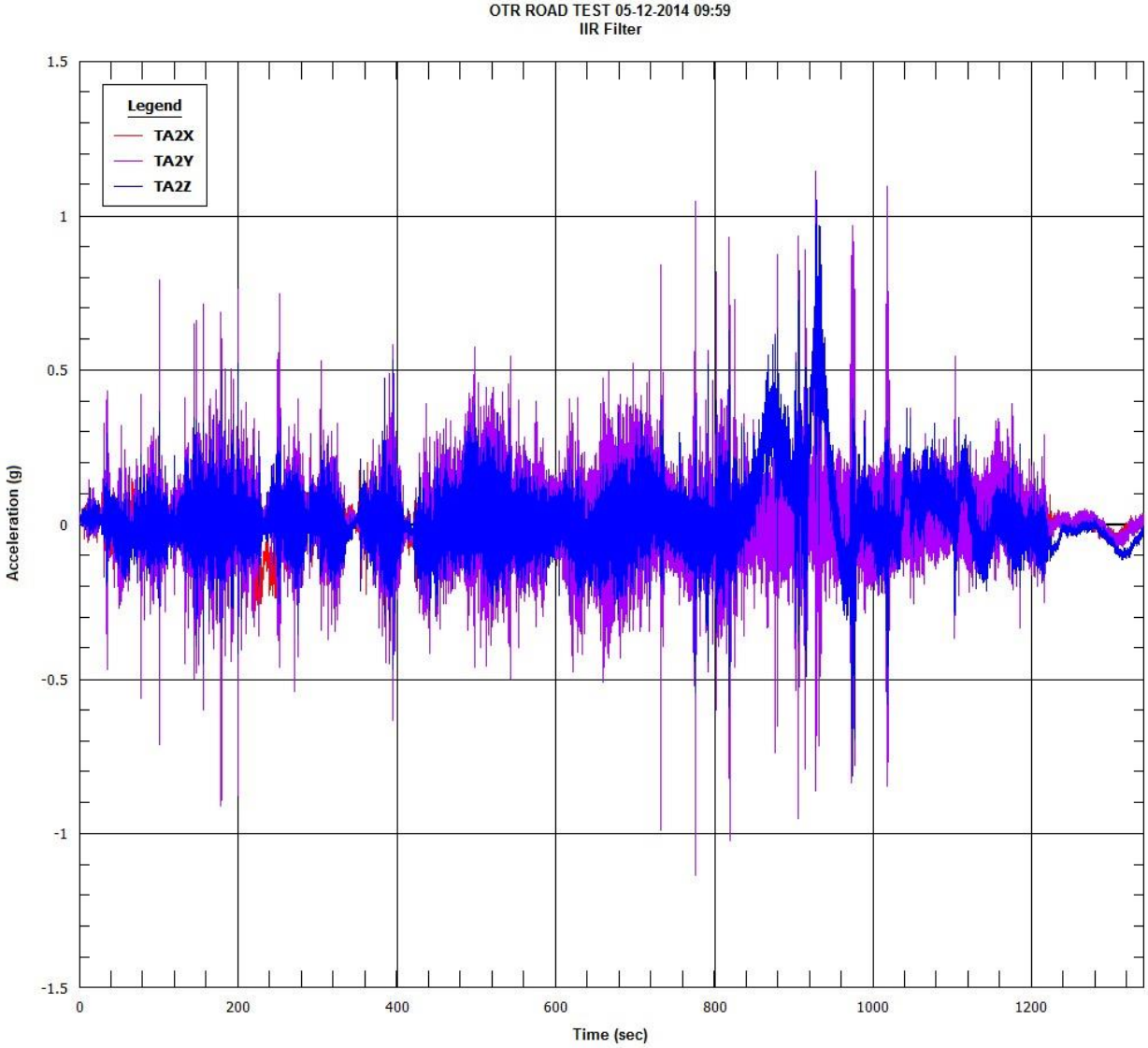

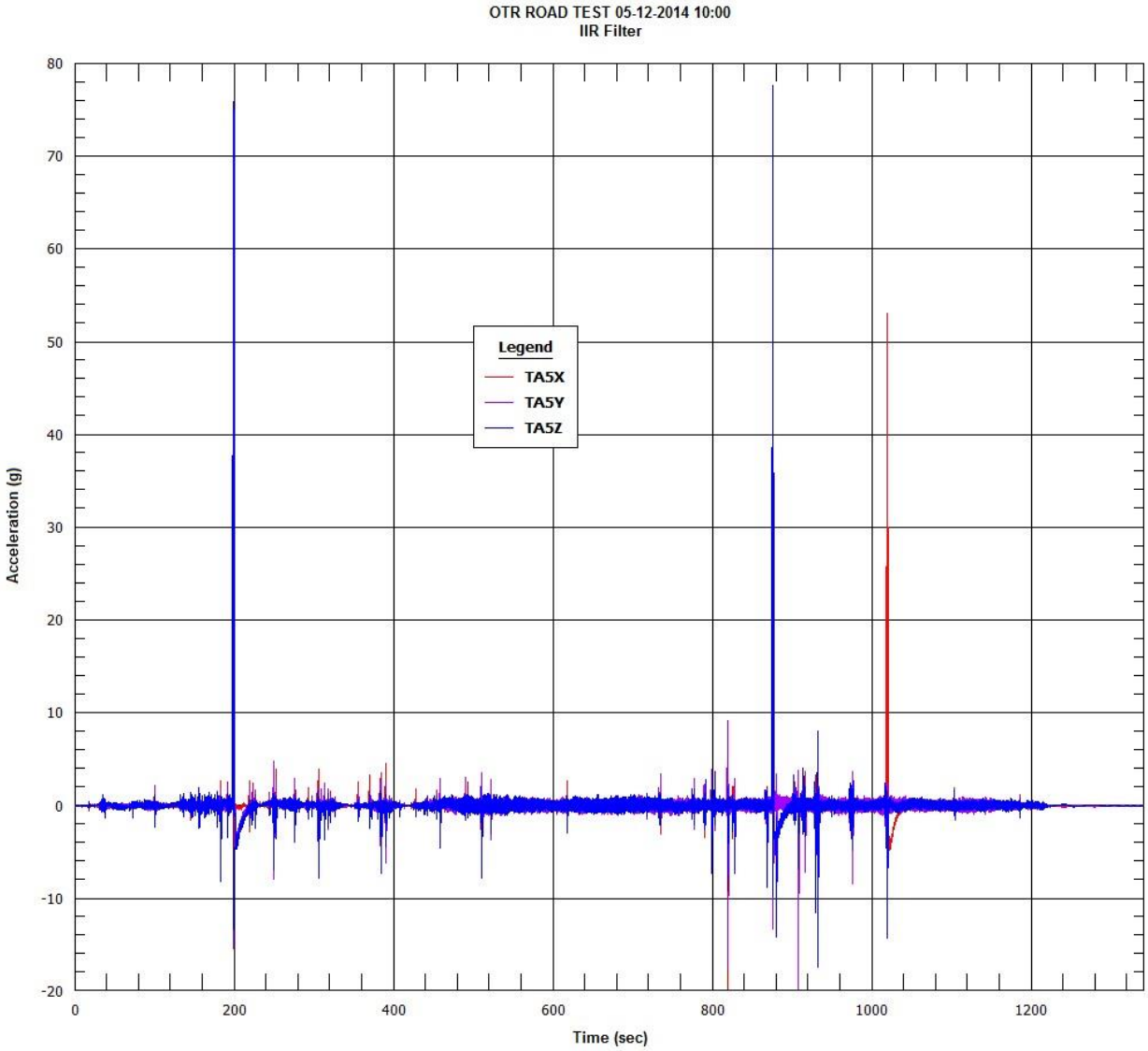
OTR ROAD TEST 05-12-2014 10:00
IIR Filter
Legend
TA5X
TA5Y
TA5Z
Acceleration (g)
Time (sec)
80
70
60
50
40
30
20
10
0
-10
-20
0
200
400
600
800
1000
1200

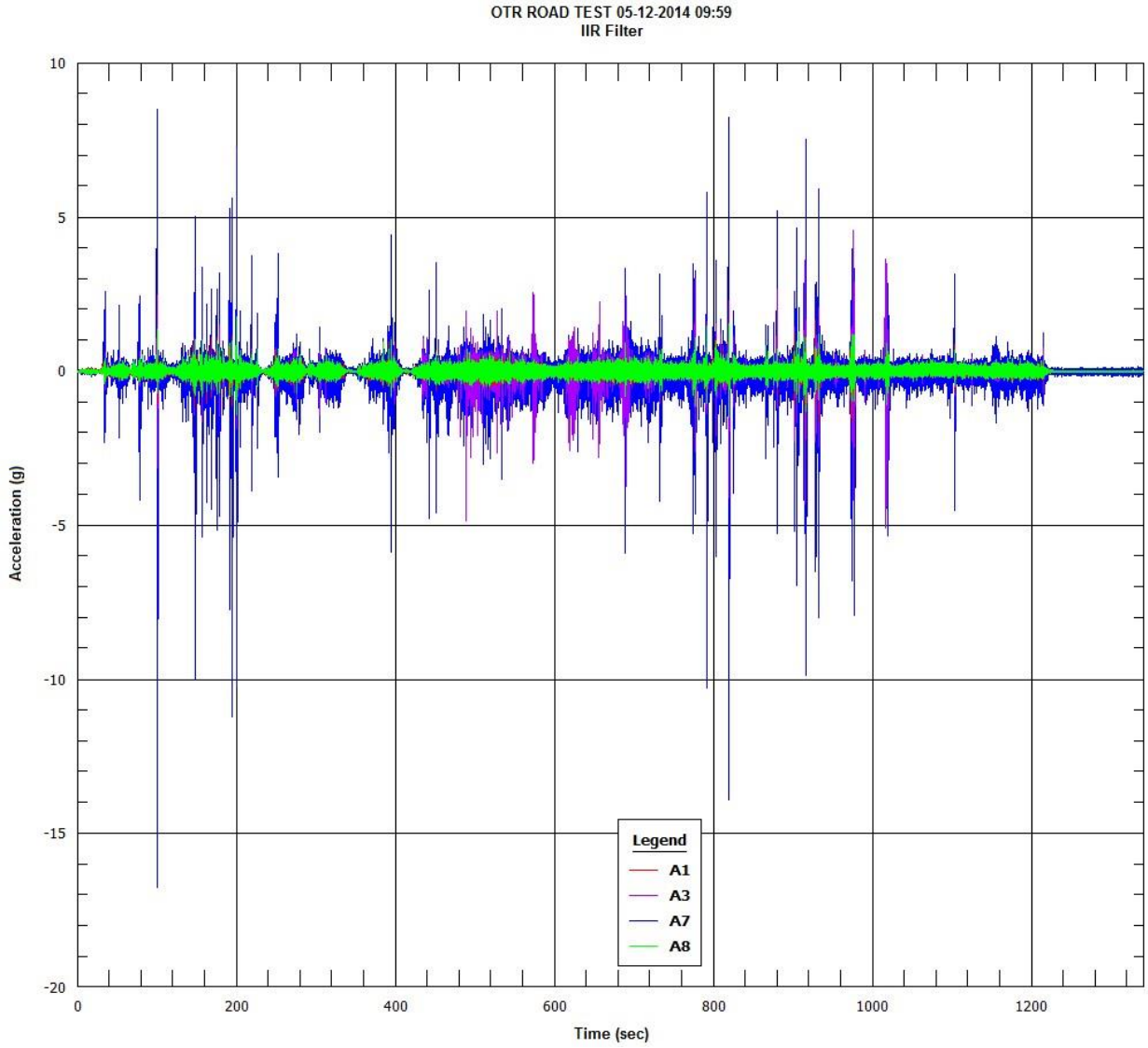

Figure 8.7 Segment 2 accelerometers time-histories

8.2.4 Accelerometer Fast Fourier Transformations (g/Hz versus Hz)

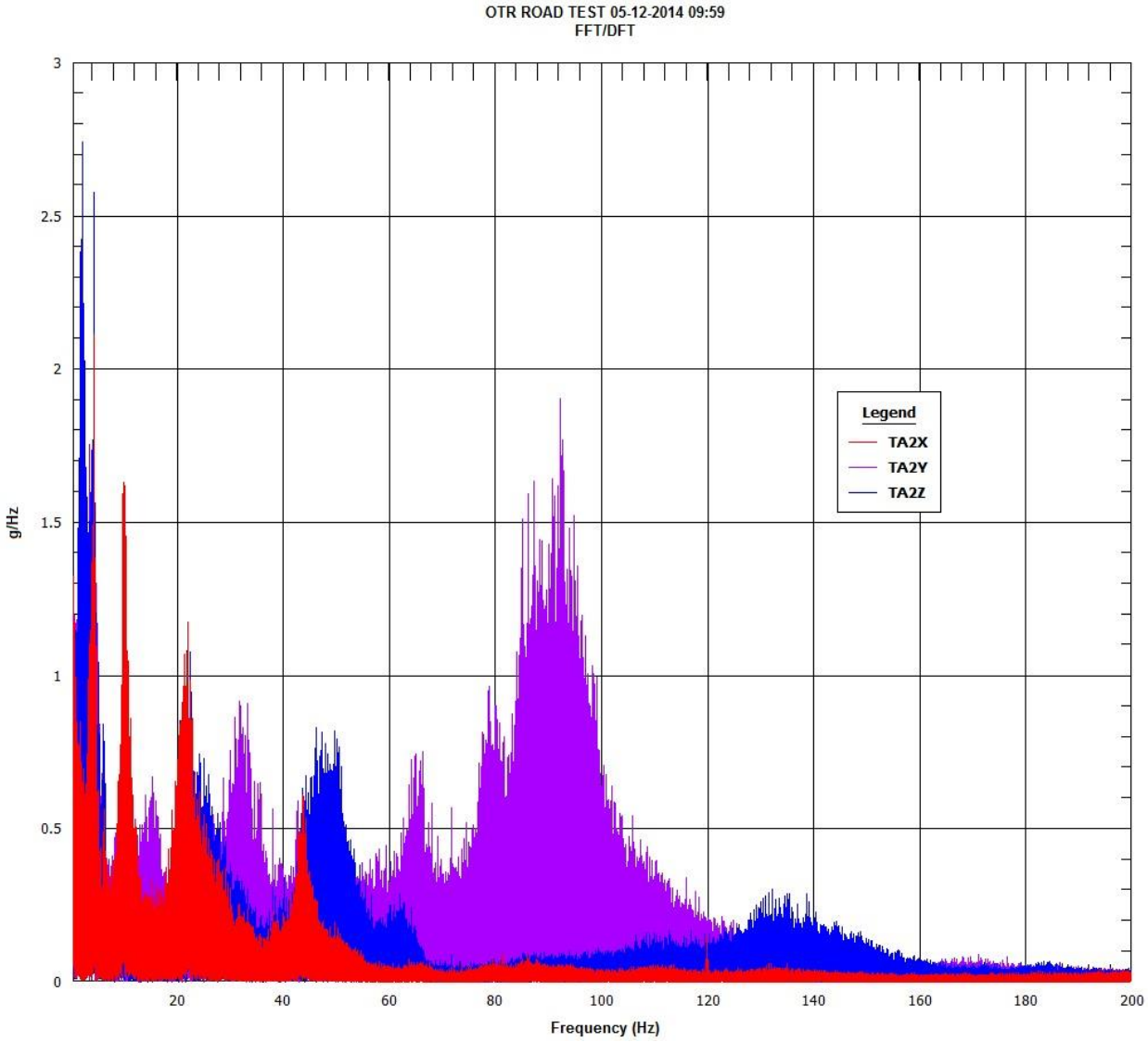

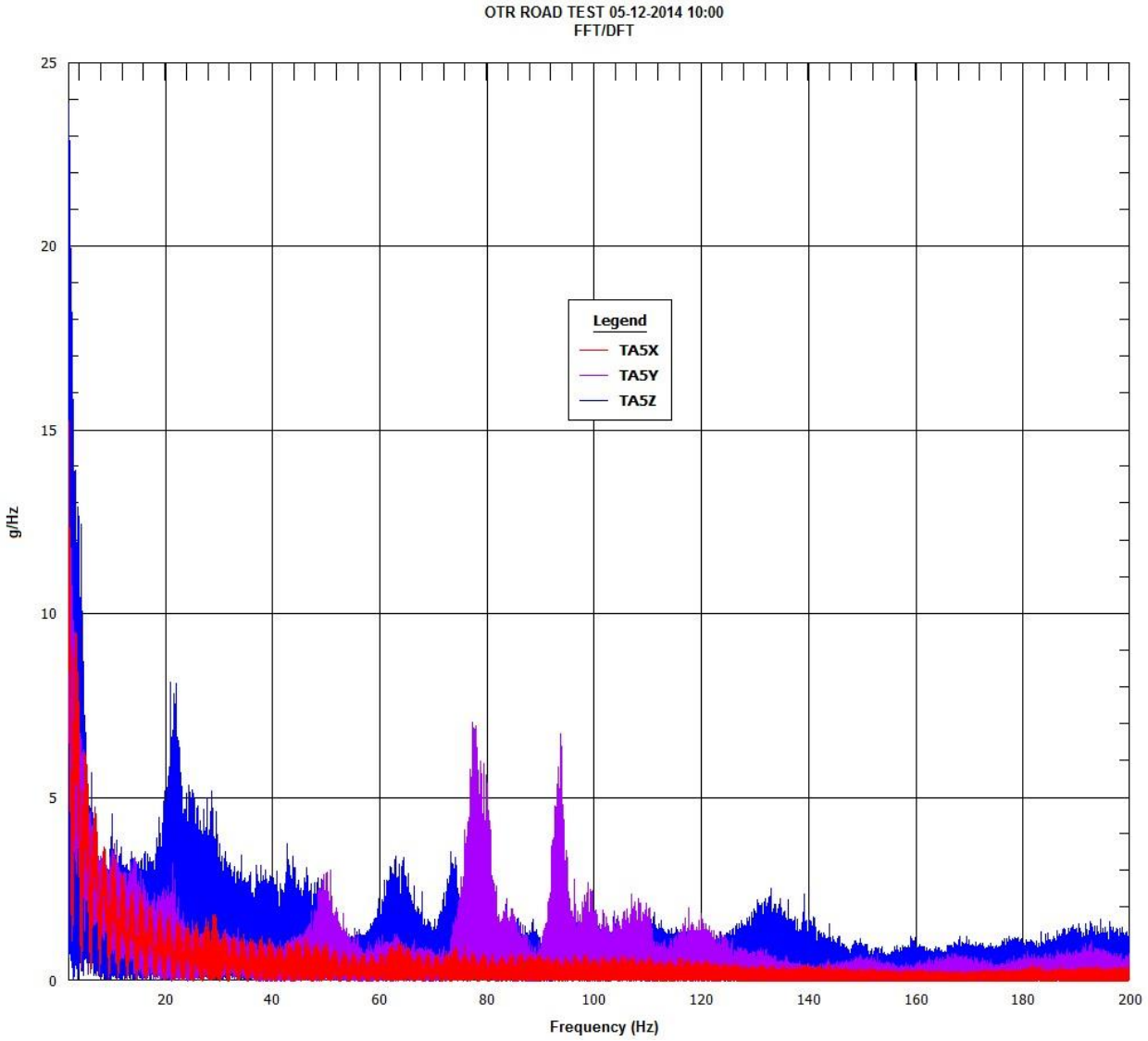
OTR ROAD TEST 05-12-2014 10:00
FFT/DFT
Legend
TA5X
TA5Y
TA5Z
g/Hz
Frequency (Hz)
0
5
10
15
20
25
20
40
60
80
100
120
140
160
180
200

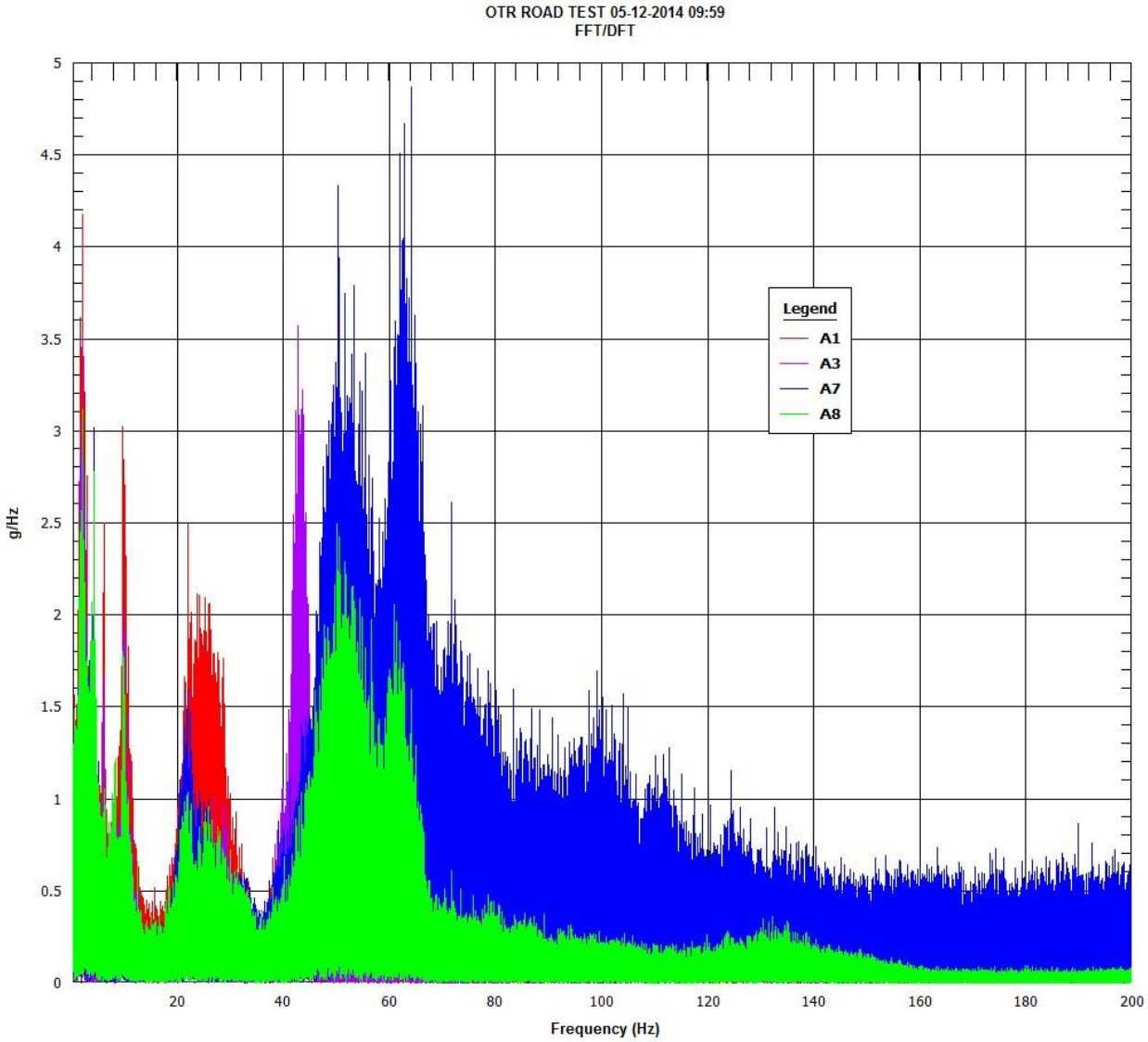

Figure 8.8 Segment 2 accelerometer FFTs

8.3 Truck Route Segment 3 Data Plots

8.3.1 Strain Gauge Time-Histories (με versus time)

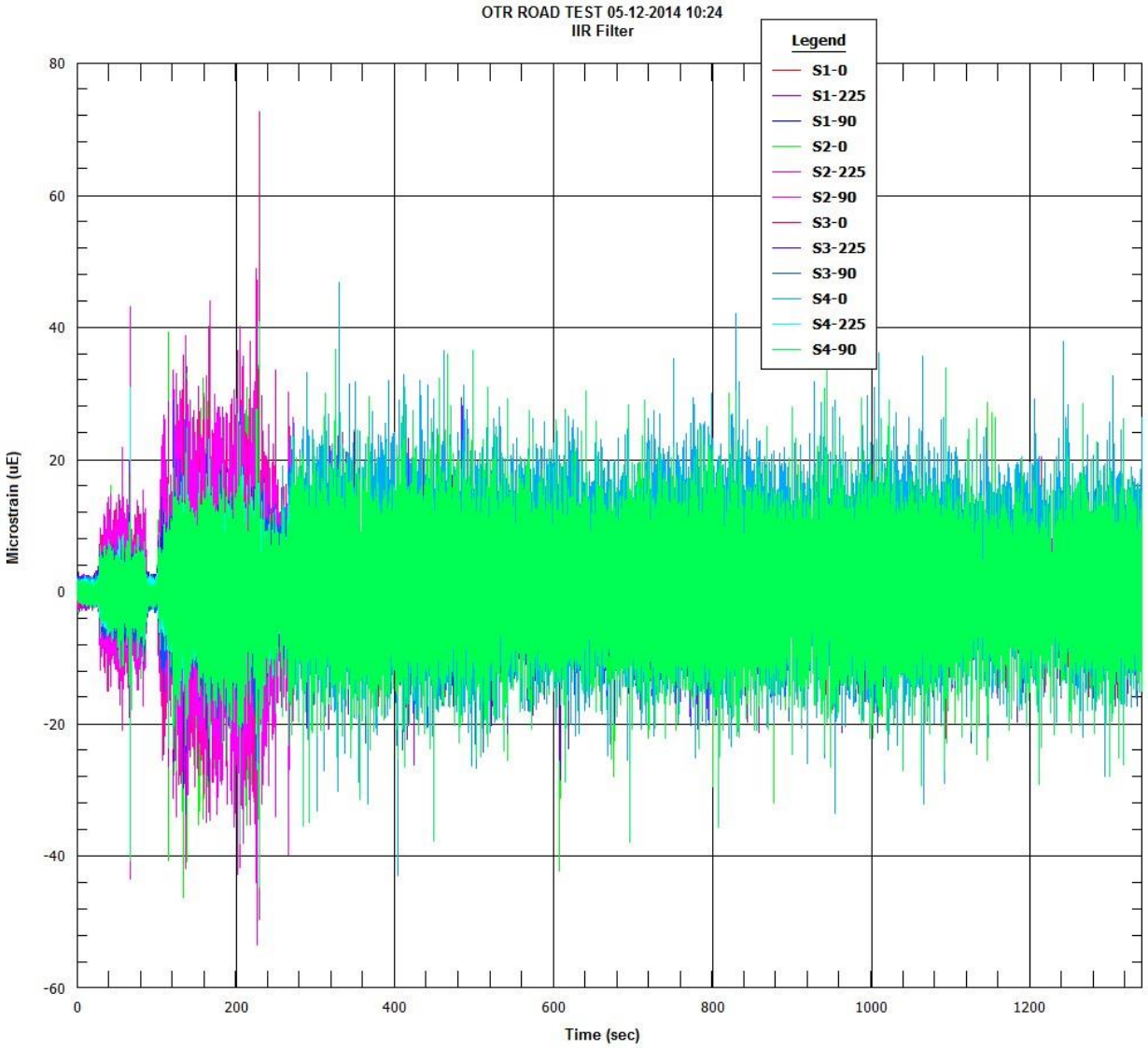

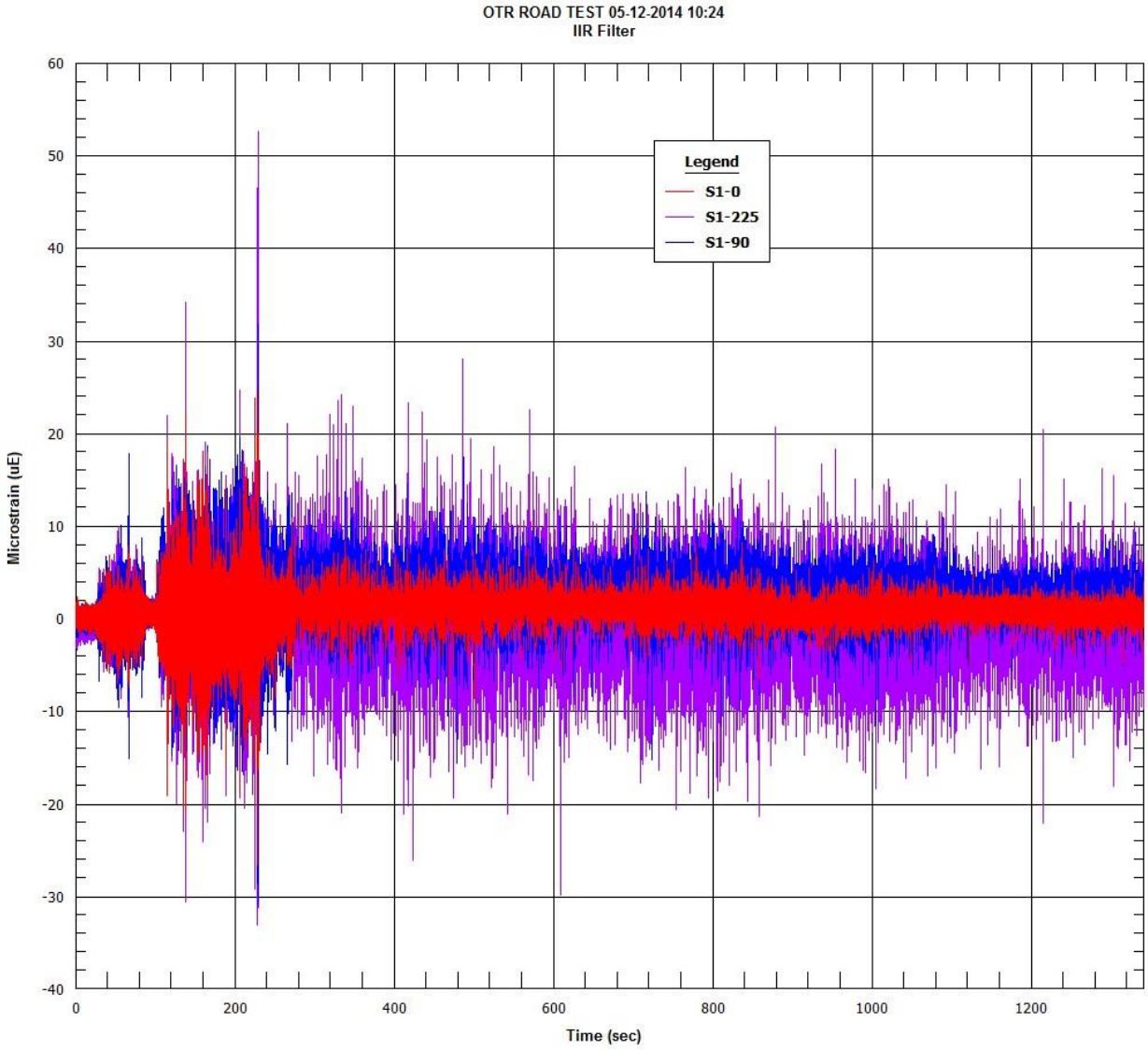
OTR ROAD TEST 05-12-2014 10:24
IIR Filter
Legend
S1-0
S1-225
S1-90
Microstrain (uE)
Time (sec)
60
50
40
30
20
10
0
-10
-20
-30
-40
0
200
400
600
800
1000
1200

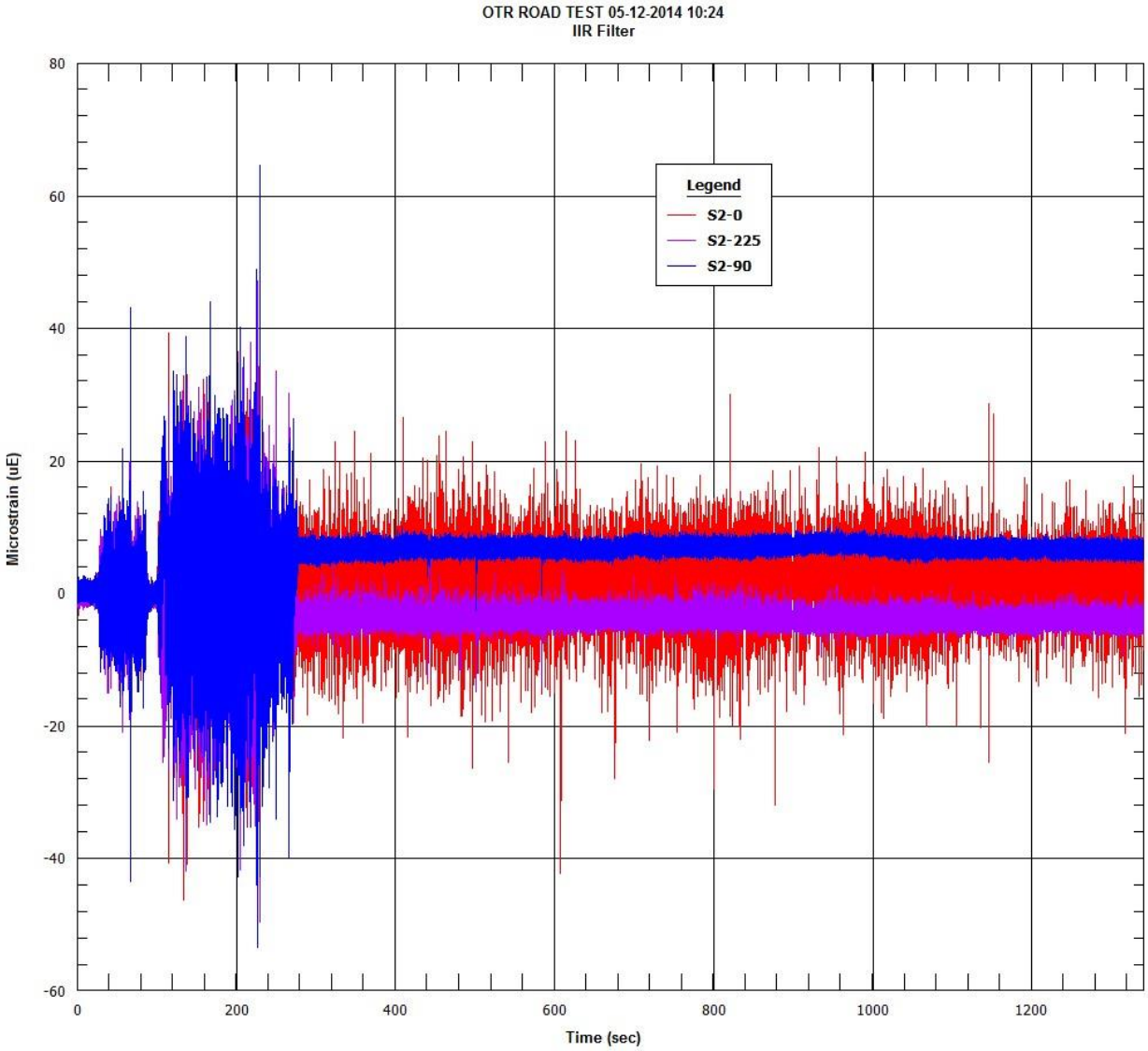
OTR ROAD TEST 05-12-2014 10:24
IIR Filter
Legend
S2-0
S2-225
S2-90
Microstrain (uE)
Time (sec)
80
60
40
20
0
-20
-40
-60
0
200
400
600
800
1000
1200

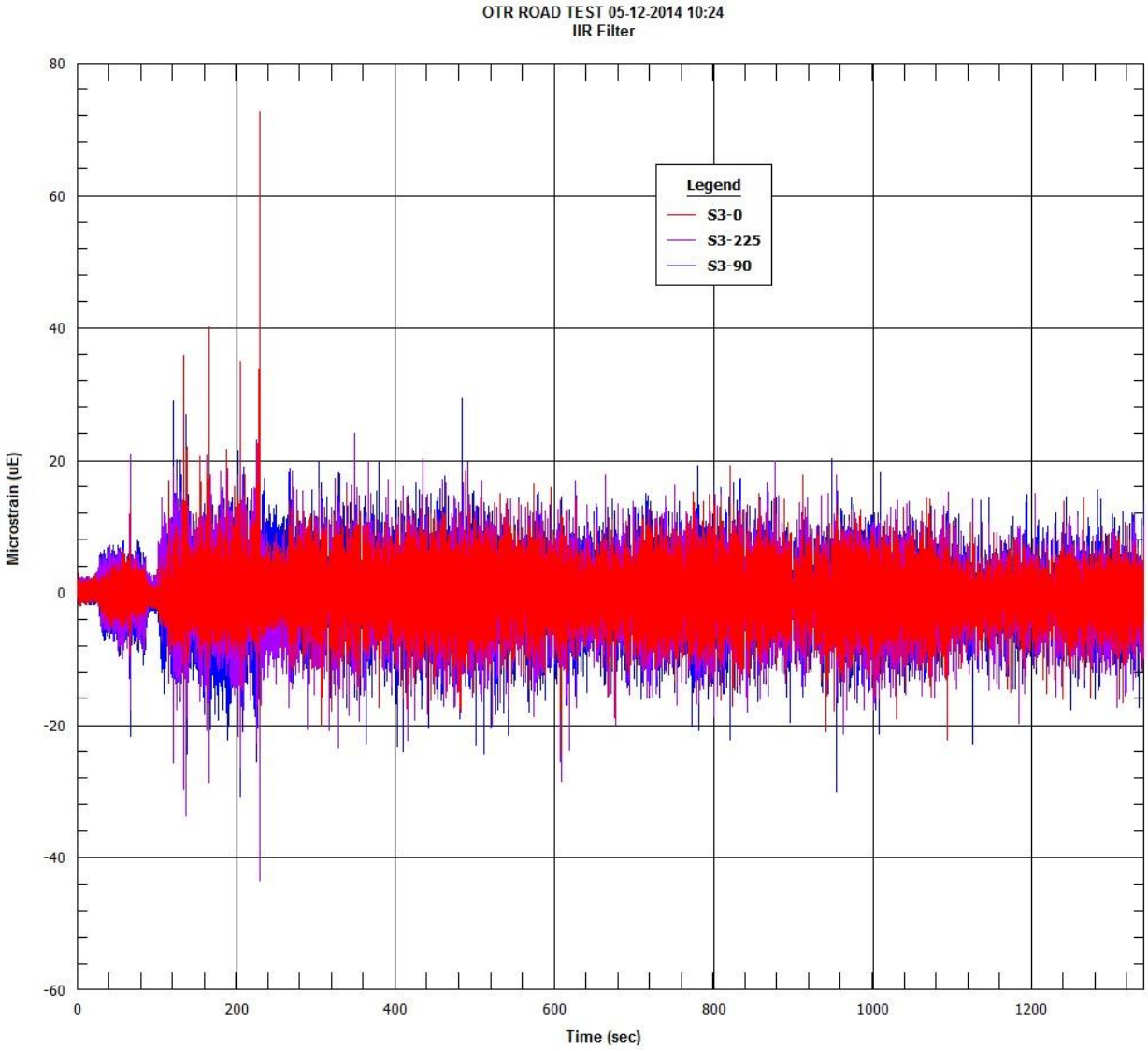
OTR ROAD TEST 05-12-2014 10:24
IIR Filter
Legend
S3-0
S3-225
S3-90
Microstrain (uE)
Time (sec)
80
60
40
20
0
-20
-40
-60
0
200
400
600
800
1000
1200

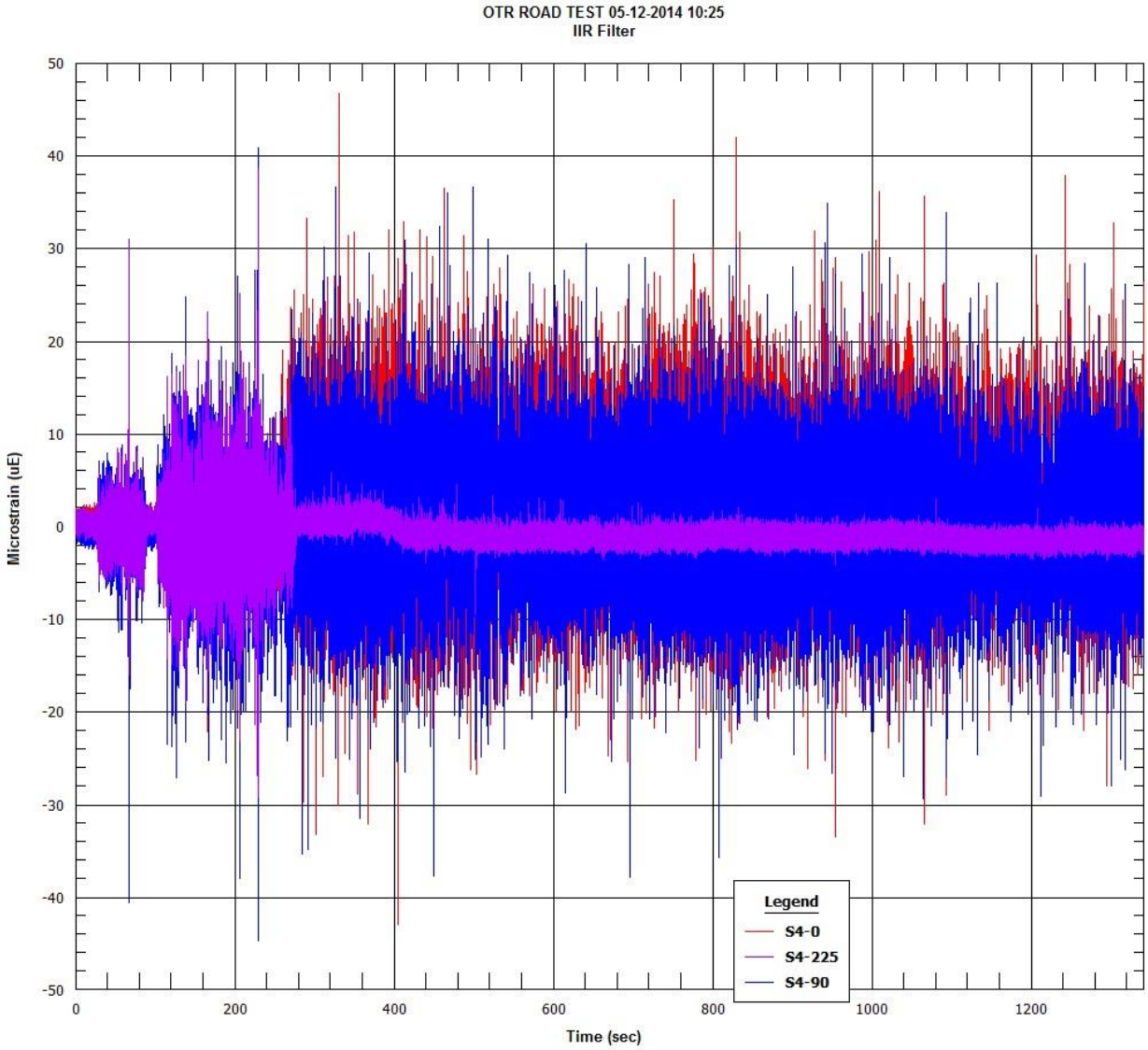

Figure 8.9 Segment 3 strain gauge time-histories

8.3.2 Strain Gauge Fast Fourier Transformations (με/Hz versus Hz)

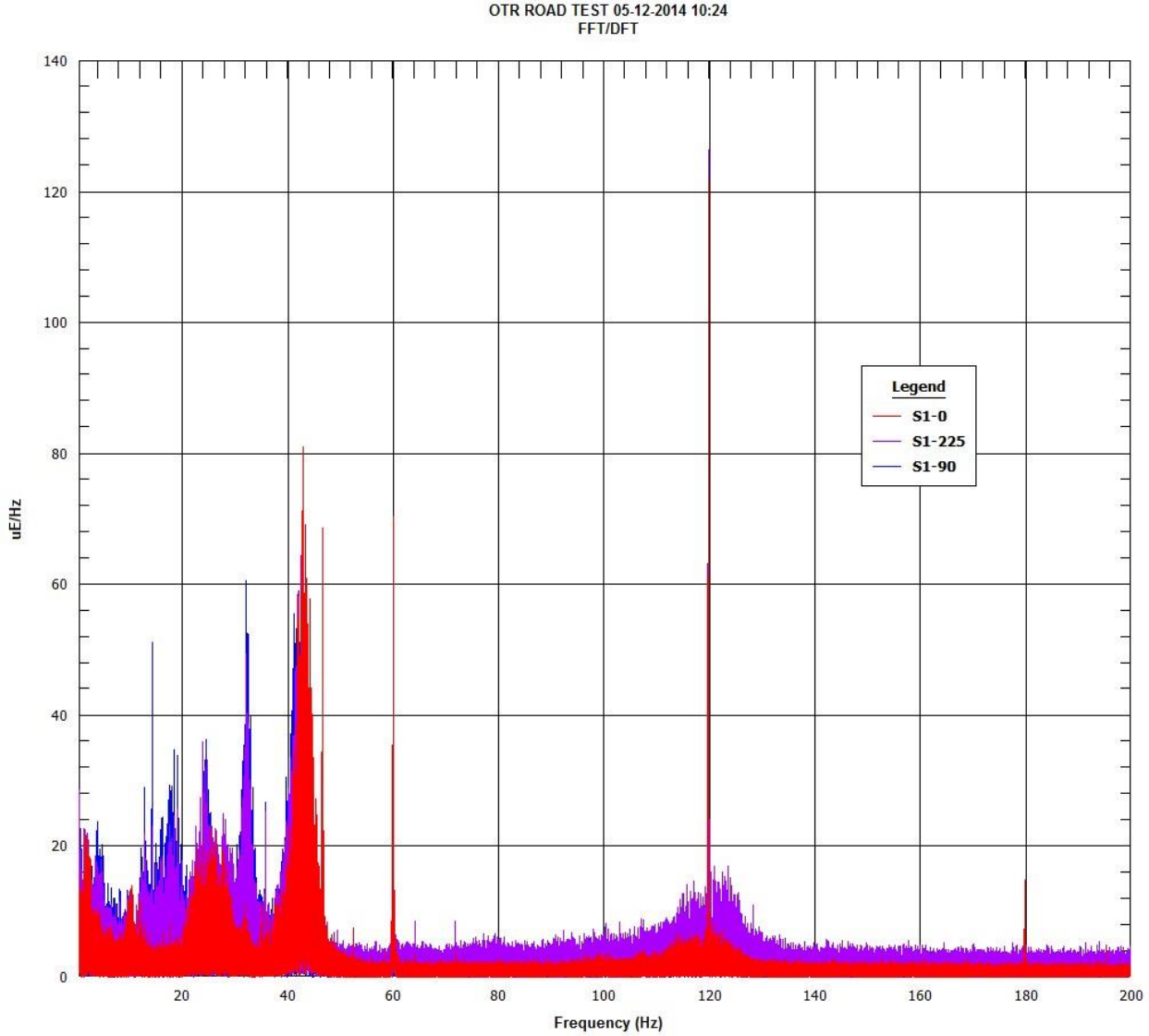

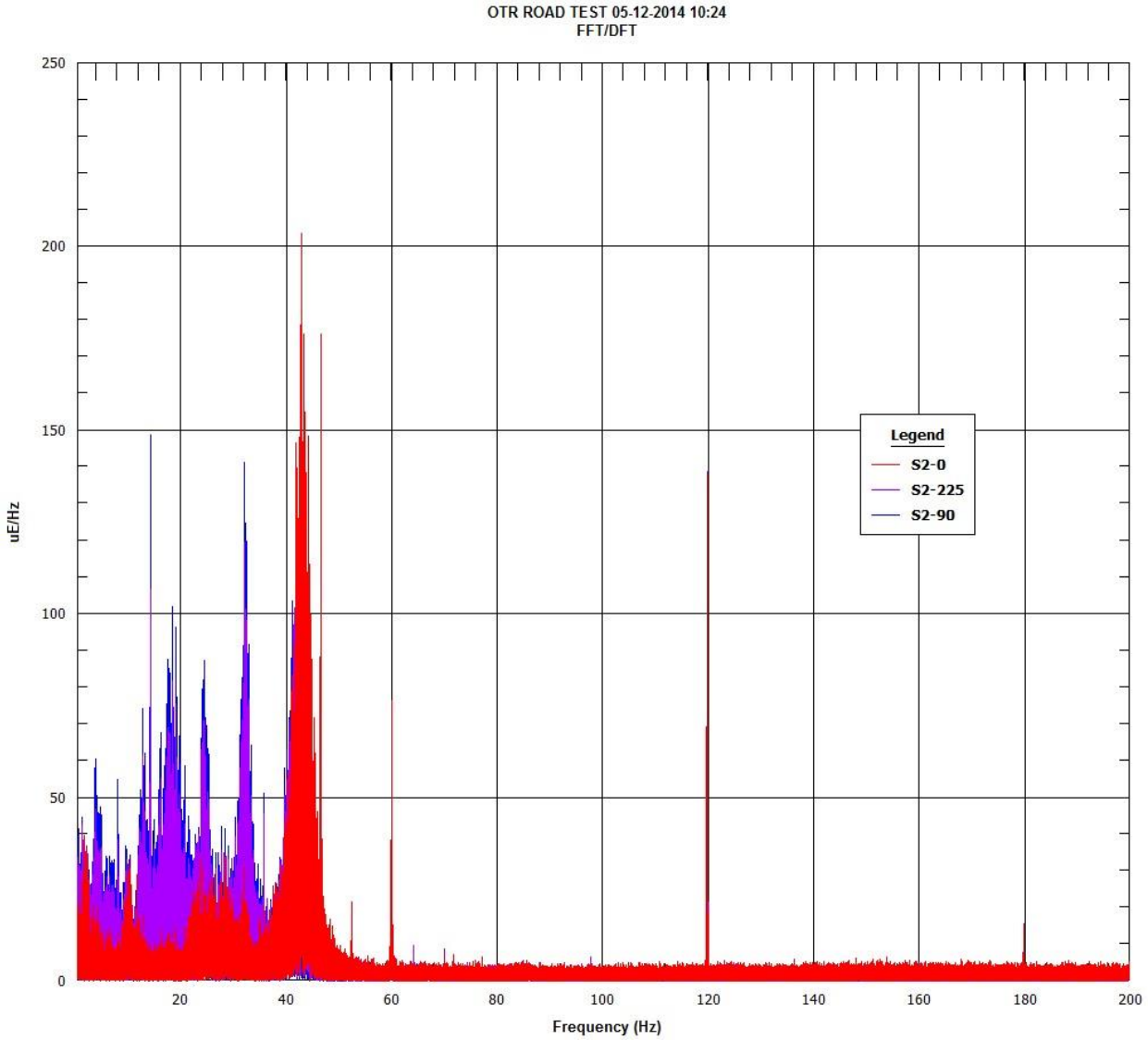
OTR ROAD TEST 05-12-2014 10:24
FFT/DFT
uE/Hz
Frequency (Hz)
Legend
S2-0
S2-225
S2-90
0
50
100
150
200
250
20
40
60
80
100
120
140
160
180
200

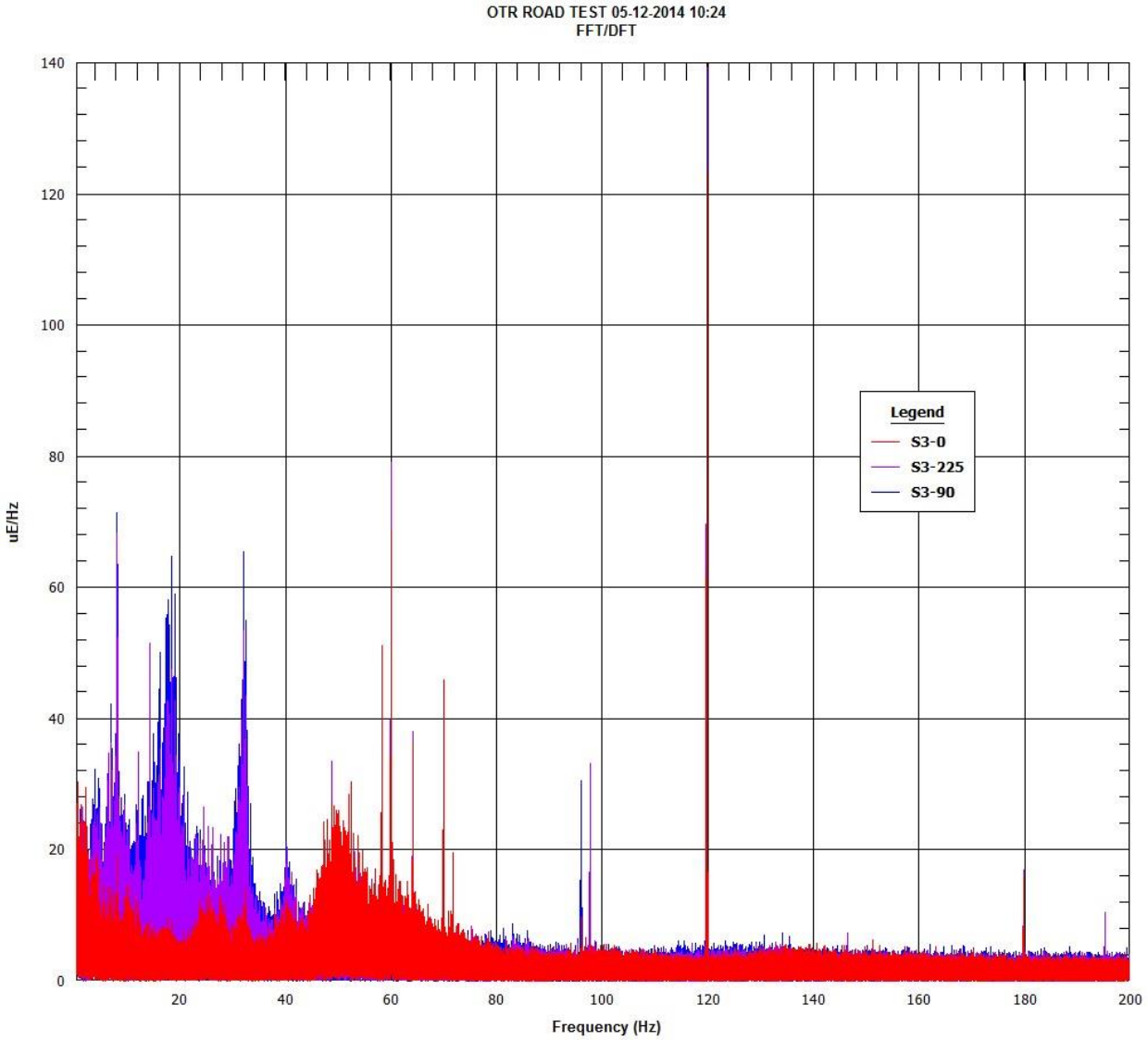
OTR ROAD TEST 05-12-2014 10:24
FFT/DFT
uE/Hz
Frequency (Hz)
Legend
S3-0
S3-225
S3-90
0
20
40
60
80
100
120
140
160
180
200

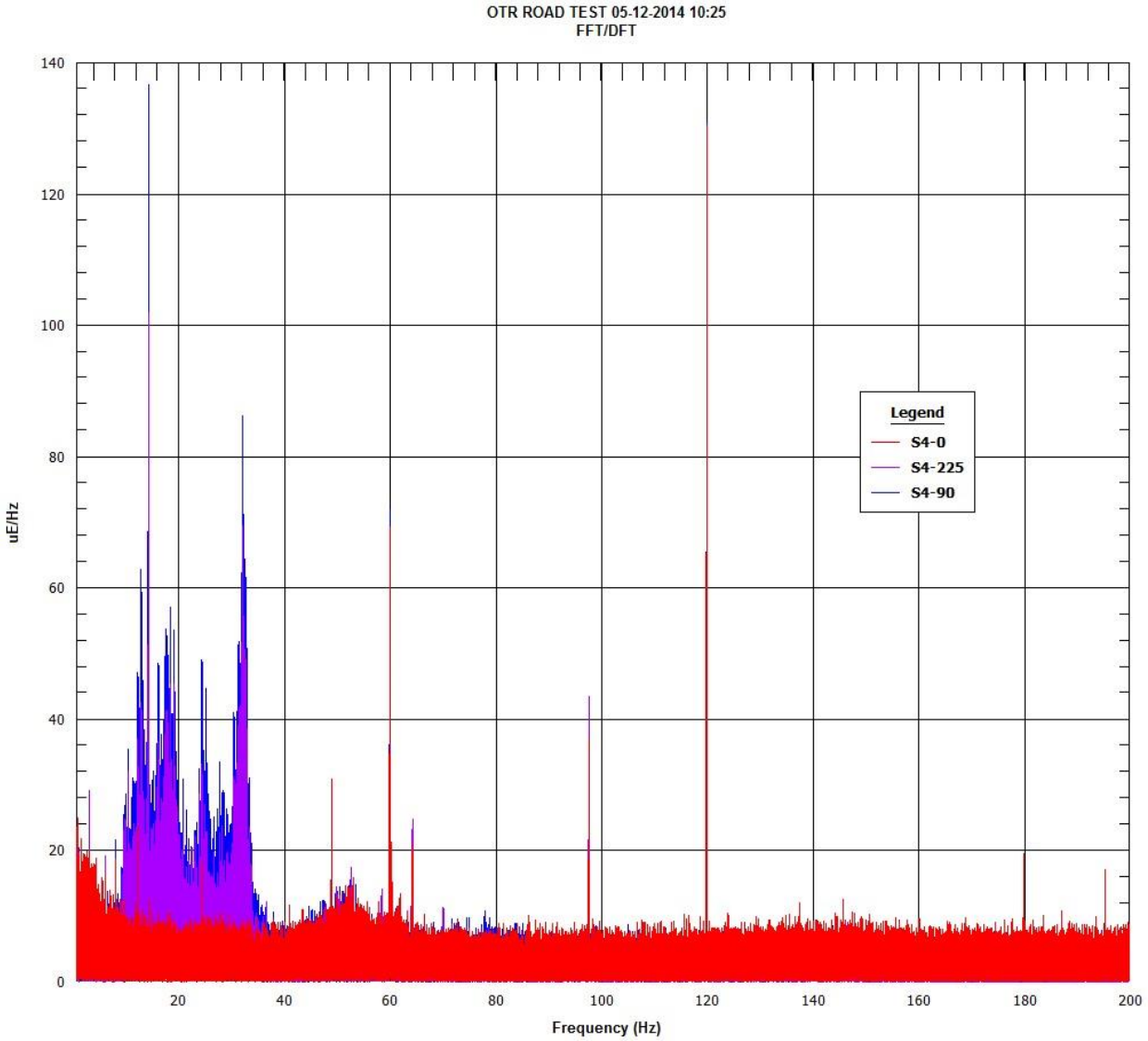

Figure 8.10 Segment 3 strain gauge FFTs

8.3.3 Accelerometer Time-Histories (g versus time)

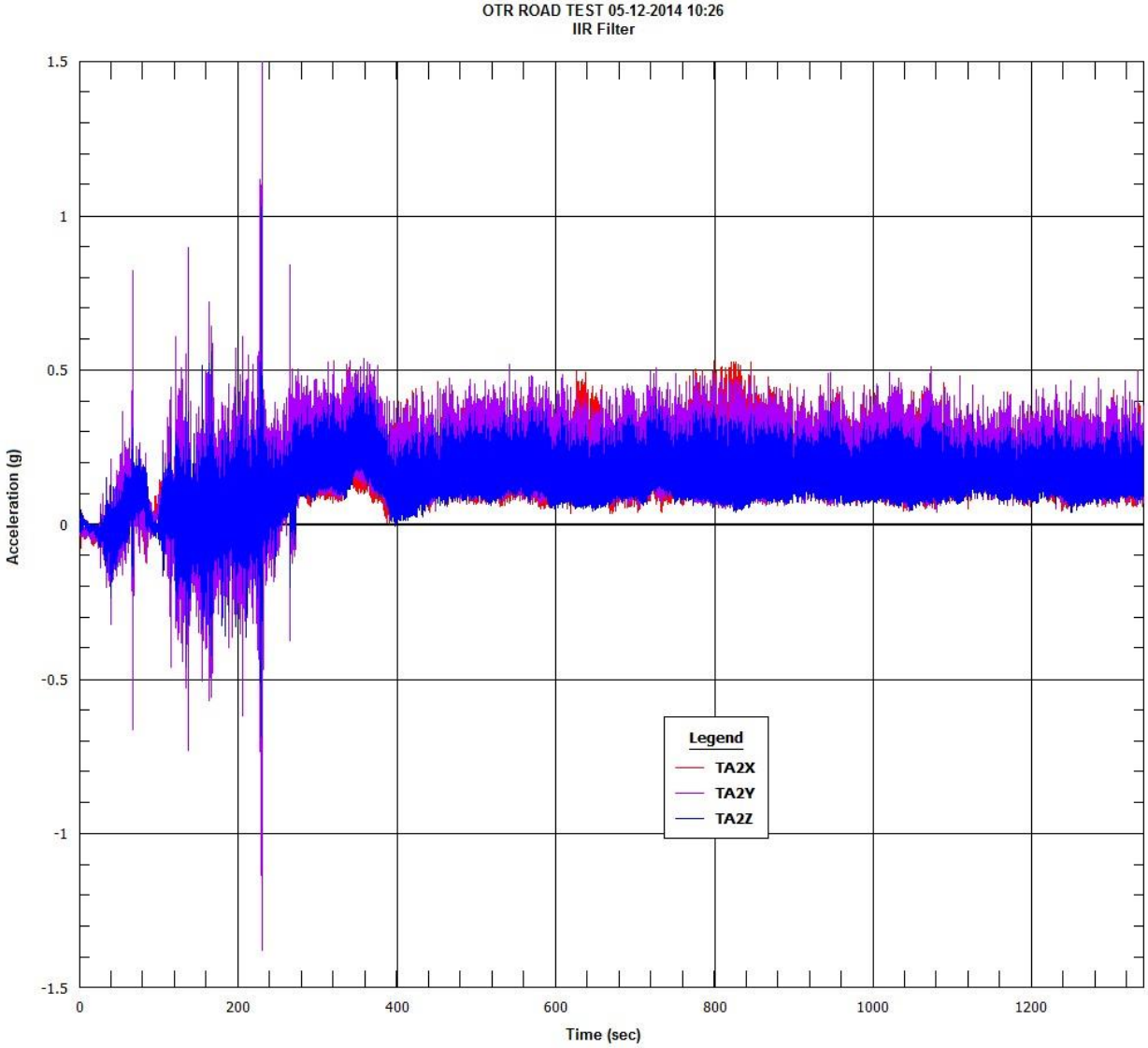

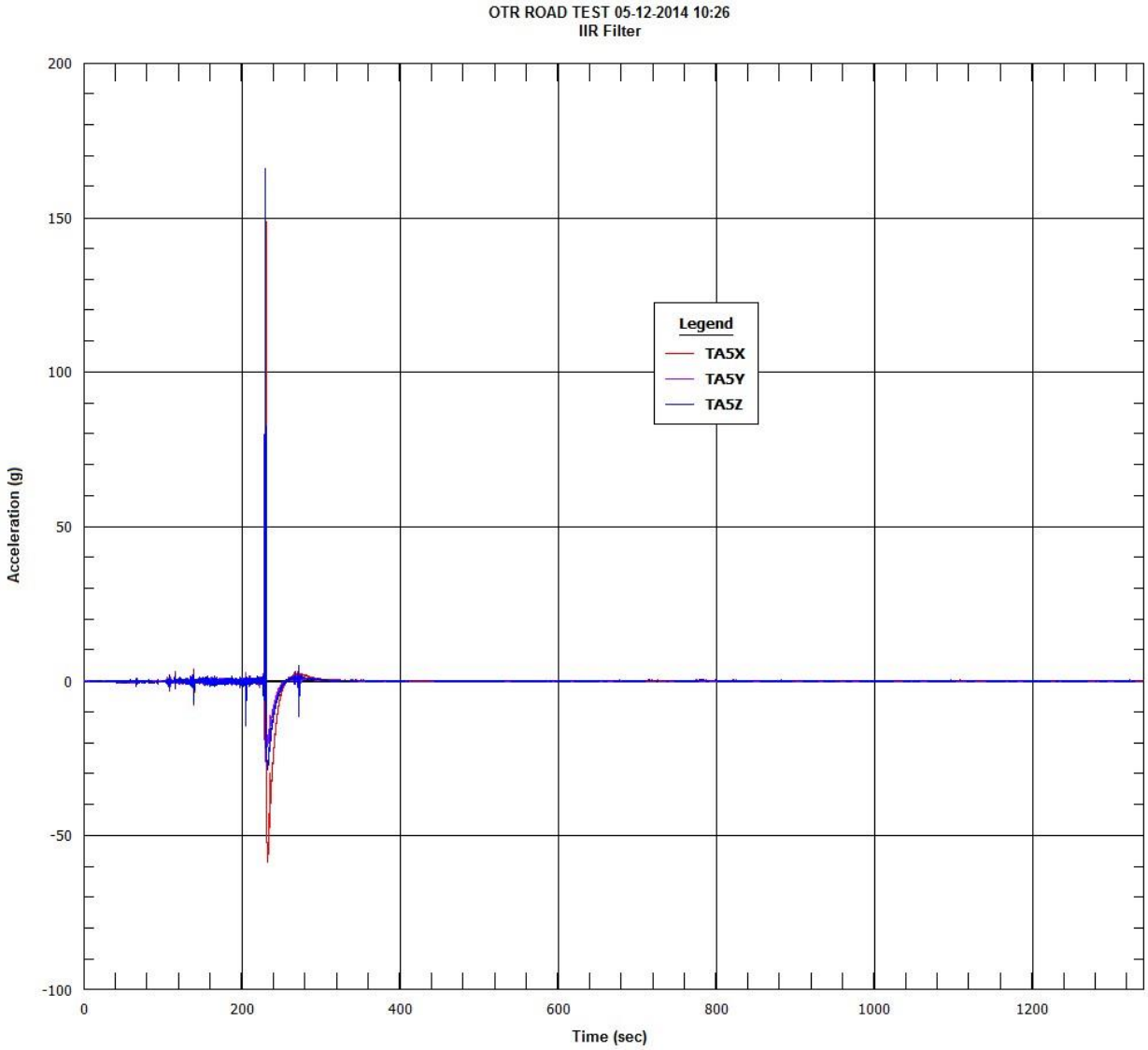
OTR ROAD TEST 05-12-2014 10:26
IIR Filter
Legend
TA5X
TA5Y
TA5Z
Acceleration (g)
Time (sec)
200
150
100
50
0
-50
-100
0
200
400
600
800
1000
1200

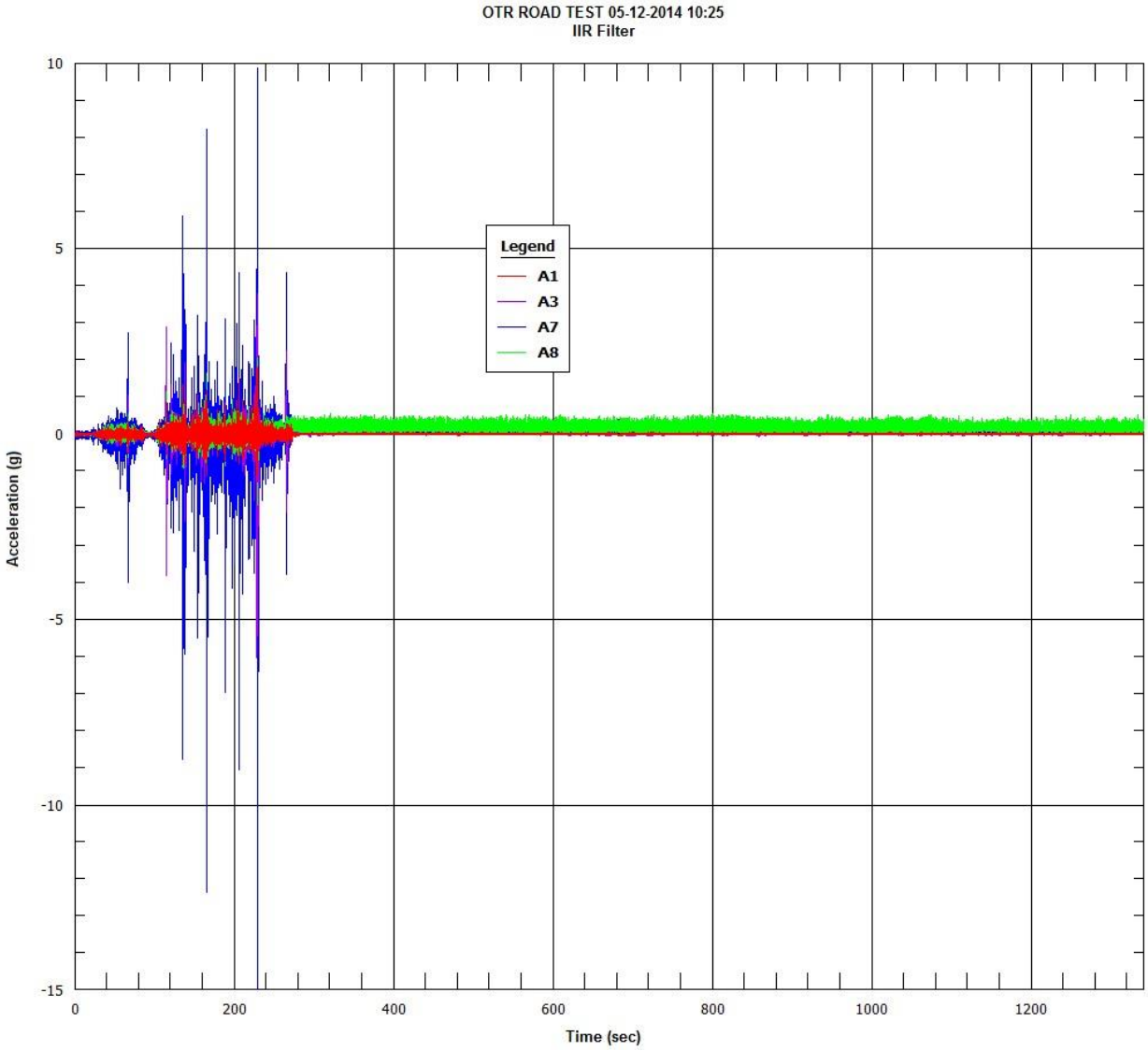

Figure 8.11 Segment 3 accelerometer time-histories

8.3.4 Accelerometer Fast Fourier Transformations (g/Hz versus Hz)

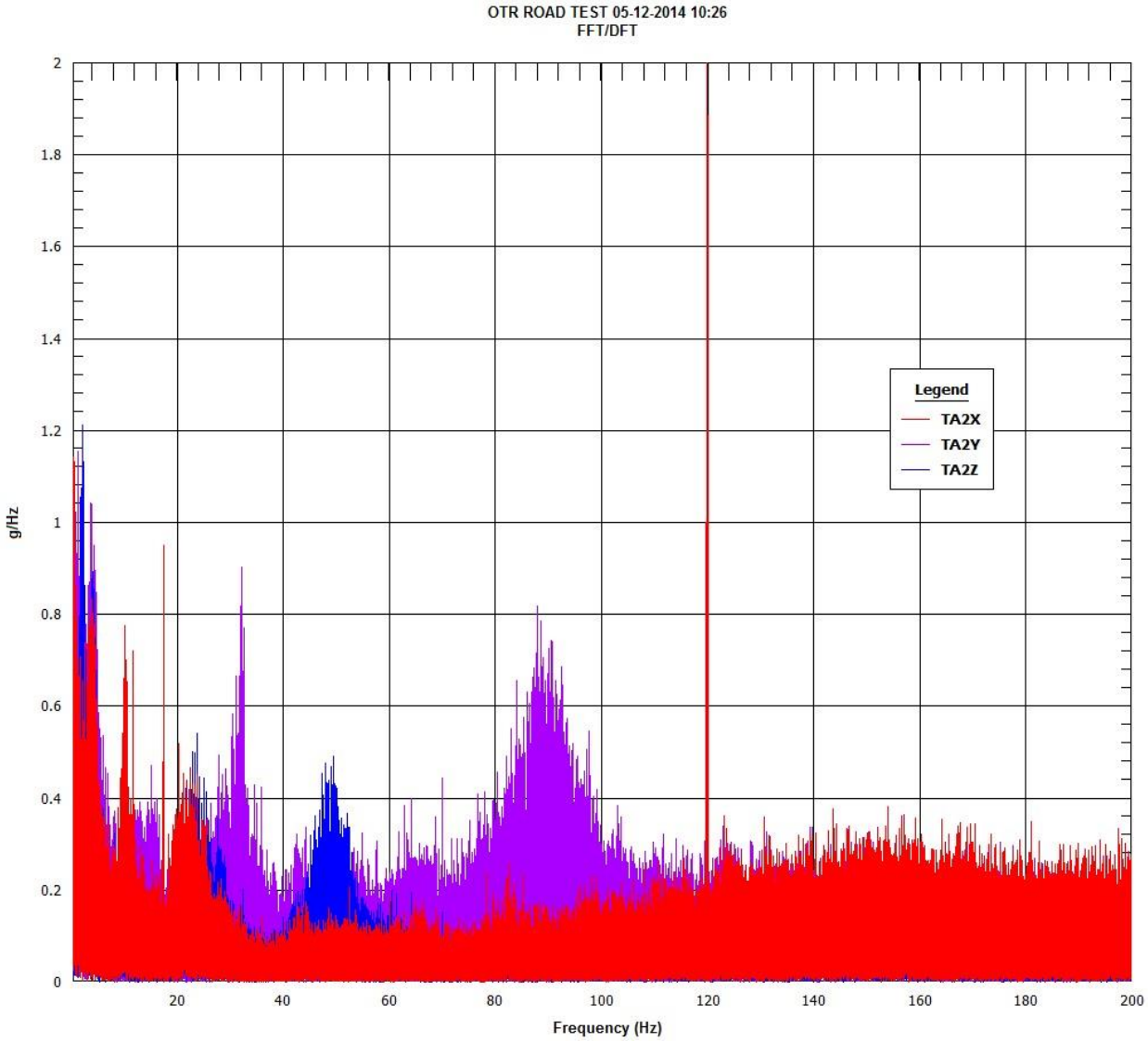

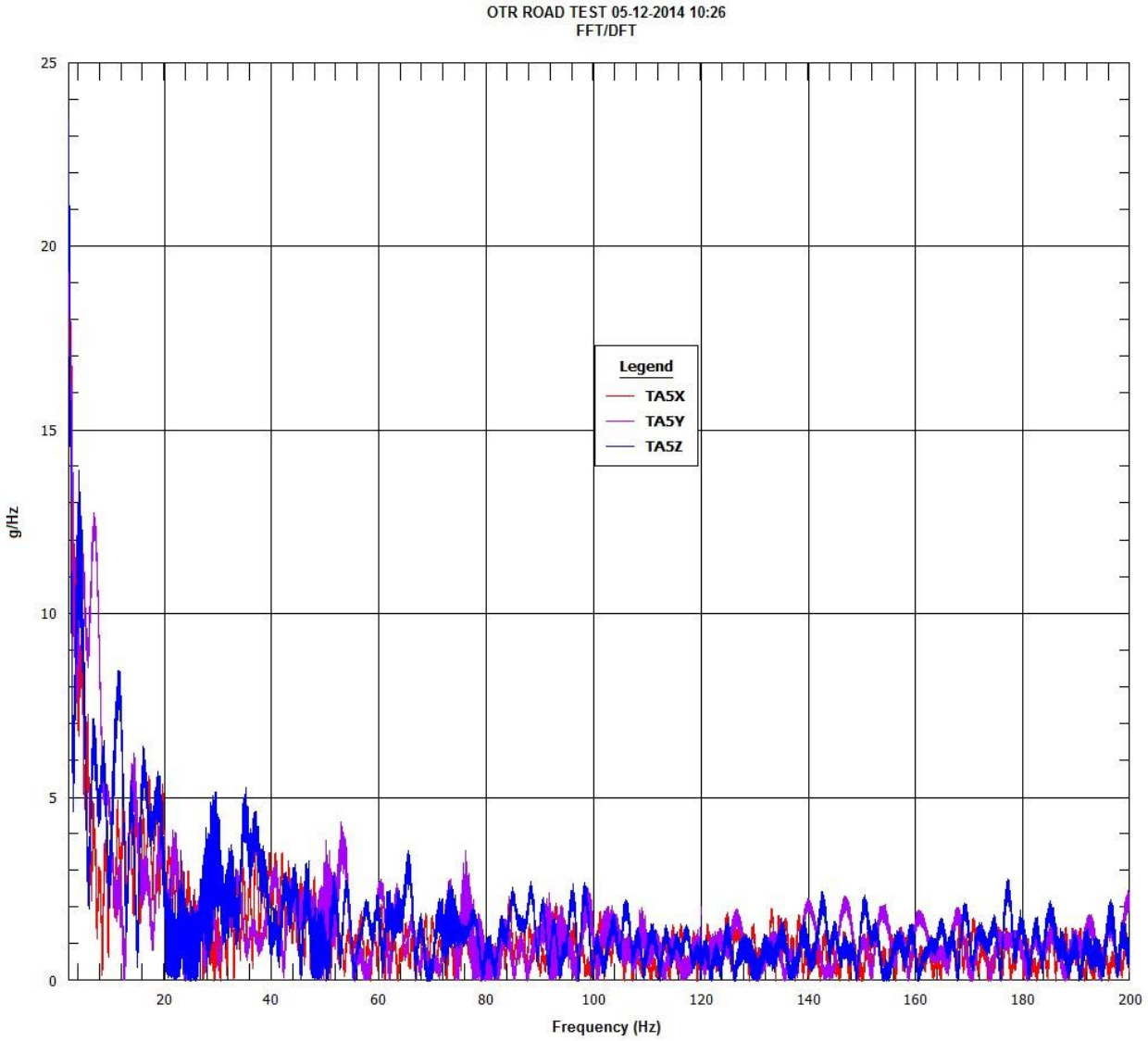
OTR ROAD TEST 05-12-2014 10:26
FFT/DFT
g/Hz
Frequency (Hz)
Legend
TA5X
TA5Y
TA5Z
0
5
10
15
20
25
20
40
60
80
100
120
140
160
180
200

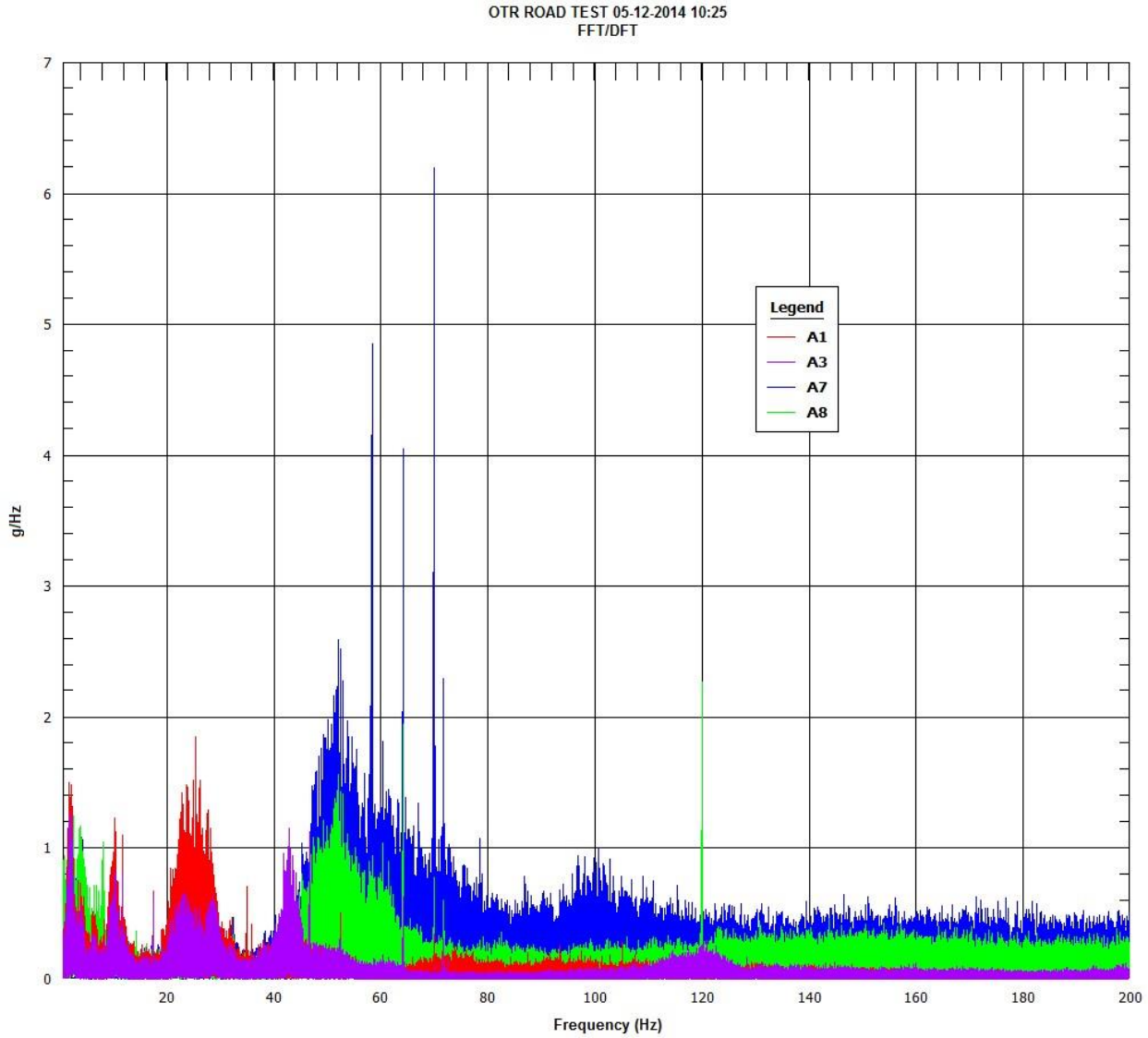

Figure 8.12 Segment 3 accelerometer FFTs

8.4 Truck Route Segment 4 Data Plots

8.4.1 Strain Gauge Time-Histories (με versus time)

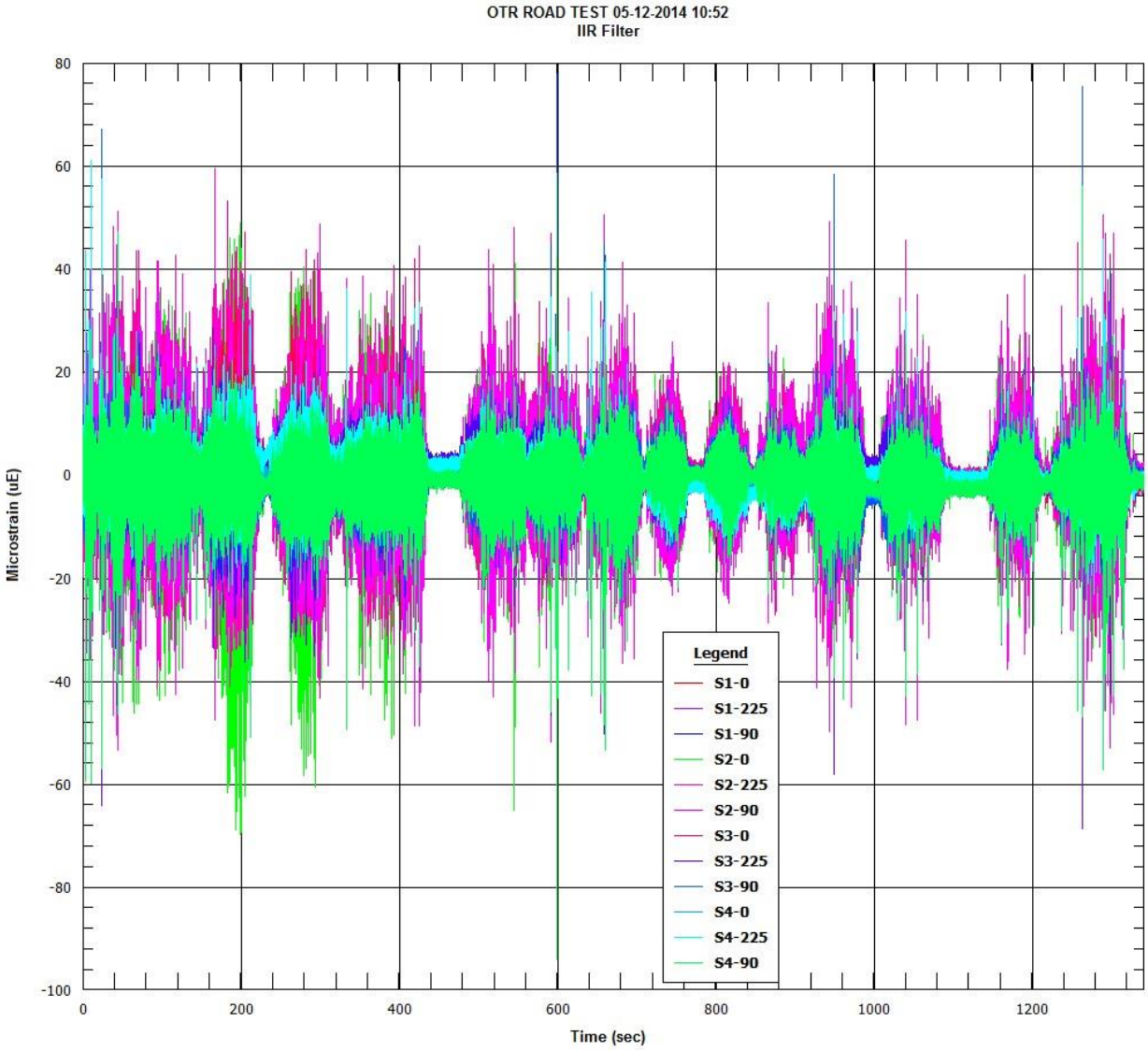

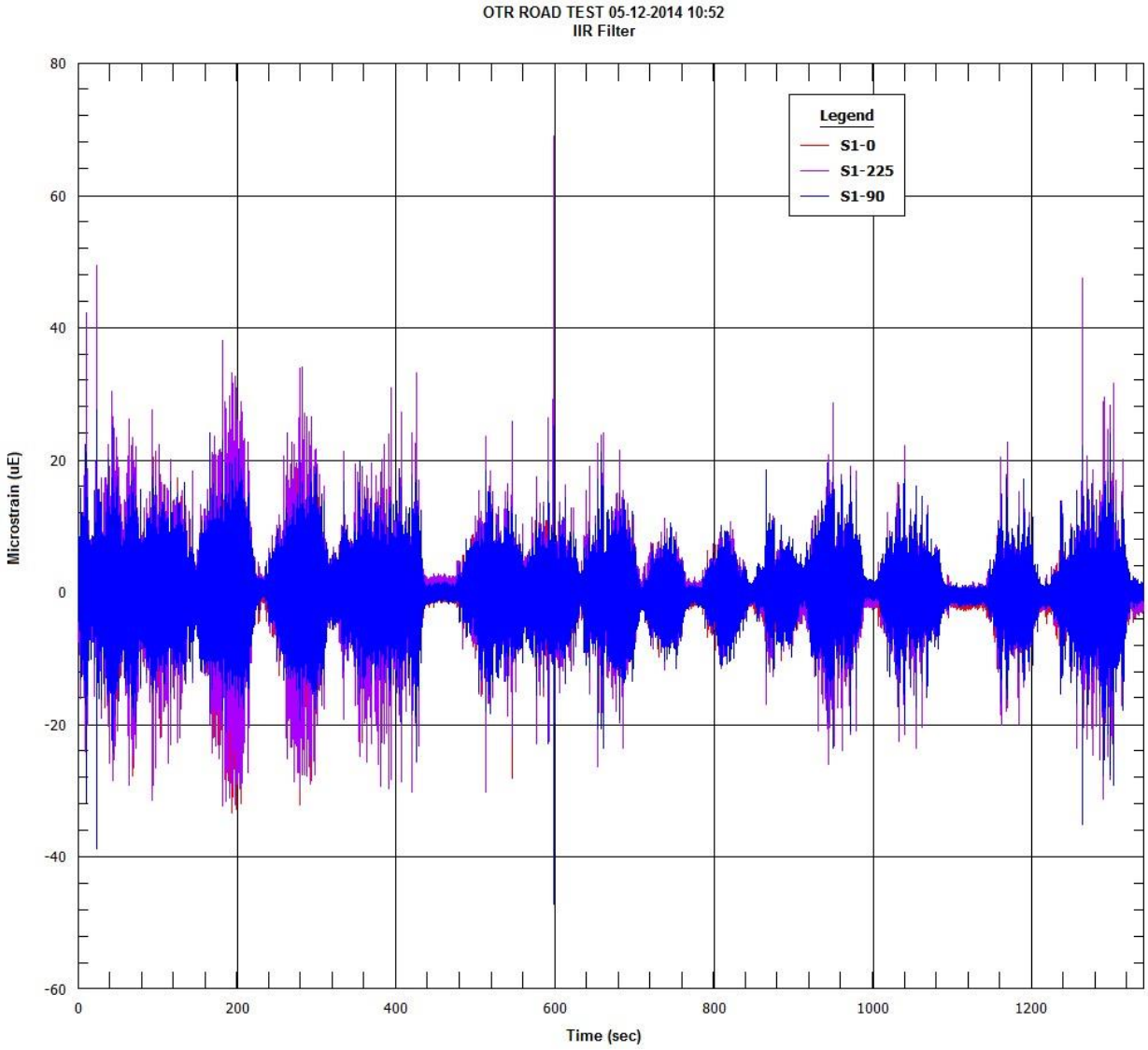
OTR ROAD TEST 05-12-2014 10:52
IIR Filter
Legend
S1-0
S1-225
S1-90
Microstrain (uE)
Time (sec)
80
60
40
20
0
-20
-40
-60
0
200
400
600
800
1000
1200

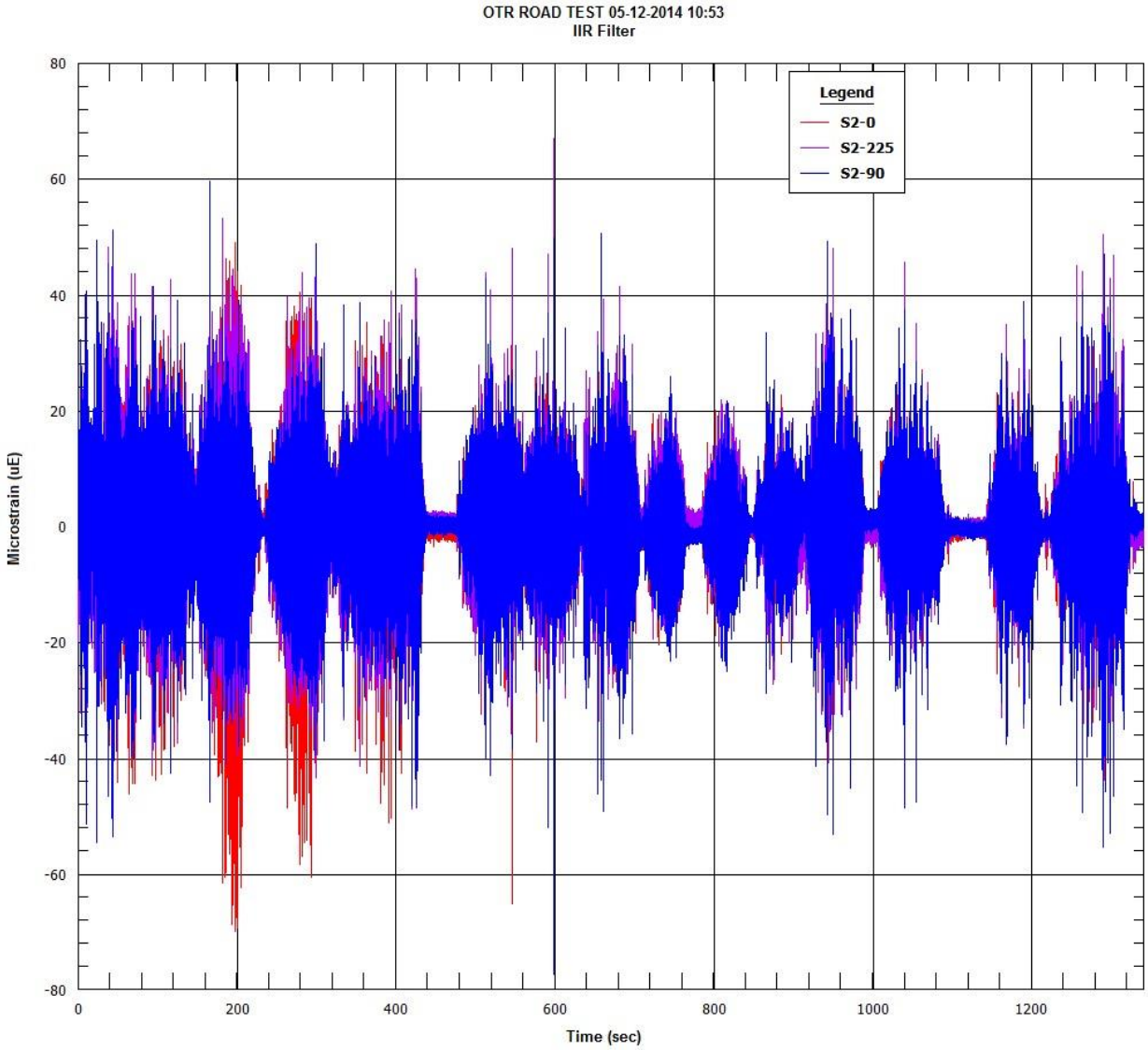
OTR ROAD TEST 05-12-2014 10:53
IIR Filter
Legend
S2-0
S2-225
S2-90
Microstrain (uE)
Time (sec)
80
60
40
20
0
-20
-40
-60
-80
0
200
400
600
800
1000
1200

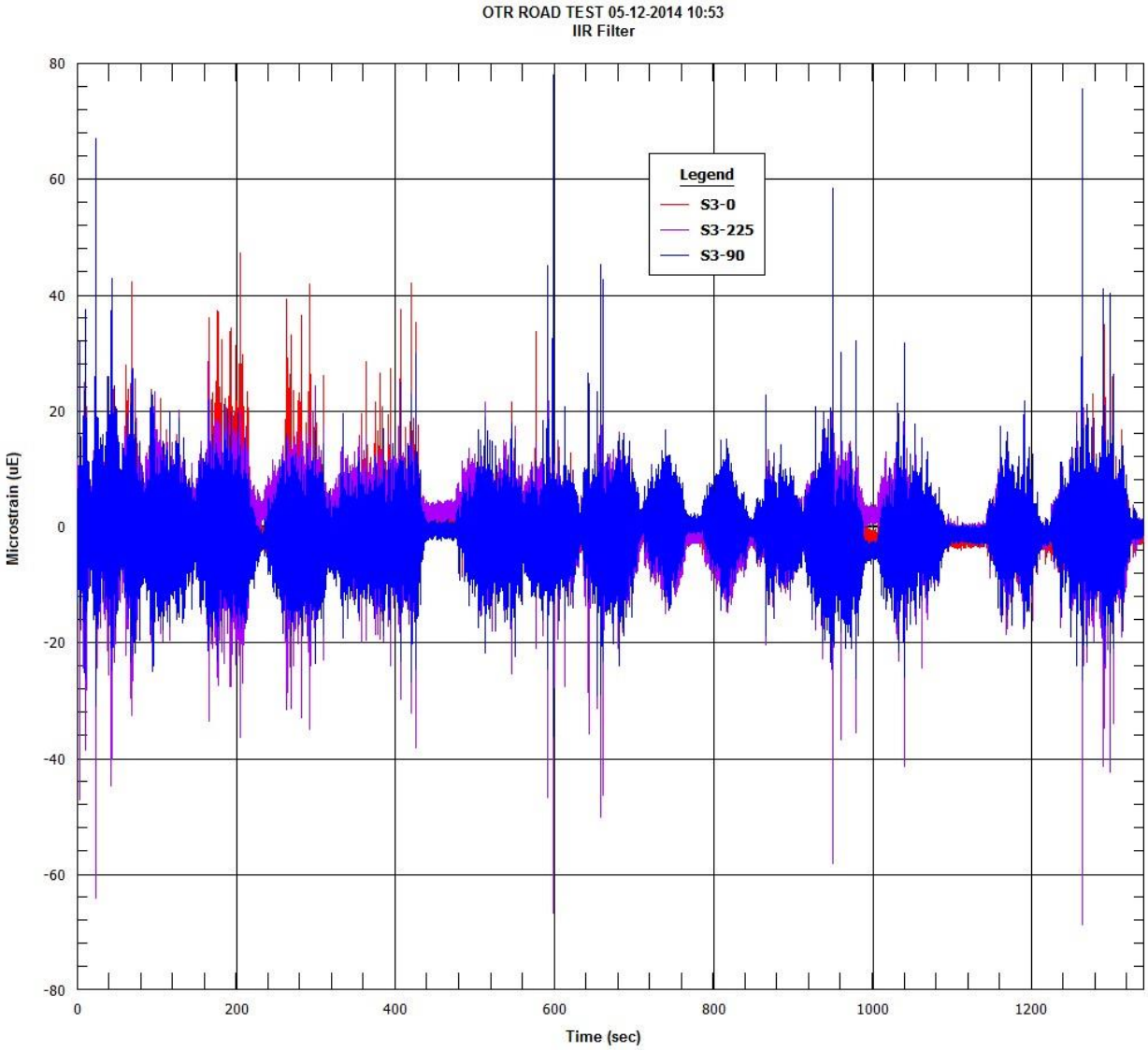
OTR ROAD TEST 05-12-2014 10:53
IIR Filter
Legend
S3-0
S3-225
S3-90
Microstrain (uE)
Time (sec)
80
60
40
20
0
-20
-40
-60
-80
0
200
400
600
800
1000
1200

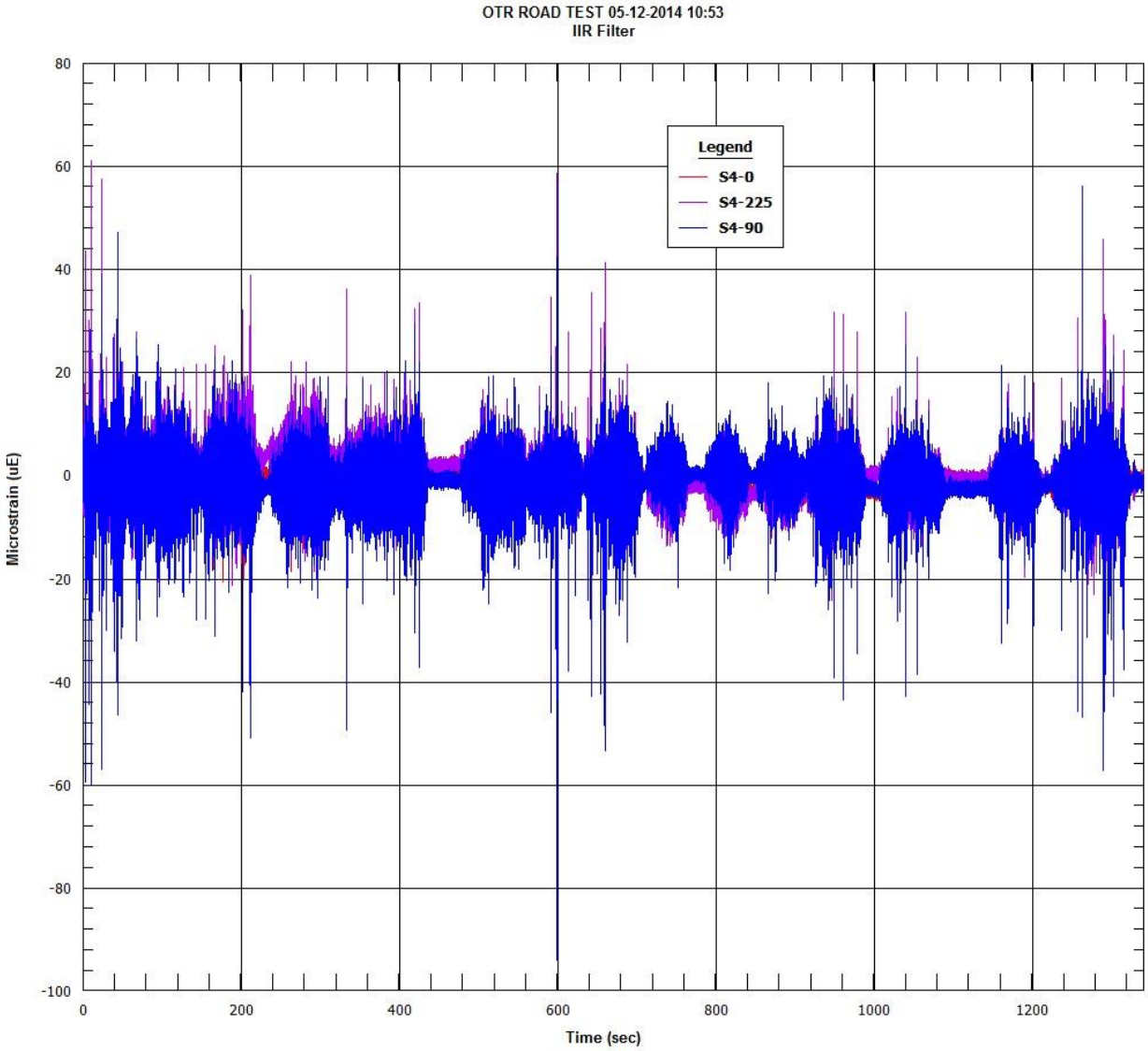

Figure 8.13 Segment 4 strain gauge time-histories

8.4.2 Strain Gauge Fast Fourier Transformations (με/Hz versus Hz)

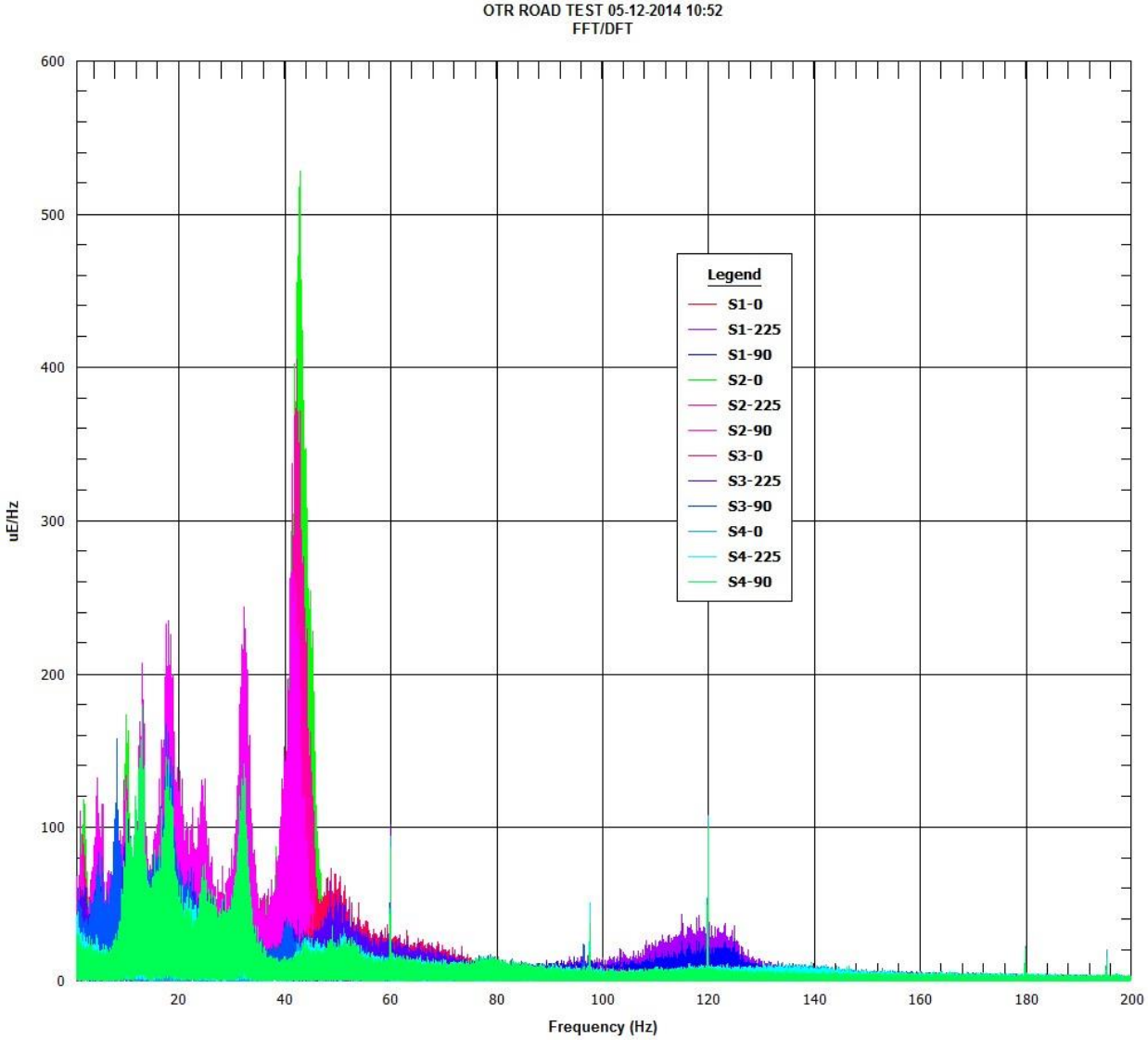

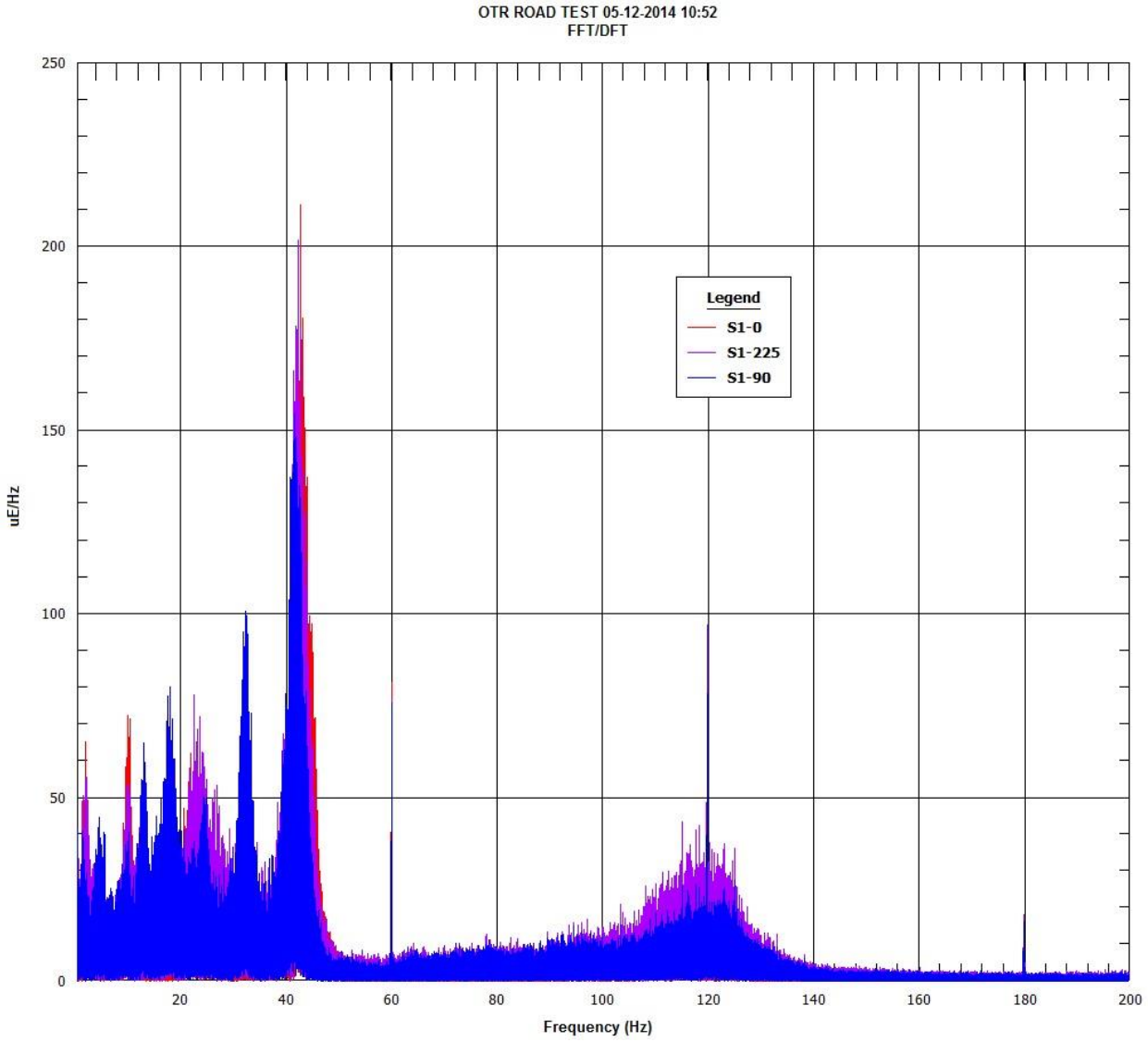
OTR ROAD TEST 05-12-2014 10:52
FFT/DFT
Legend
S1-0
S1-225
S1-90
uE/Hz
Frequency (Hz)
0
50
100
150
200
250
20
40
60
80
100
120
140
160
180
200

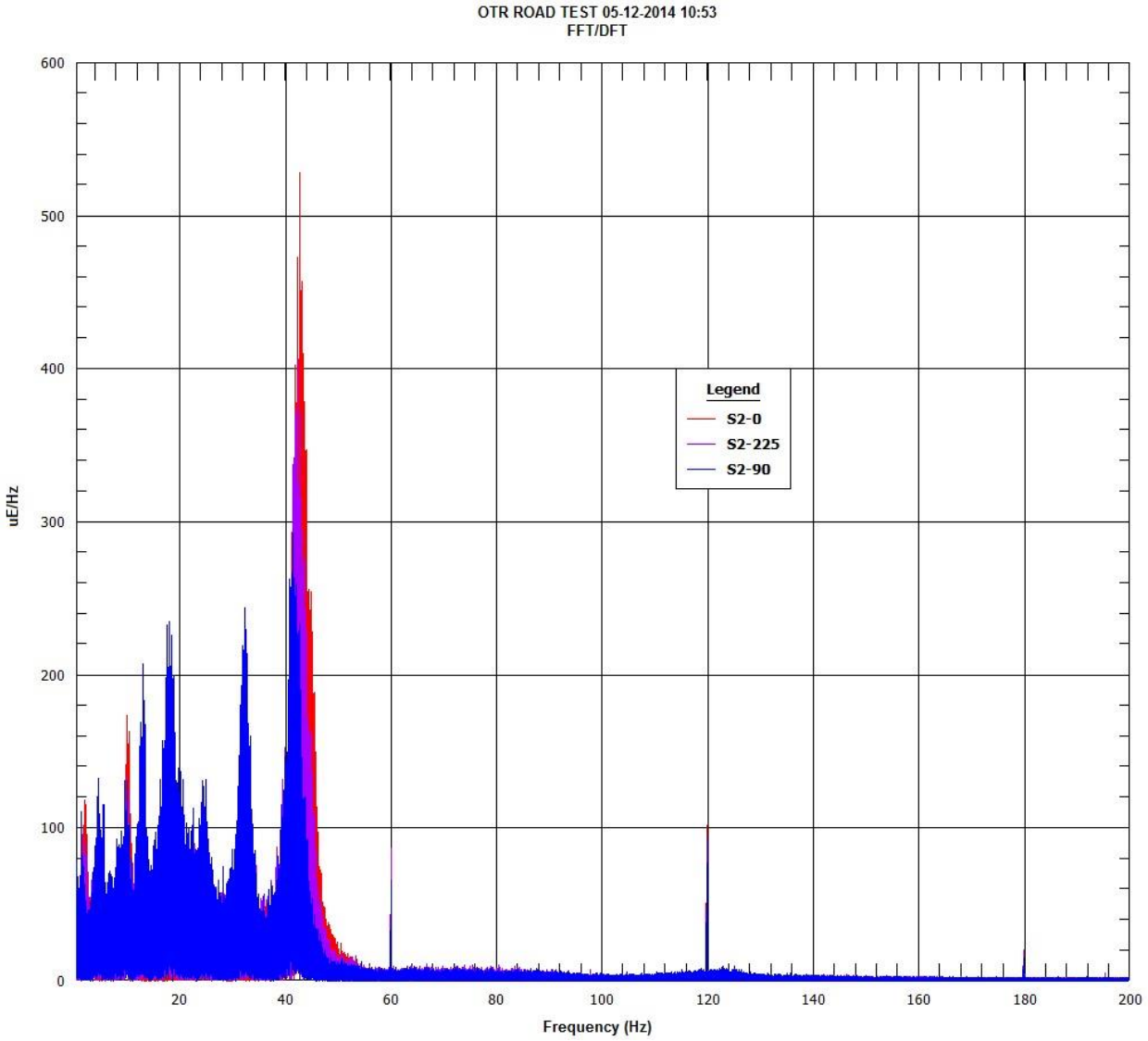
OTR ROAD TEST 05-12-2014 10:53
FFT/DFT
uE/Hz
Frequency (Hz)
Legend
S2-0
S2-225
S2-90
0
100
200
300
400
500
600
20
40
60
80
100
120
140
160
180
200

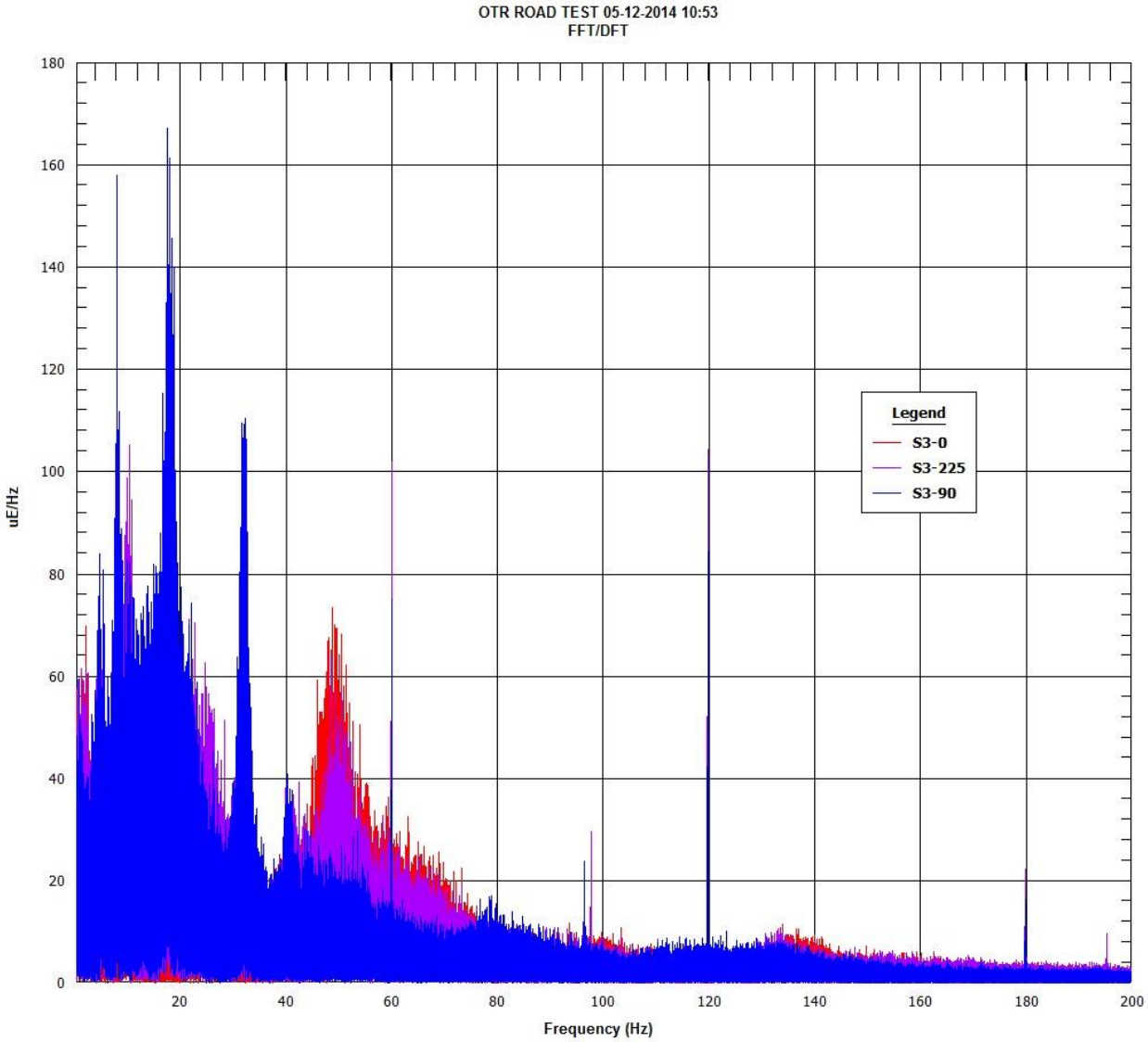
OTR ROAD TEST 05-12-2014 10:53
FFT/DFT
uE/Hz
Frequency (Hz)
Legend
S3-0
S3-225
S3-90
0
20
40
60
80
100
120
140
160
180
200

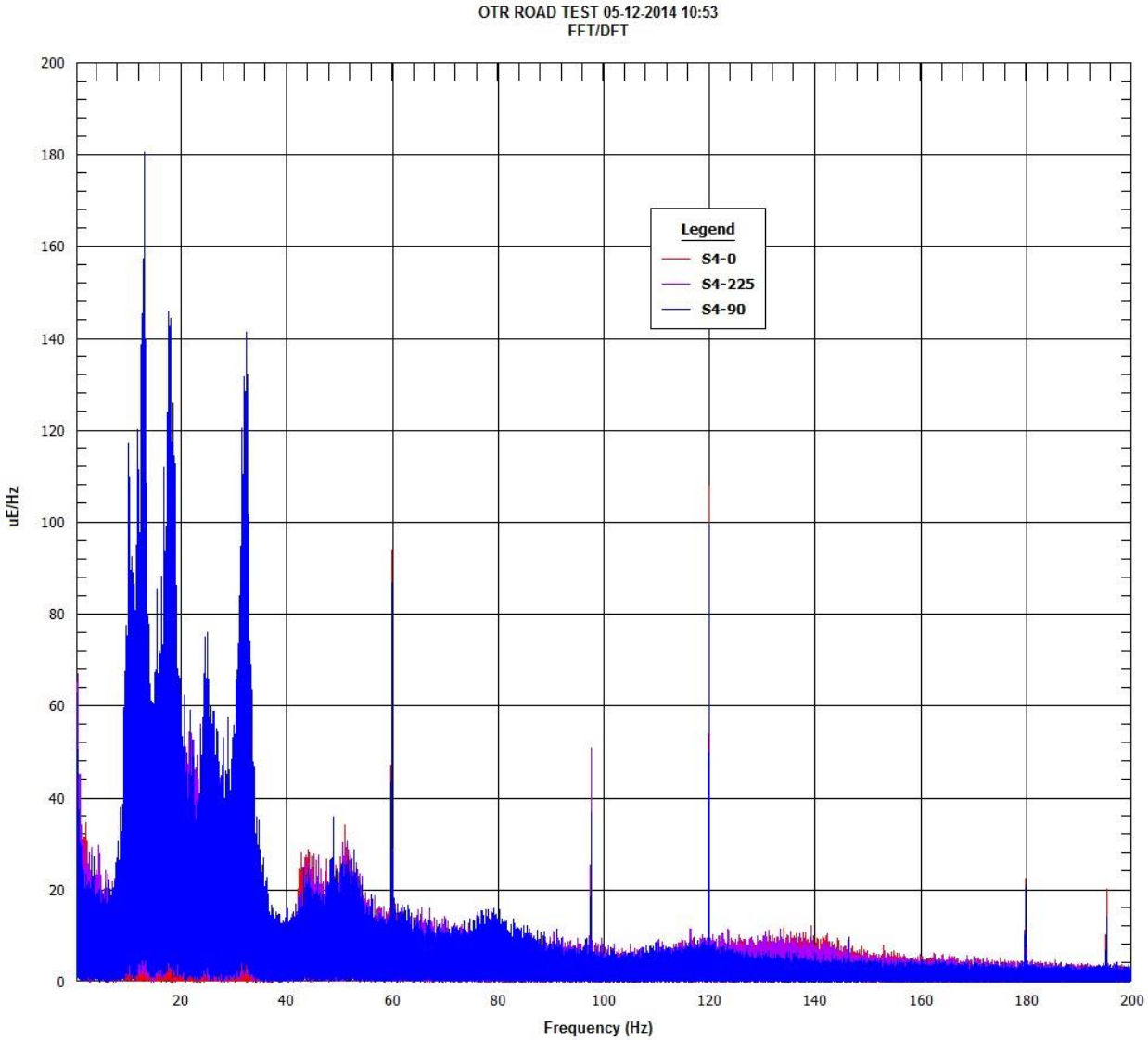

Figure 8.14 Segment 4 strain gauge FFTs

8.4.3 Accelerometer Time-Histories (g versus time)

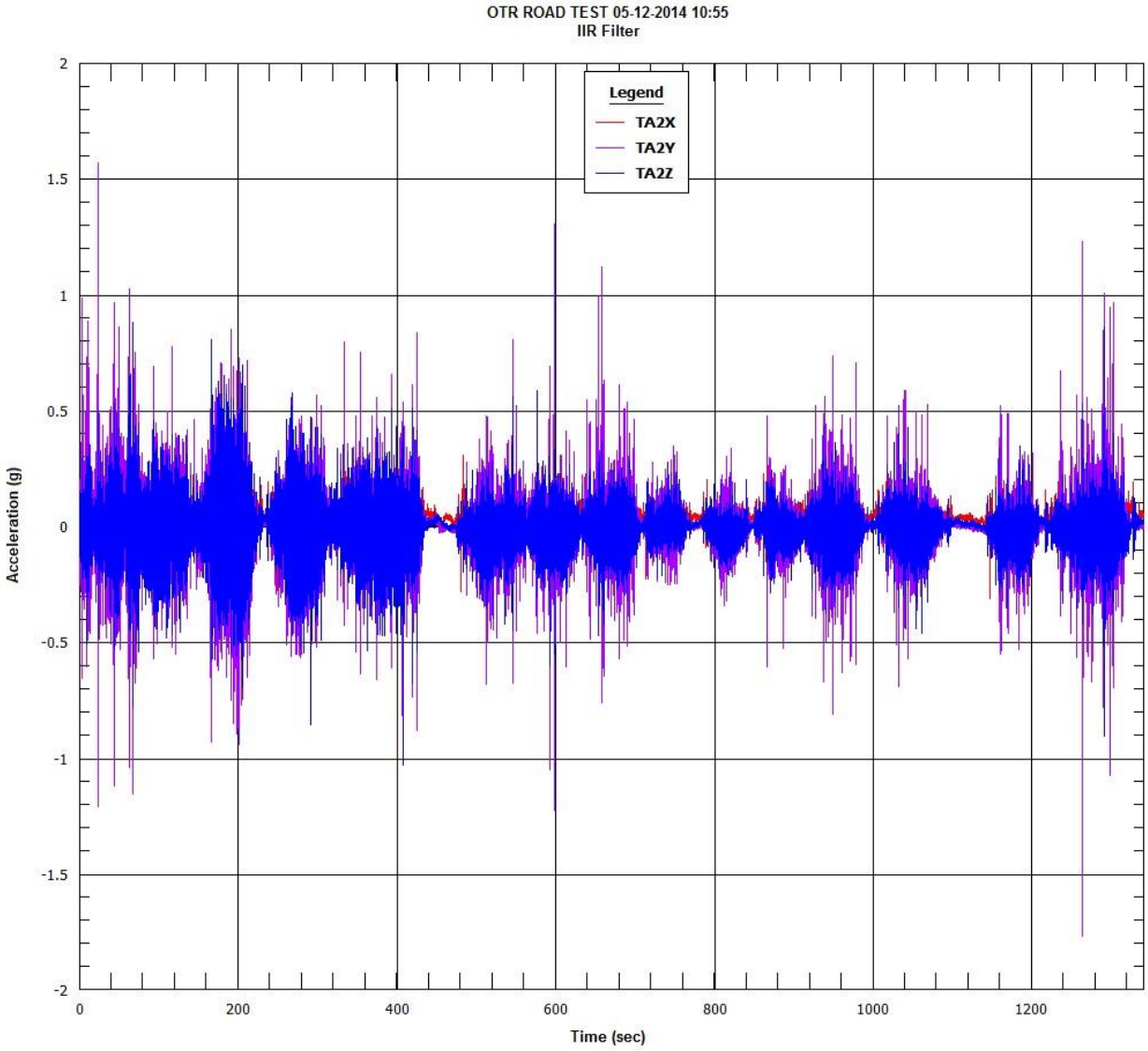

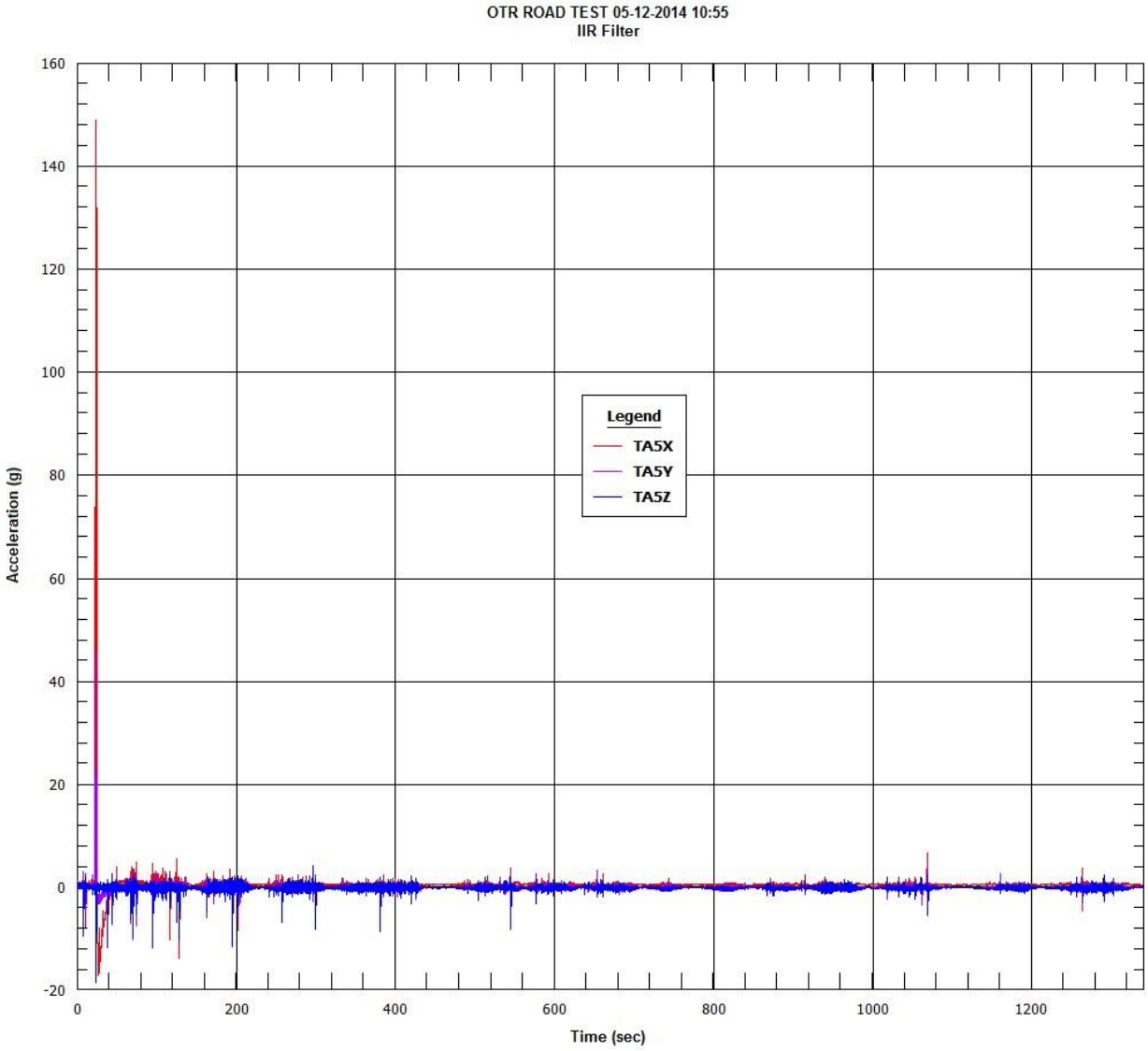
OTR ROAD TEST 05-12-2014 10:55
IIR Filter
Legend
TA5X
TA5Y
TA5Z
Acceleration (g)
Time (sec)
160
140
120
100
80
60
40
20
0
-20
0
200
400
600
800
1000
1200

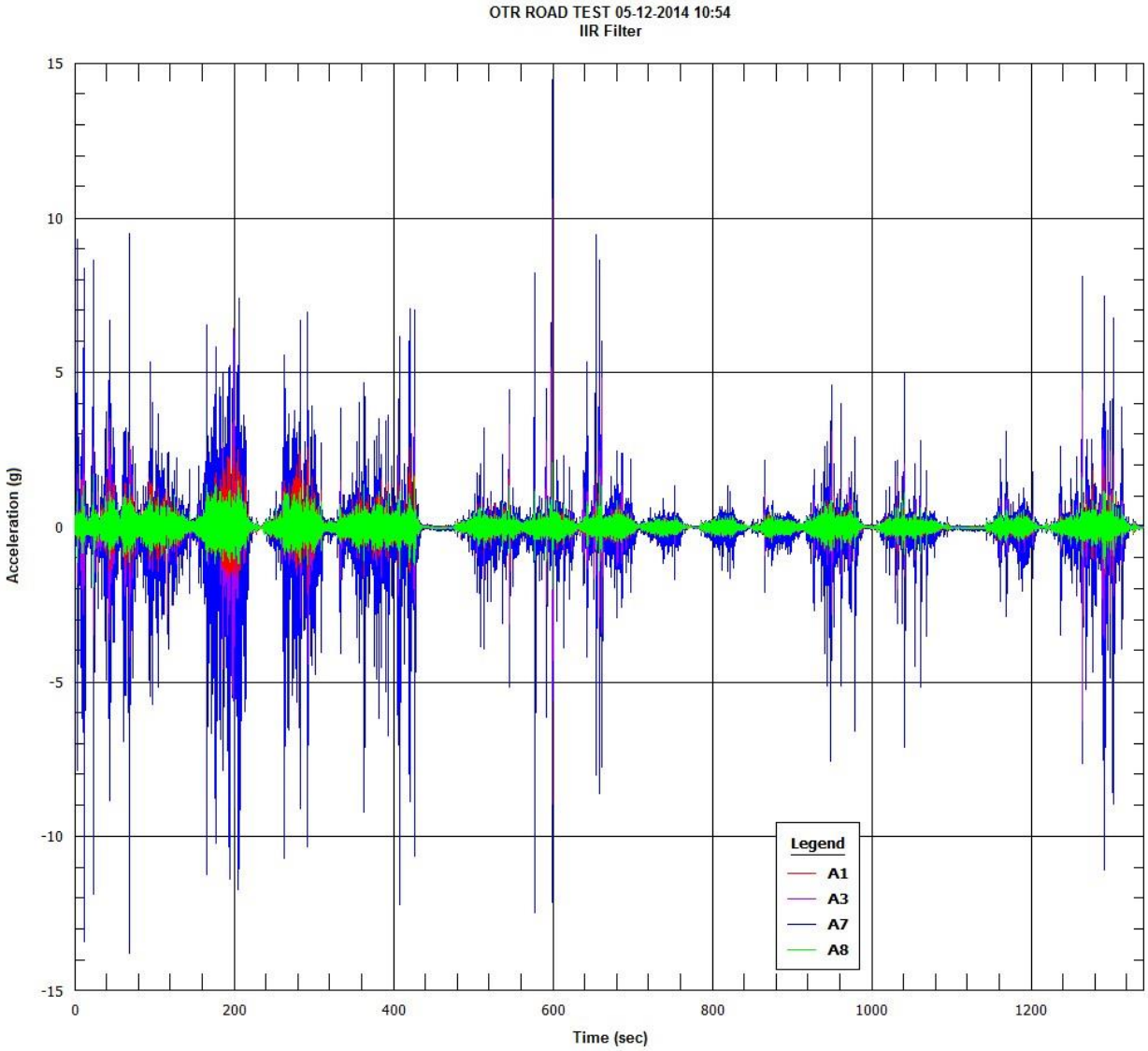

Figure 8.15 Segment 4 accelerometer time-histories

8.4.4 Accelerometer Fast Fourier Transformations (g/Hz versus Hz)

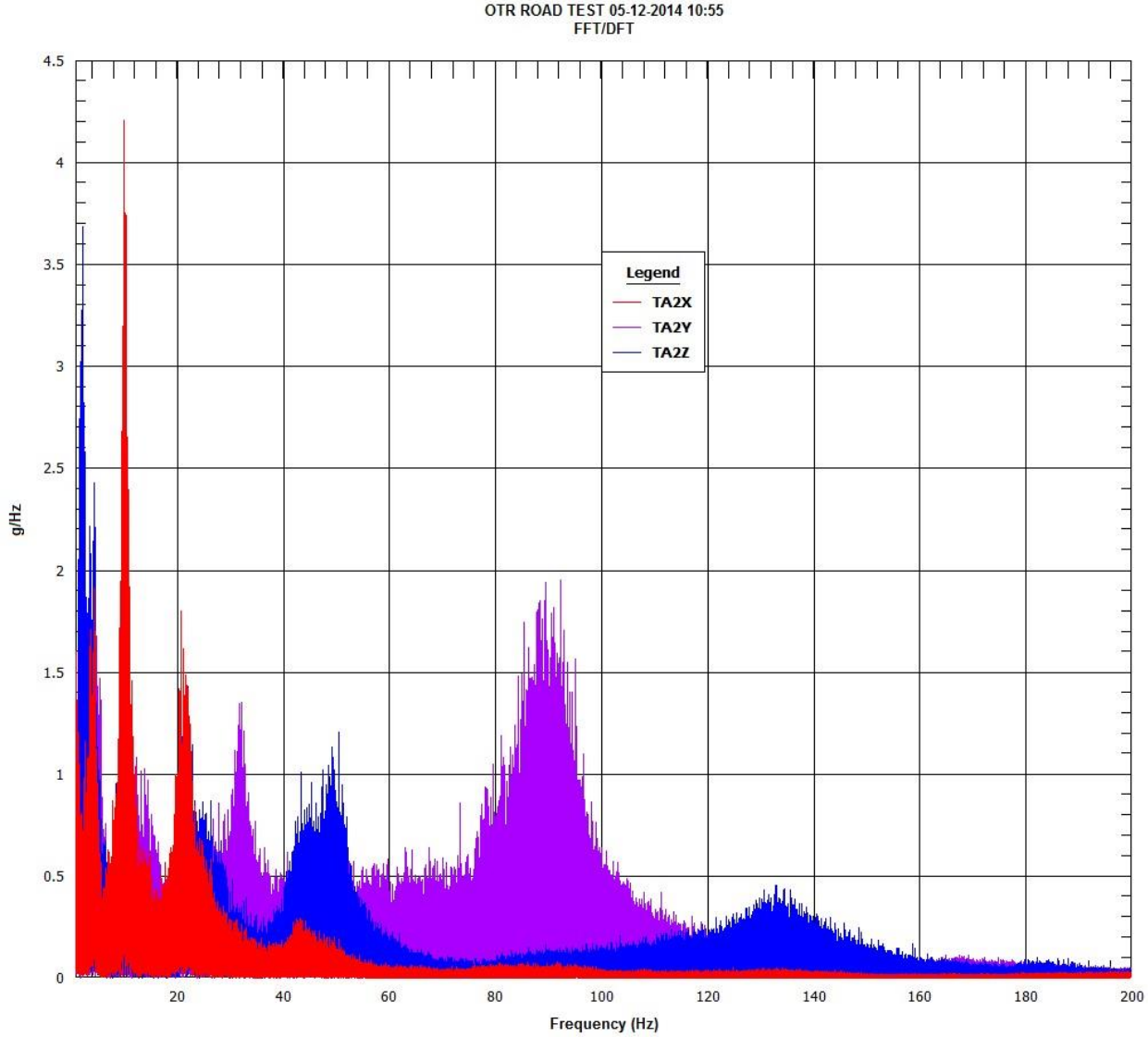

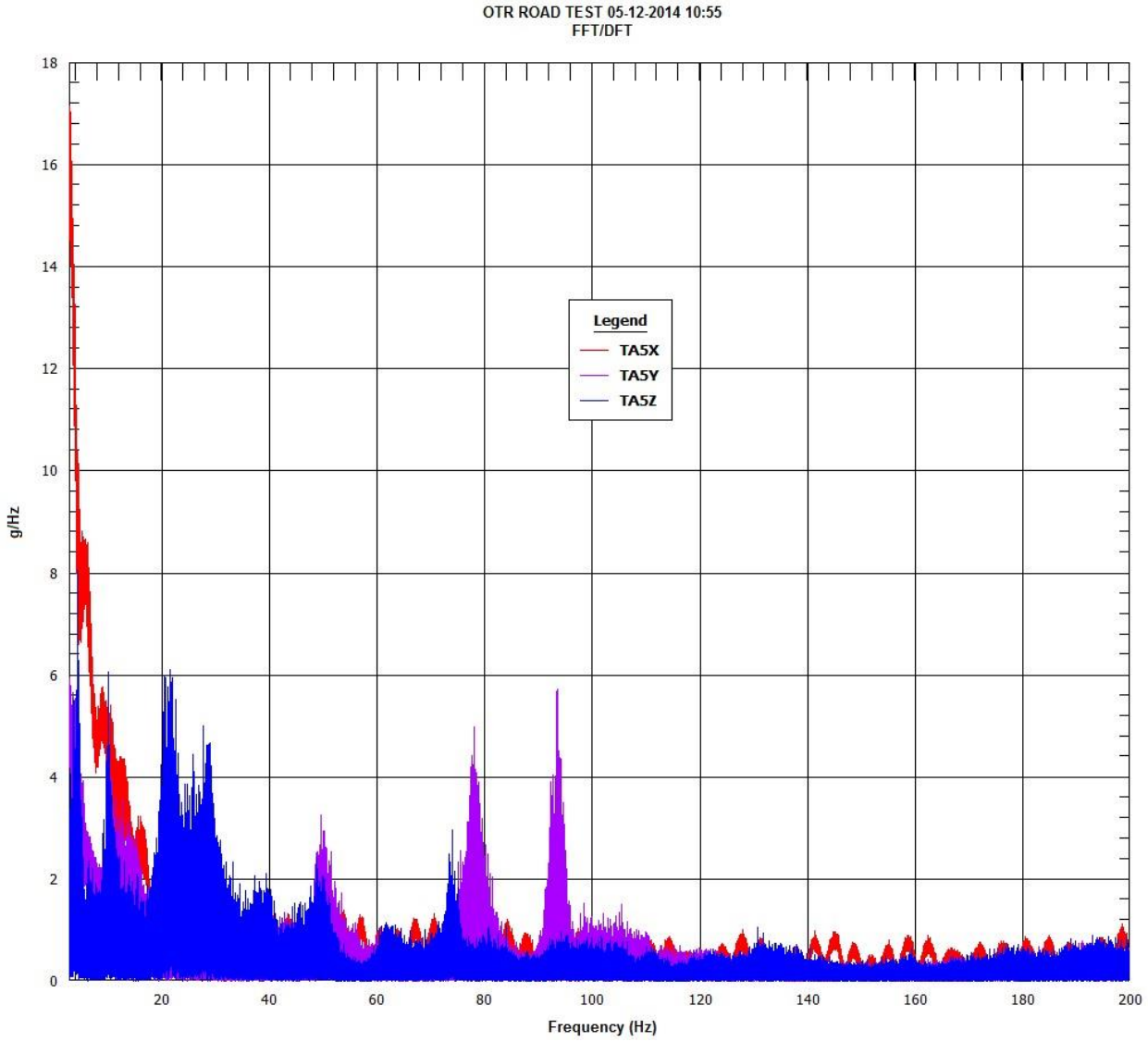
OTR ROAD TEST 05-12-2014 10:55
FFT/DFT
Legend
TA5X
TA5Y
TA5Z
g/Hz
Frequency (Hz)
0
2
4
6
8
10
12
14
16
18
20
40
60
80
100
120
140
160
180
200

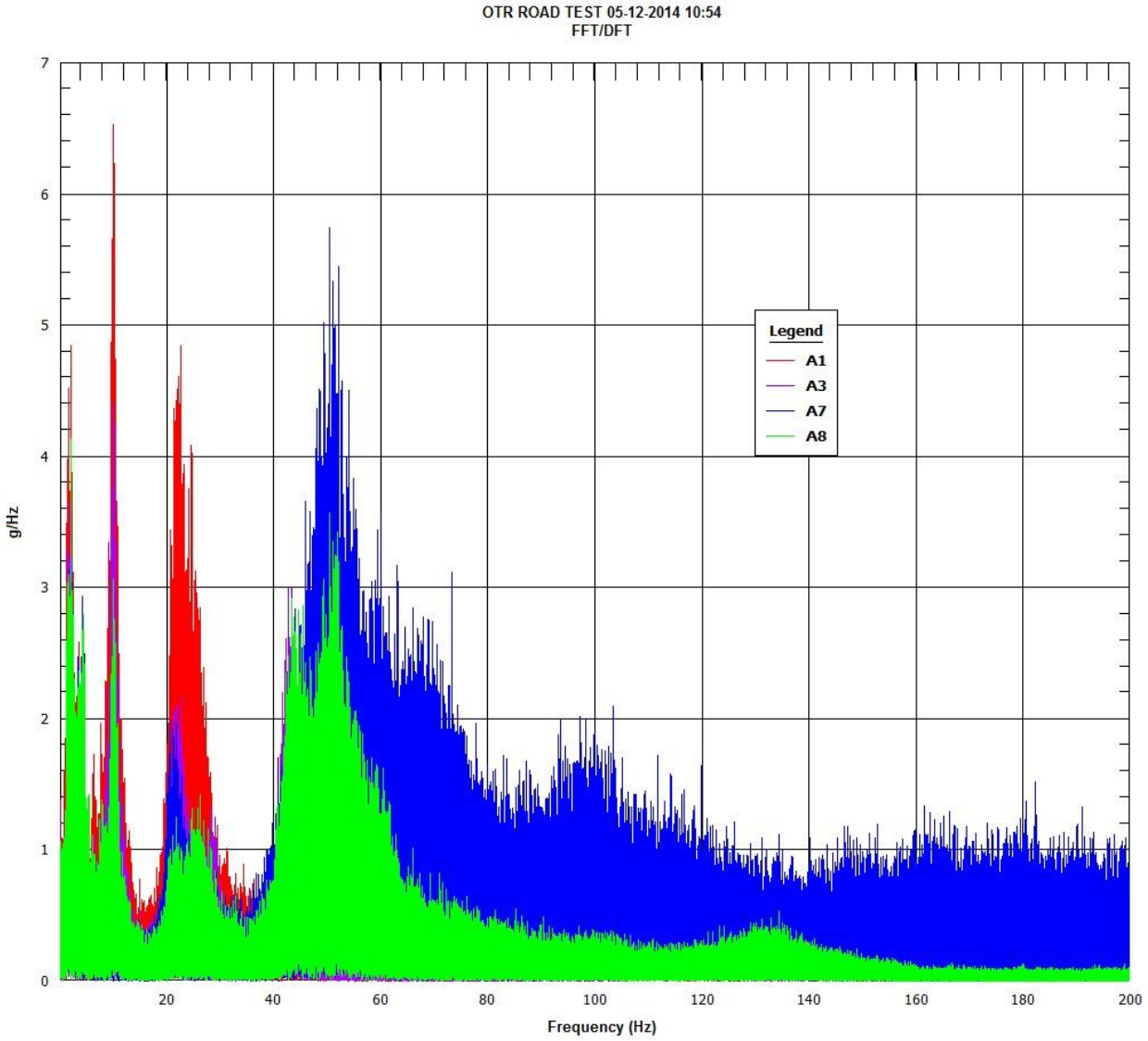

Figure 8.16 Segment 4 accelerometer FFTs

8.5 Truck Route Segment 5 Data Plots

8.5.1 Strain Gauge Time-Histories (με versus time)

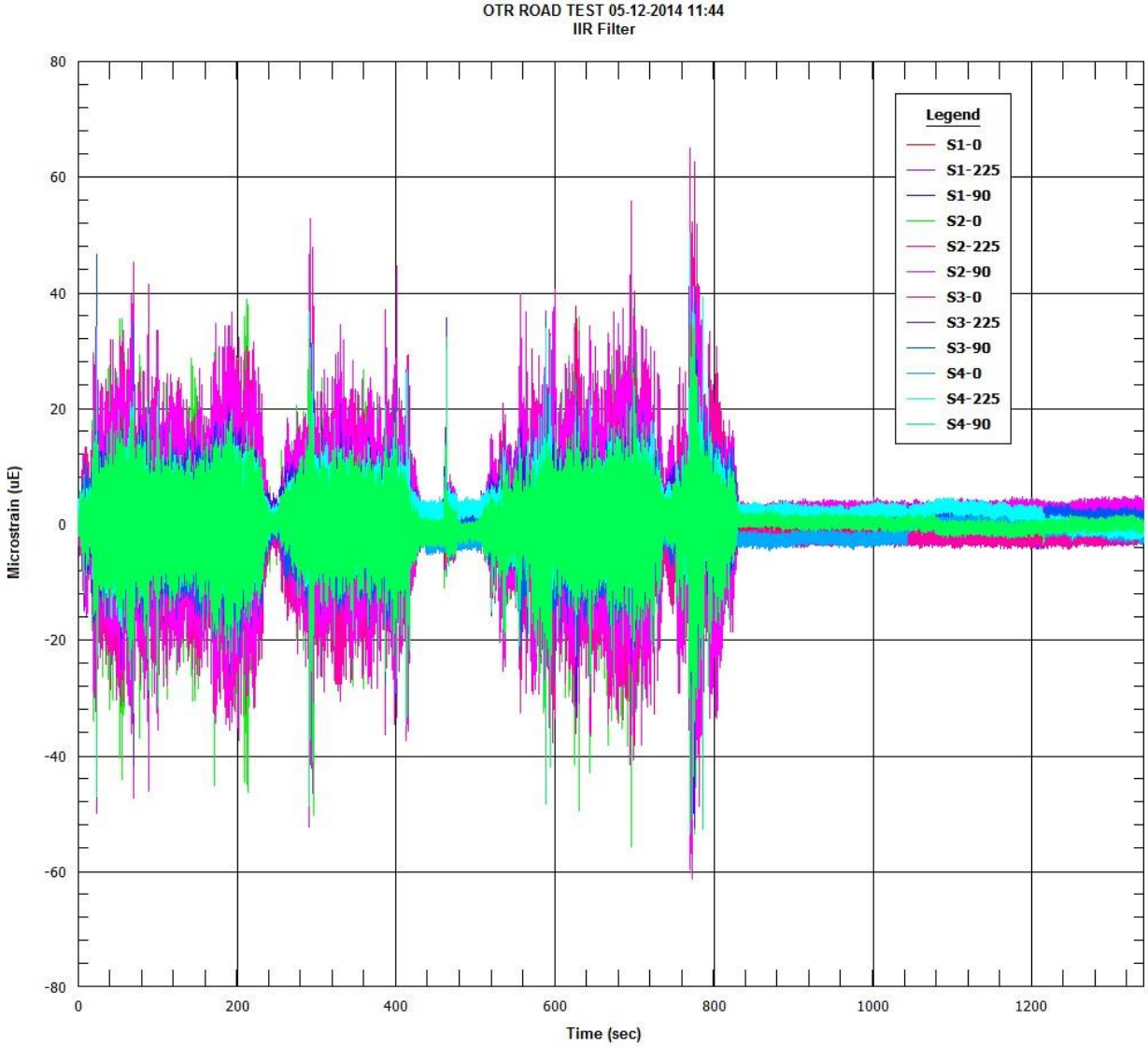

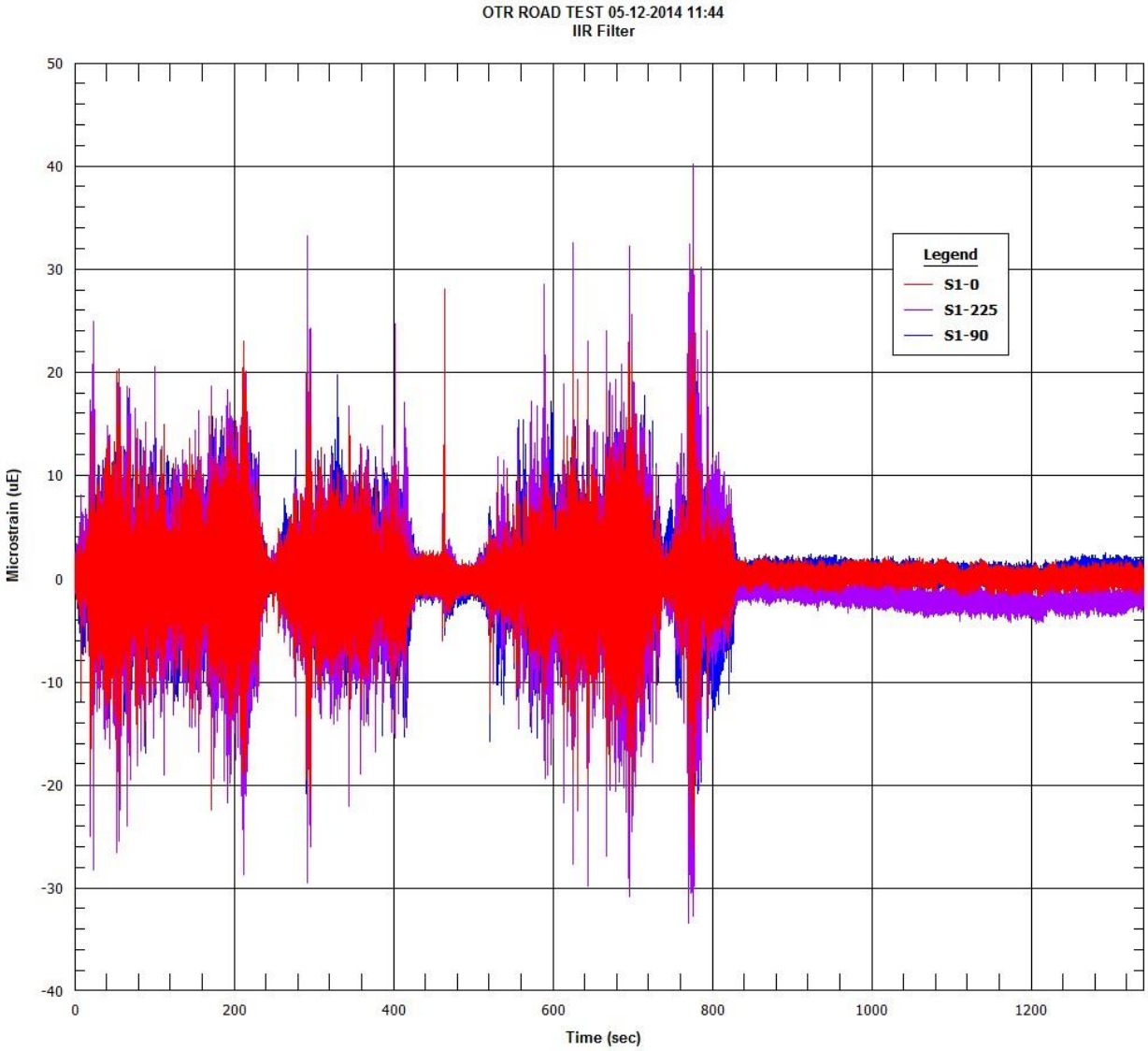
OTR ROAD TEST 05-12-2014 11:44
IIR Filter
Legend
S1-0
S1-225
S1-90
Microstrain (uE)
Time (sec)
50
40
30
20
10
0
-10
-20
-30
-40
0
200
400
600
800
1000
1200

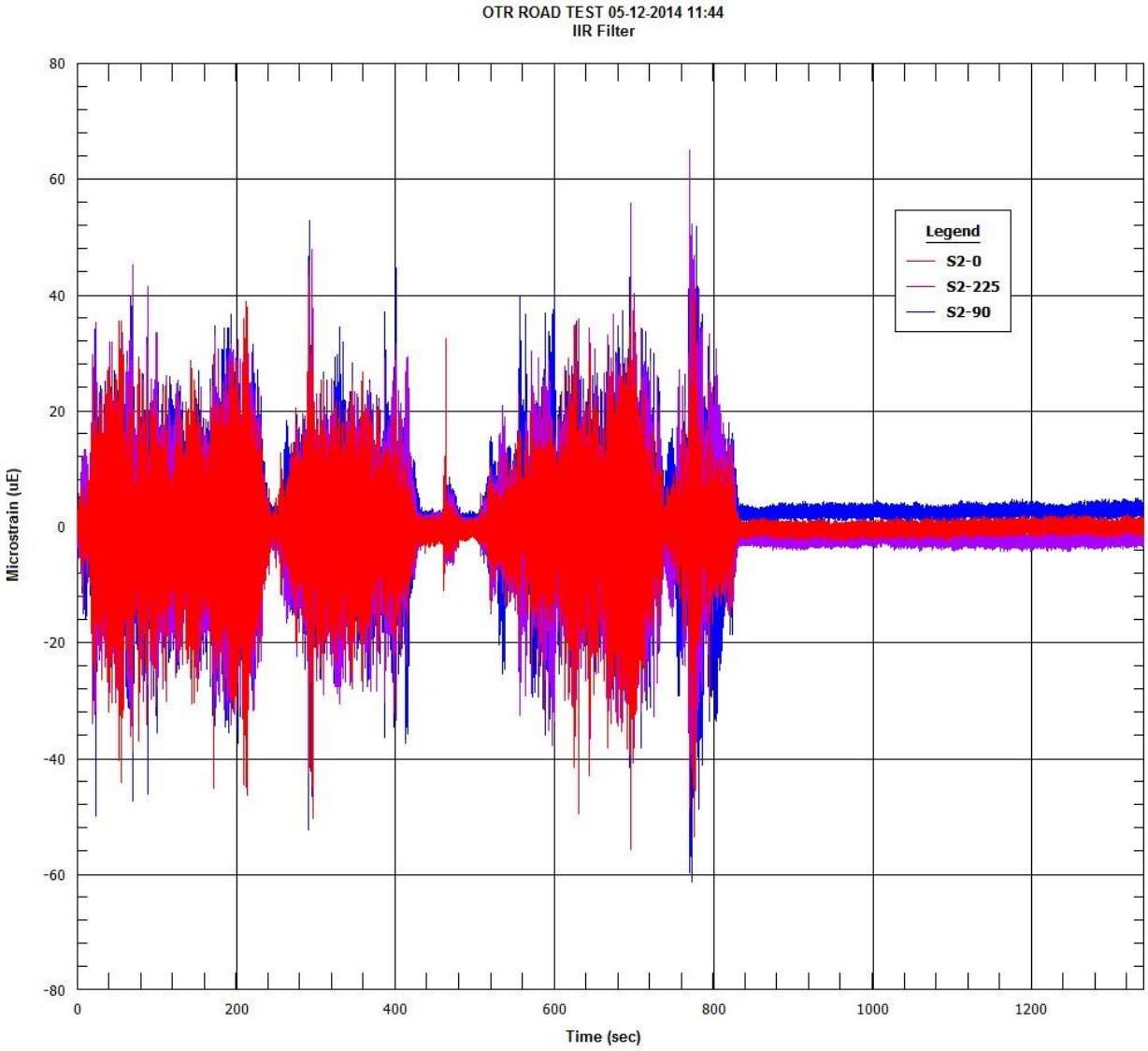
OTR ROAD TEST 05-12-2014 11:44
IIR Filter
Legend
S2-0
S2-225
S2-90
Microstrain (uE)
Time (sec)
80
60
40
20
0
-20
-40
-60
-80
0
200
400
600
800
1000
1200

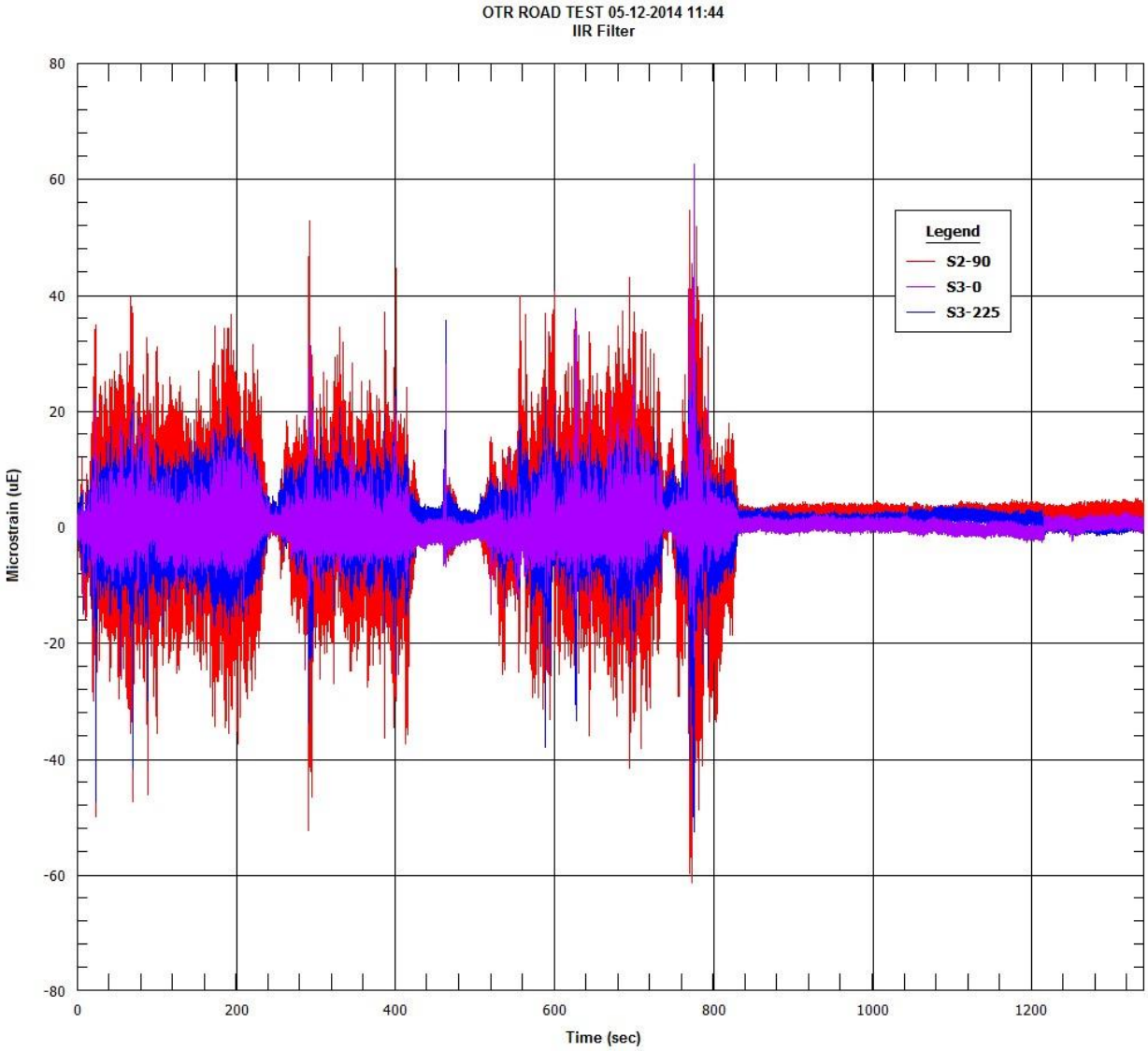
OTR ROAD TEST 05-12-2014 11:44
IIR Filter
Legend
S2-90
S3-0
S3-225
Microstrain (uE)
Time (sec)
80
60
40
20
0
-20
-40
-60
-80
0
200
400
600
800
1000
1200

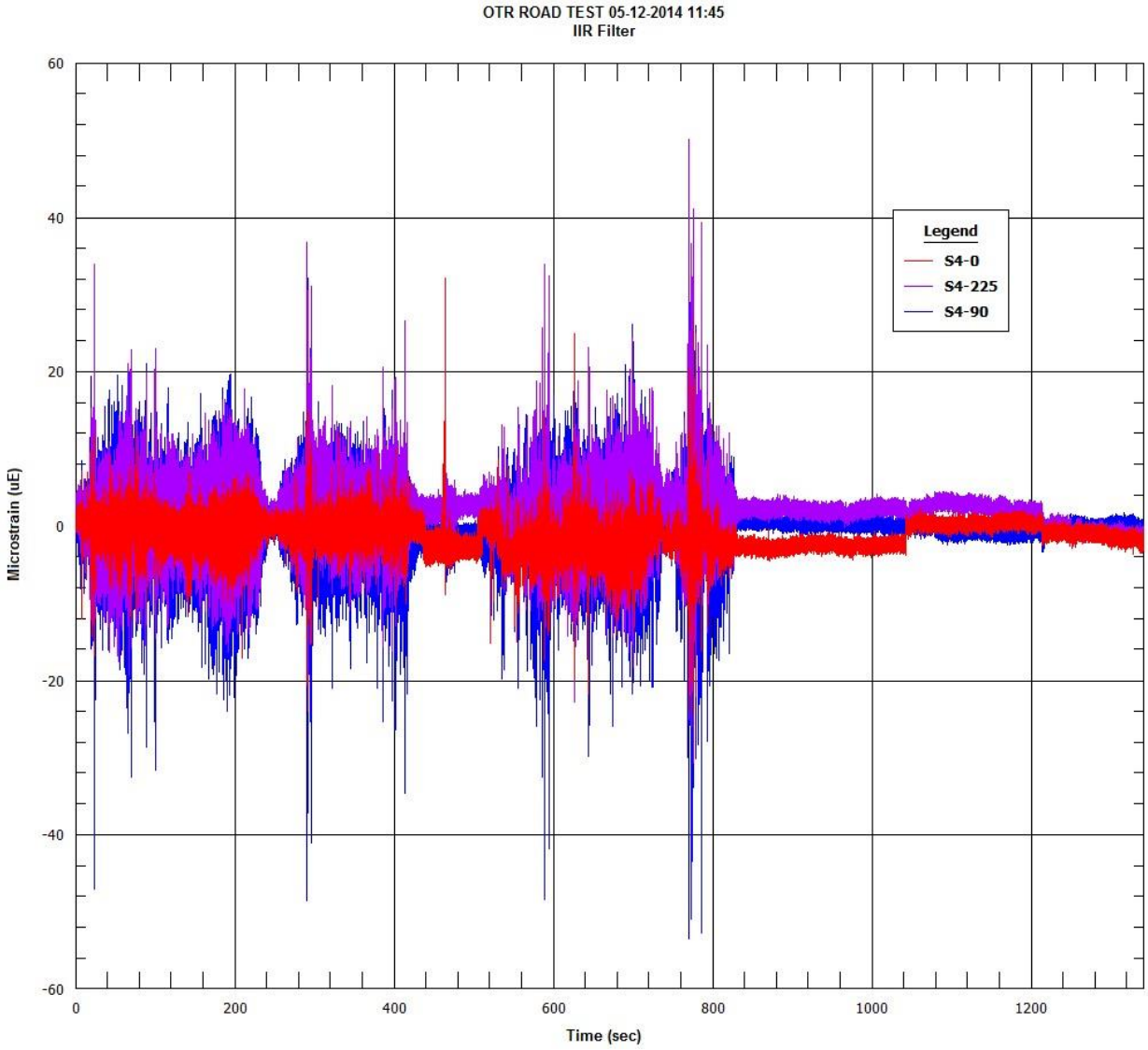

Figure 8.17 Segment 5 strain gauge time-histories

8.5.2 Strain Gauge Fast Fourier Transformations (με/Hz versus Hz)

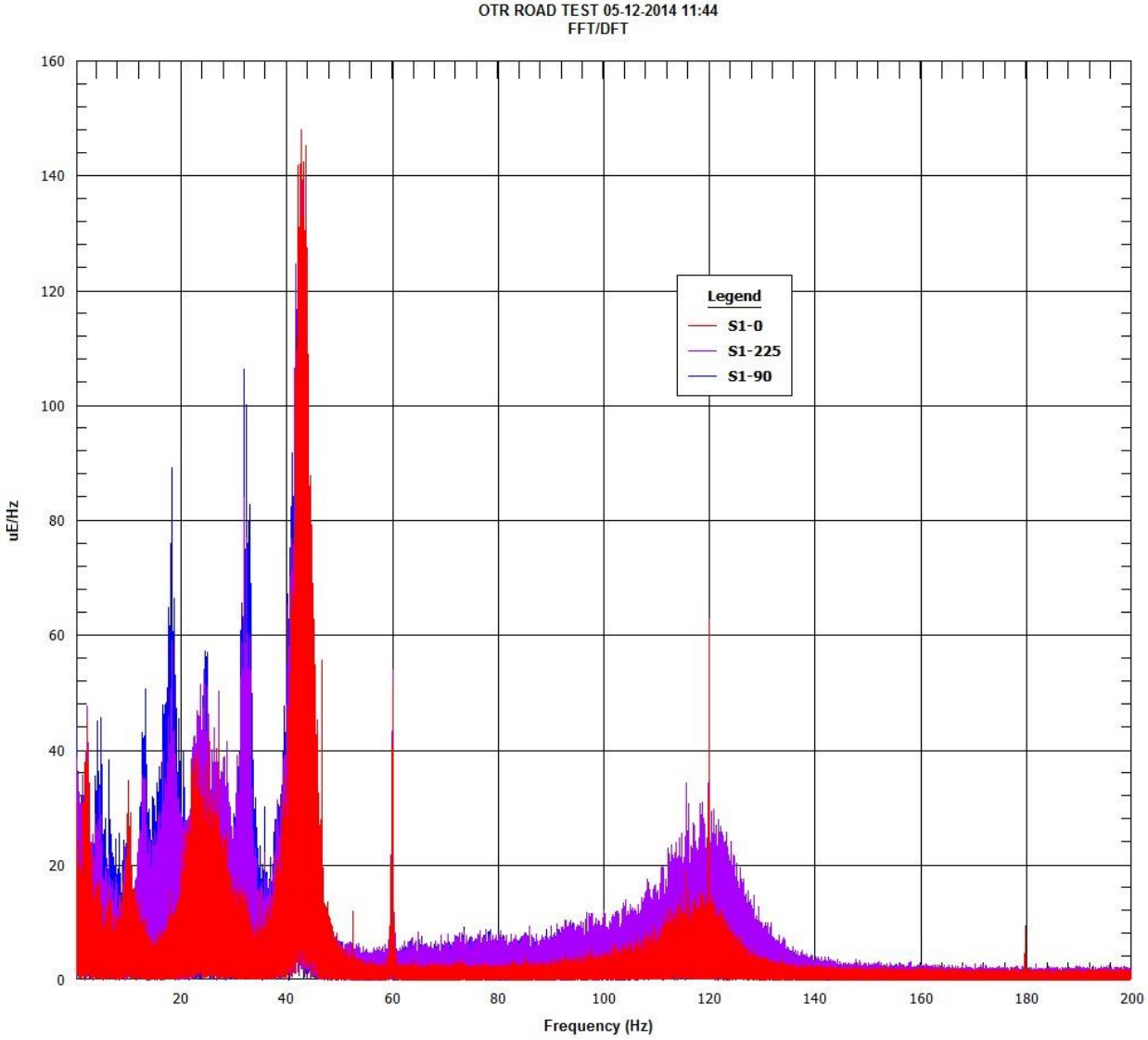

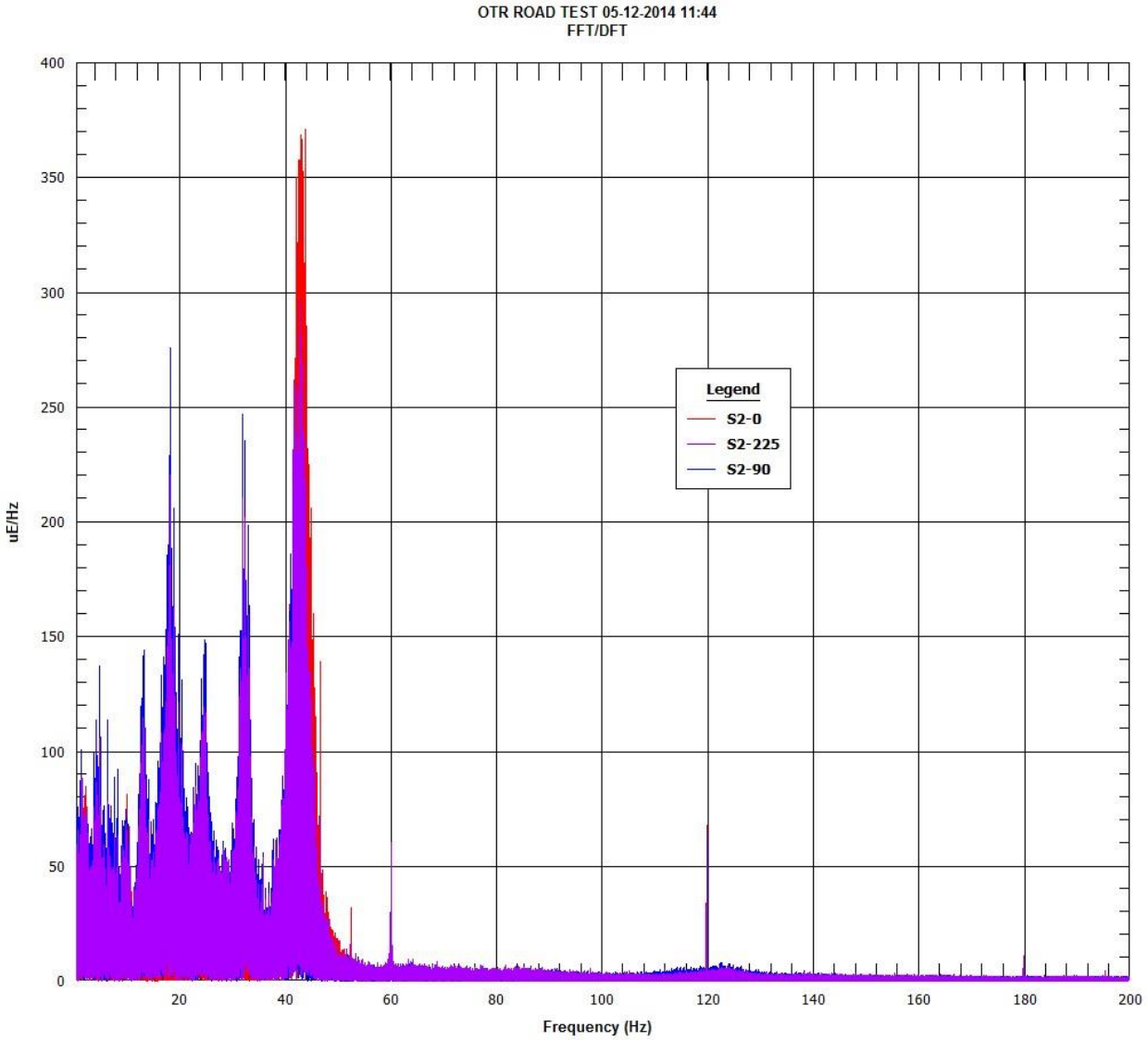
OTR ROAD TEST 05-12-2014 11:44
FFT/DFT
uE/Hz
Frequency (Hz)
Legend
S2-0
S2-225
S2-90
0
50
100
150
200
250
300
350
400
20
40
60
80
100
120
140
160
180
200

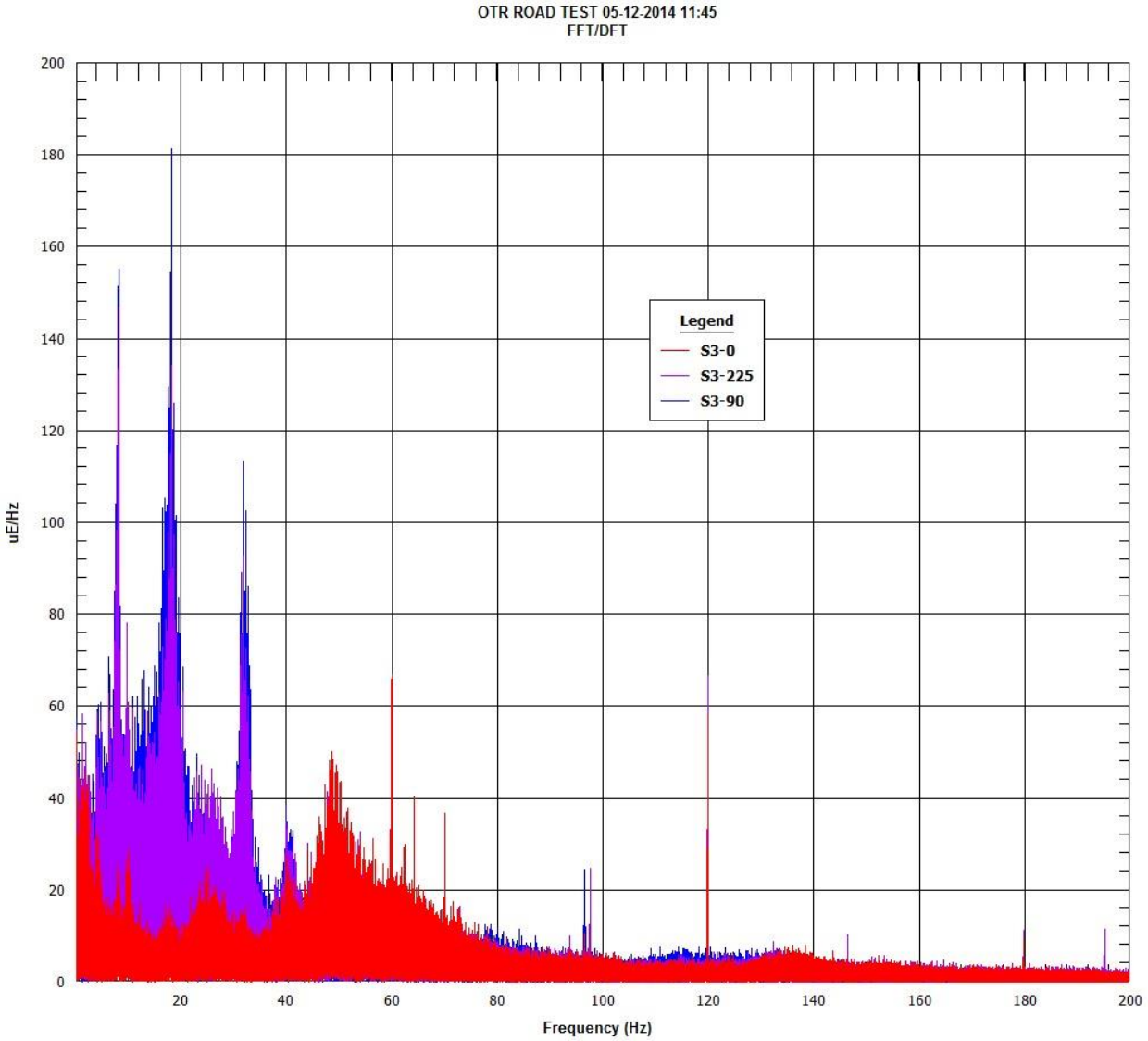
OTR ROAD TEST 05-12-2014 11:45
FFT/DFT
Legend
S3-0
S3-225
S3-90
uE/Hz
Frequency (Hz)
0
20
40
60
80
100
120
140
160
180
200

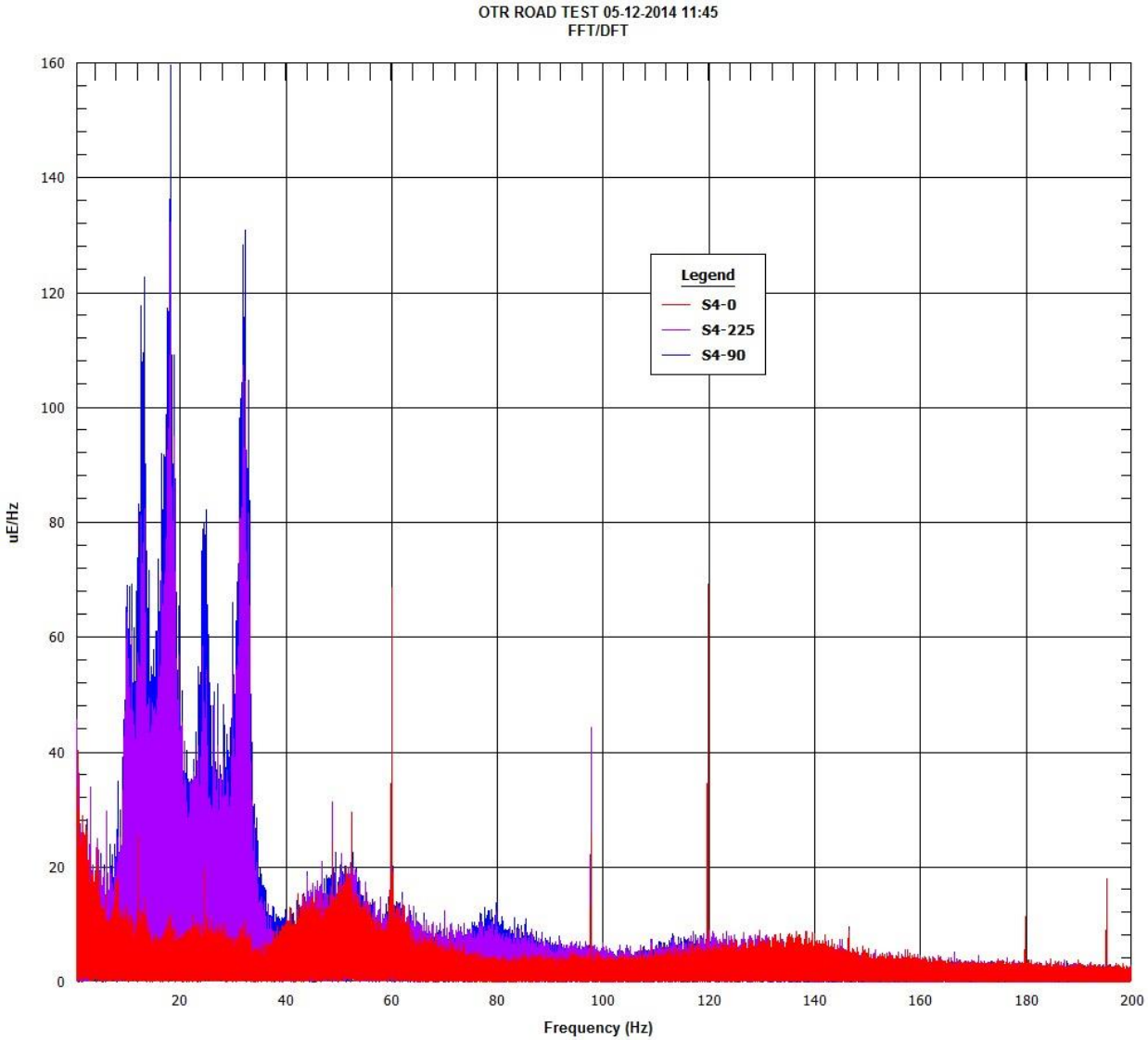

Figure 8.18 Segment 5 strain gauge FFTs

8.5.3 Accelerometer Time-Histories (g versus time)

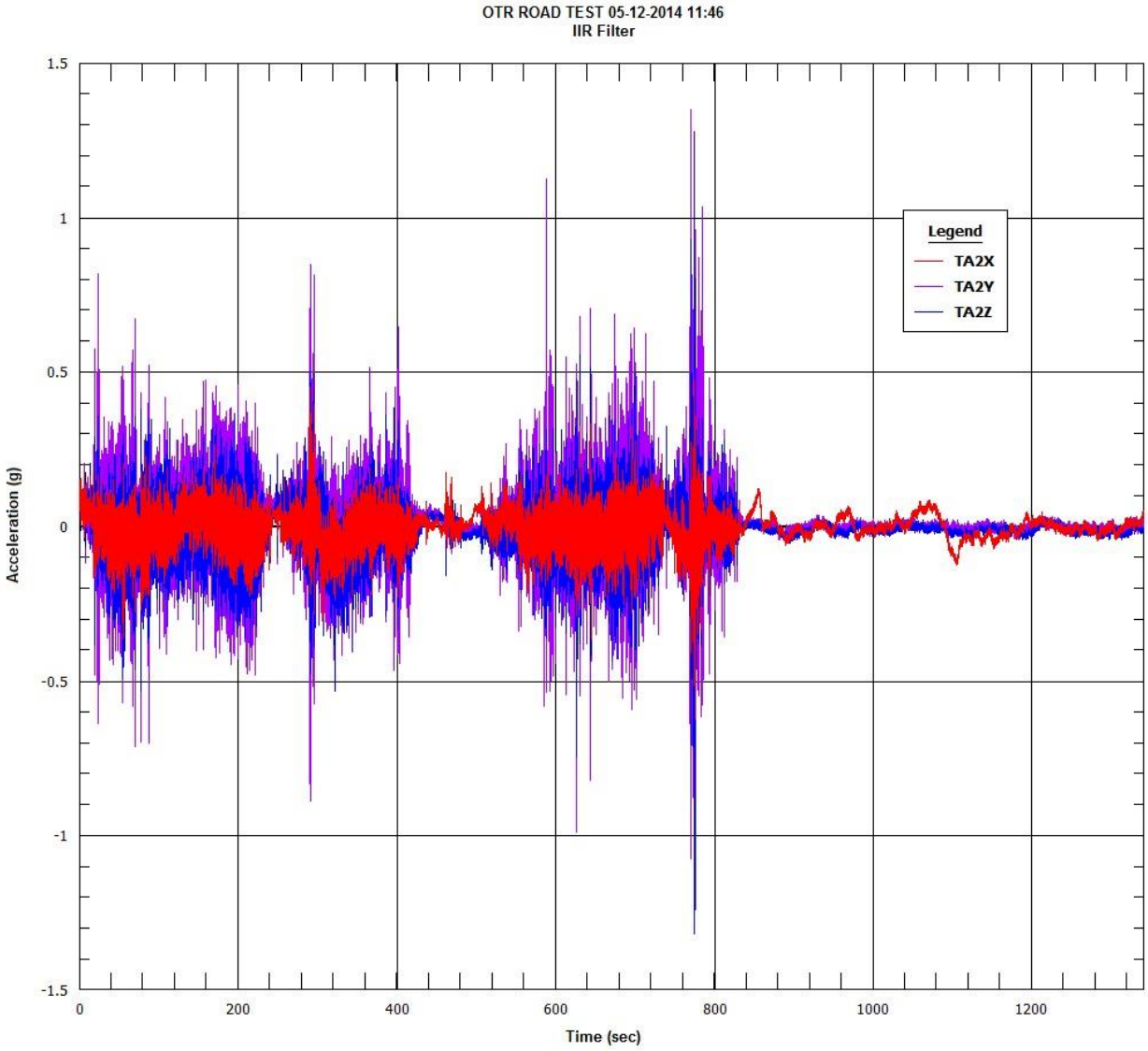

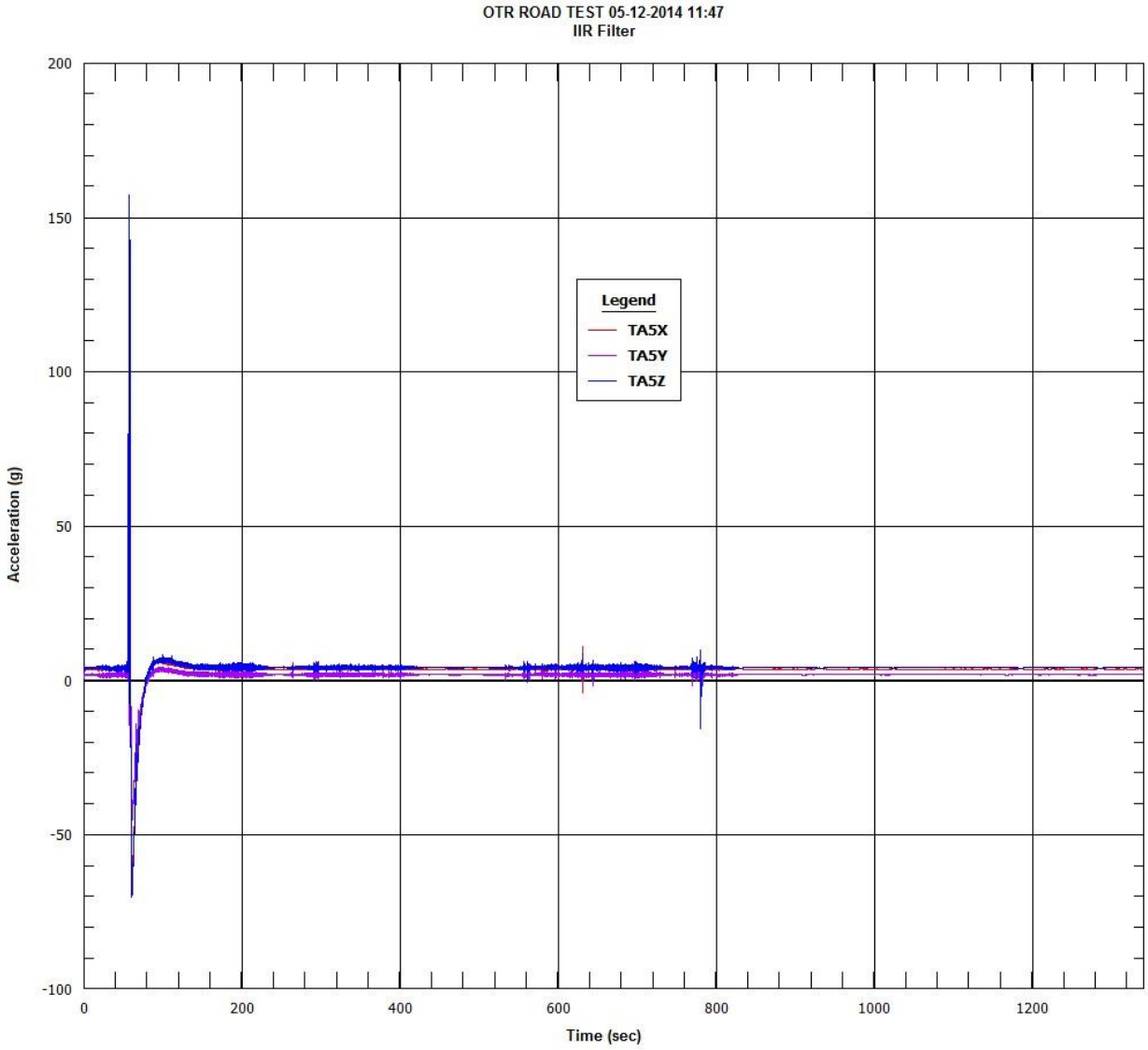
OTR ROAD TEST 05-12-2014 11:47
IIR Filter
Legend
TA5X
TA5Y
TA5Z
Acceleration (g)
Time (sec)
200
150
100
50
0
-50
-100
0
200
400
600
800
1000
1200

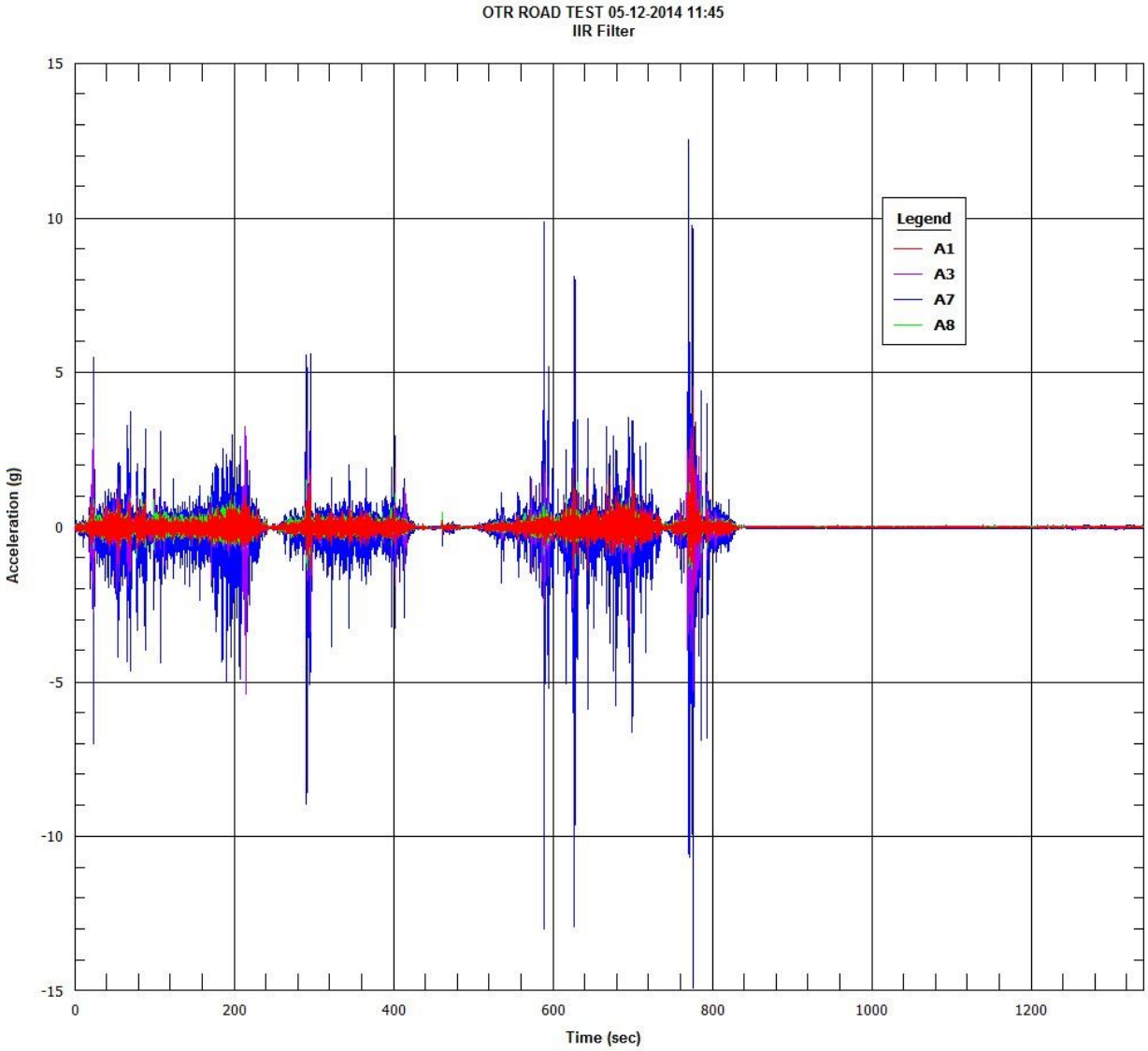

Figure 8.19 Segment 5 accelerometer time-histories

8.5.4 Accelerometer Fast Fourier Transformations (g/Hz versus Hz)

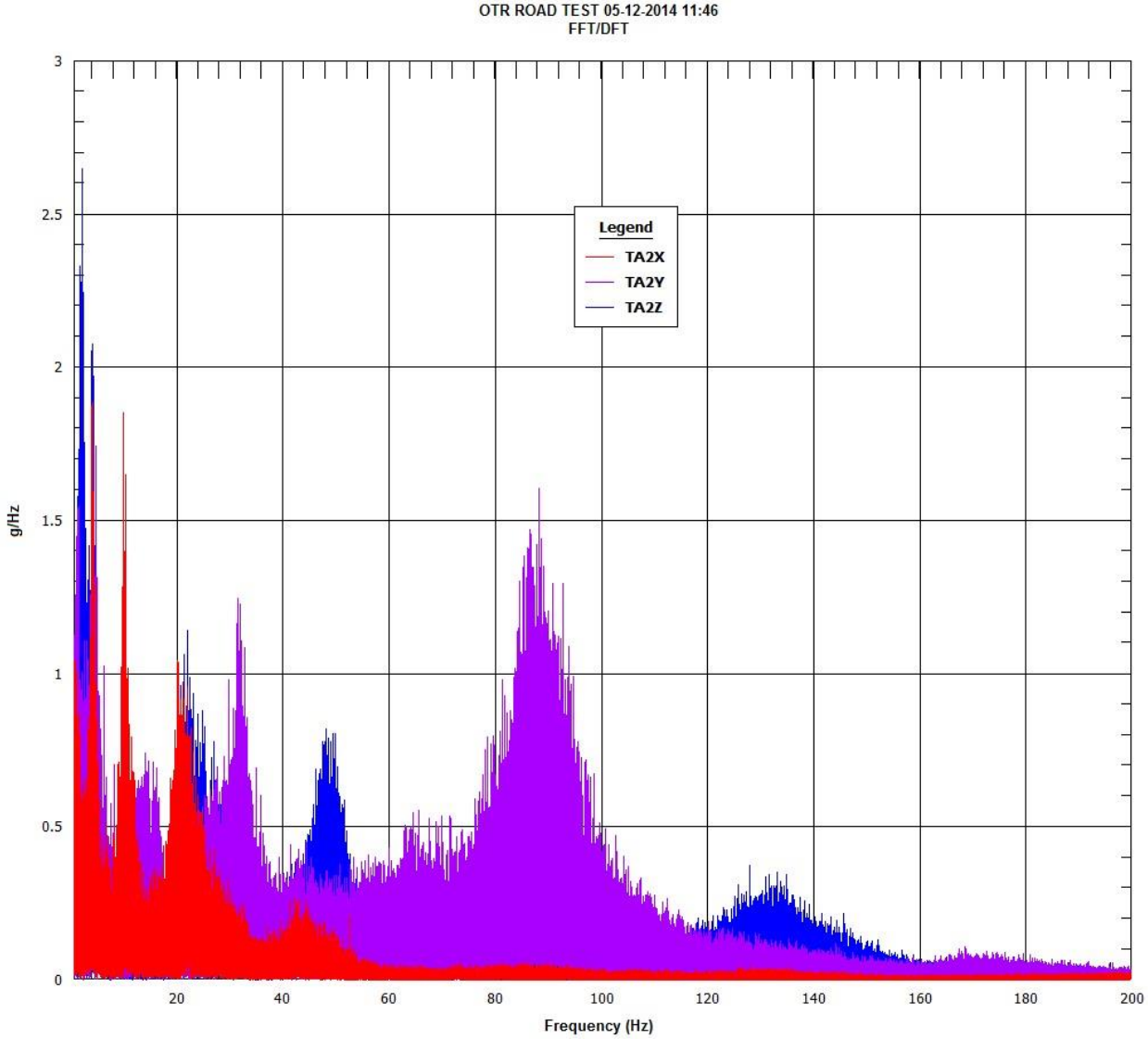

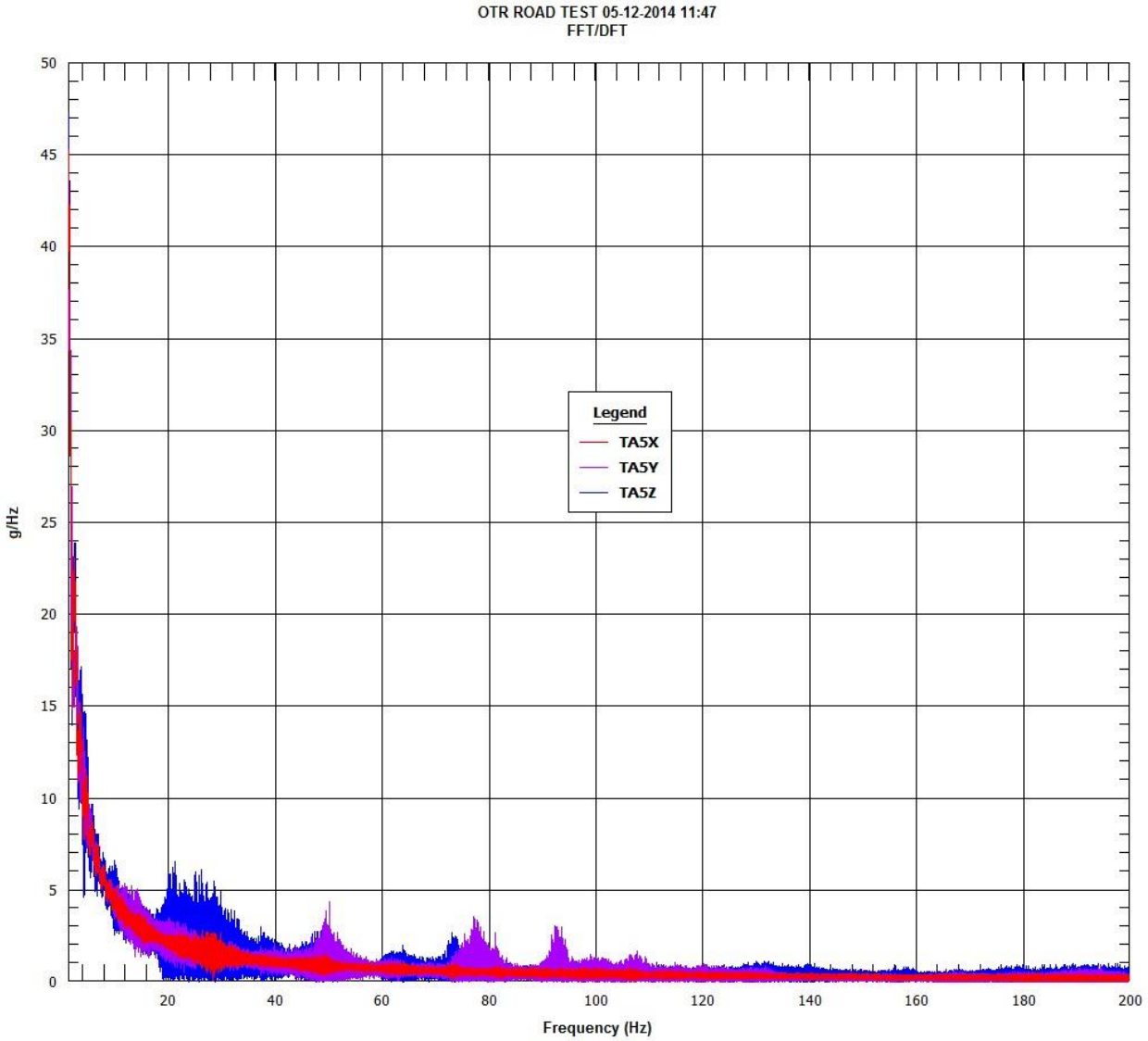
OTR ROAD TEST 05-12-2014 11:47
FFT/DFT
Legend
TA5X
TA5Y
TA5Z
g/Hz
Frequency (Hz)
0
5
10
15
20
25
30
35
40
45
50
20
40
60
80
100
120
140
160
180
200

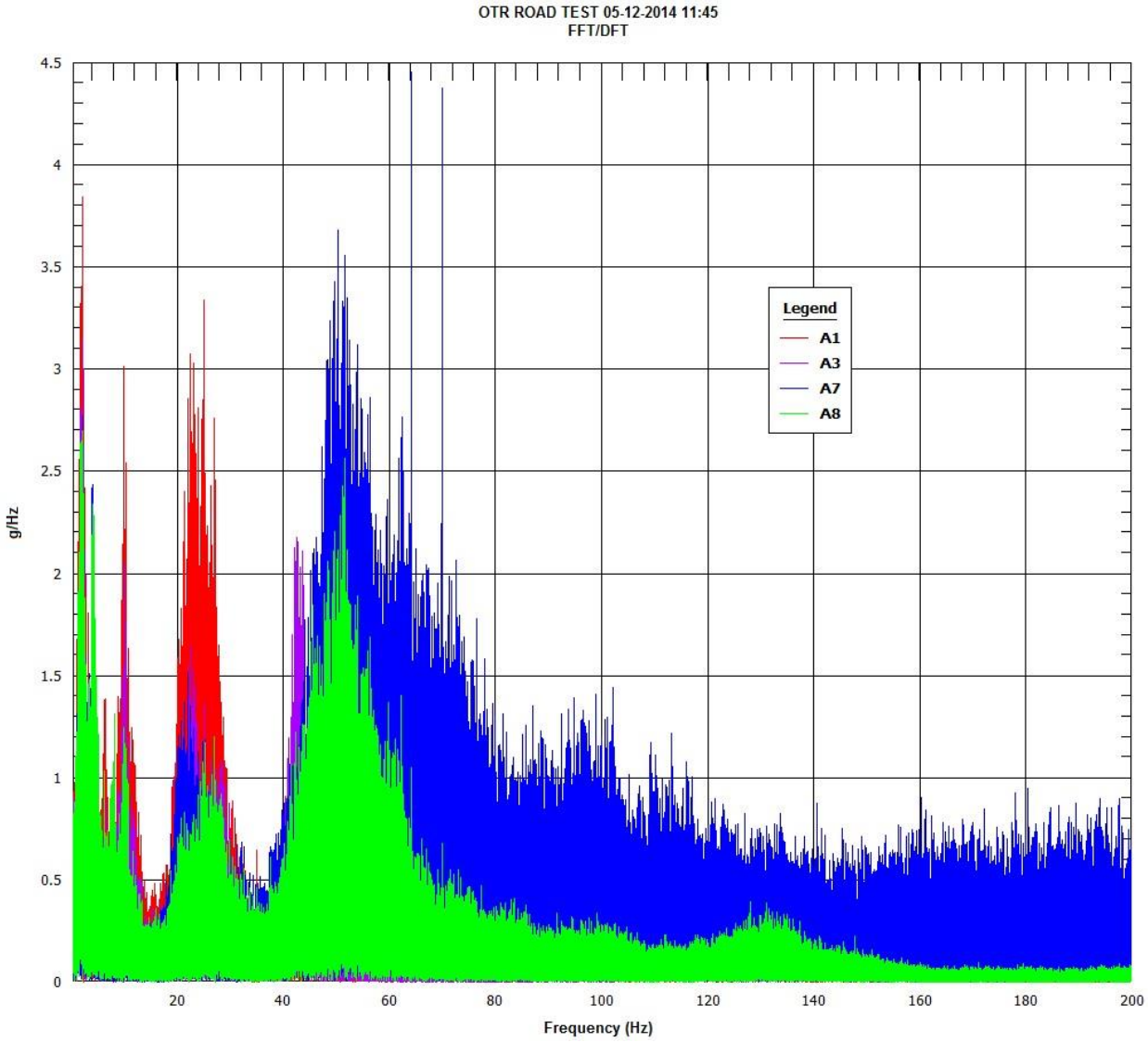

Figure 8.20 Segment 5 accelerometer FFTs